CZECH TECHNICAL UNIVERSITY IN PRAGUE
FACULTY OF ELECTRICAL ENGINEERING

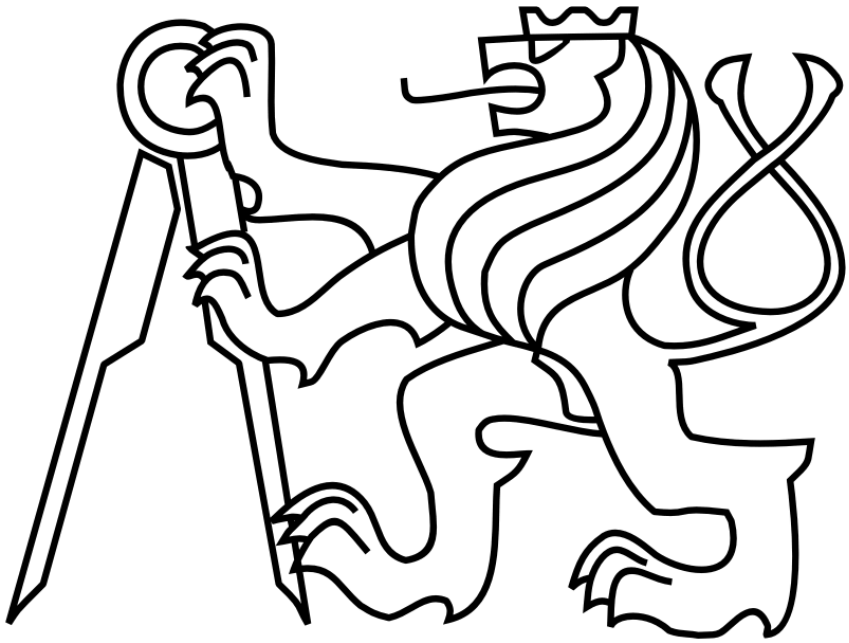

HABILITATION THESIS

MODERN SENSORS IN AIDED NAVIGATION SYSTEMS

Prague, 2013

Jan ROHAC, PhD.

ABSTRACT

This habilitation thesis is focused on advanced algorithms and methodology concerning aided navigation systems predominantly using MEMS based inertial sensors and aiding systems. It mainly describes the contribution of the applicant in areas involving a complex design and development of such navigation systems. Thus, it deals with principles of navigation, methods of system parameters estimation, calibration techniques, modeling, and signal/data processing. The thesis presents particular solutions and their direct impact on the system performance and accuracy. In addition, results published as well as unpublished are presented.

ANOTACE

Předkládaná habilitační práce se věnuje pokročilým algoritmům a metodám užívaným v oblasti navigačních systémů převážně využívajících MEMS inerciálních senzorů a doplňkových pomocných měřicích systémů. Práce popisuje přínos žadatele v oblasti výzkumu a vývoje těchto navigačních systémů. Práce se zabývá navigačními principy, metodami odhadu parametrů systému, kalibračními metodami, modelováním a zpracování signálu a dat. Práce dále uvádí konkrétní řešení a jejich vliv na funkčnost a přesnost navigačního systému. Vše je dokládáno výsledky jak publikovanými, tak i nepublikovanými.

ACKNOWLEDGMENTS

First of all I would like to thank all my colleagues and friends who have supported me and helped me during my present career as well as who have cooperated with me on research and results publishing.

Special thanks to:

- Karel Draxler, associate professor at the Dept. of Measurement, Faculty of Electrical Engineering, CTU in Prague, who is my main advisor and supporter at the department guided me during my PhD. study and in my career at the department.
- My PhD. students (Michal Reinštein, Martin Šipoš, Petr Nováček, Jakub Šimánek), to whom I have been honored to be a supervisor specialist. We became an excellent group cooperating on research, publishing papers, and on lots of other work.
- Daniel Hanus, associate professor at the Dept. of Air Transport, Faculty of Transportation Sciences, CTU in Prague, who I have been working with in the field of international relationships and cooperation.

I am aware of missing many other people here who deserve to be thanked; I apologize for it and I beg for their understanding. Nevertheless, my greatest thanks belong to my family and closest friends for their support, friendship, and pushing me still ahead.

CONTENTS

1. INTRODUCTION

This habilitation thesis provides the overview of the applicant's activities in the field of aided navigation systems. The applicant has been supervising a navigation group at the Department of Measurement, so he has participated on the majority of activities done within this group in the form of consultation, leadership, or putting hands on. He has been a supervisor specialist of four PhD. students who have worked on topics corresponding to the field of inertial navigation and aiding systems.

Since accuracy of navigation systems is always directly related with a sensors choice, the thesis also includes short part introducing sensors suitable for cost-effective navigation systems and those which the applicant has used in his research projects. As the area of navigation systems using a cost-effective solution is complex, the thesis covers all phases of their design and development procedures which the applicant has been dealing with. It includes the topics concerning deterministic and stochastic sensor parameters evaluation methods, sensor error model design, signal and data pre-processing, data validation techniques, data fusion, and evaluation of navigation equations. All these have been applied in projects determined to experimental research from which several publications in SCI journals and conferences arose and several entire navigation systems were developed. In chapter 2 a reader can find a basis of background commonly used in navigation systems which also provides information about the current state-of-the-art in technology and methodology applied in these systems. Following chapters describe the applicant particular work, his motivation and contribution, as well as results and conclusions of his activities. Chapter 3 summarizes the applicant areas of research followed by chapter 4 which is composed of selected journal and conference proceedings papers describing the applicant work and contribution. Chapter 5 supplements the previous one with additional description of his work and contribution which have not been published yet. It has a supportive character for a reader to see at which direction the applicant research activities have been aimed. Chapter 6 provides the information about areas of research on which the applicant wants to focus in the future. At the end chapter 7 concludes the applicant activities and work.

2. CURRENT STATE-OF-THE-ART IN NAVIGATION SYSTEMS

This chapter forms a part of introduction to the field of navigation systems for a reader to understand the current-state-of-the-art and learn technology and methodology the applicant has been dealing with.

2.1. NAVIGATION SYSTEMS TECHNOLOGY AND ITS PROGRESS

Navigation systems providing the tracking of an object attitude, position, and velocity play a key role in a wide range of applications, e.g. in aeronautics, astronautics, robotics, automotive industry, underwater vehicles, or human body observation. A common technique to do so is via a dead reckoning. One form of a dead reckoning technique is using an initial position, velocity, and attitude related to a predetermined coordinate frame and consecutive update calculations based on acceleration and angular rate measurements. These measurements are generally provided by 3-axis accelerometer (ACC) and 3-axis angular rate sensor (ARS) or gyroscopes (gyros) forming so called Inertial Measurement Unit (IMU). According to required precision of navigation and economical aspects suitable inertial sensors have to be chosen. The sensors are a major source of errors in navigation systems; therefore, the type of an application should be considered as well. In the case of ARS/gyros required precision related to determined applications is denoted in Fig. 1, for the case of ACC it is shown in Fig. 2.

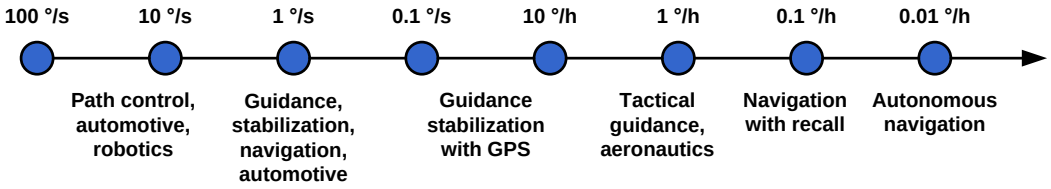

Fig. 1 - Required precision of sensed angular rate according to specified applications [2.1]

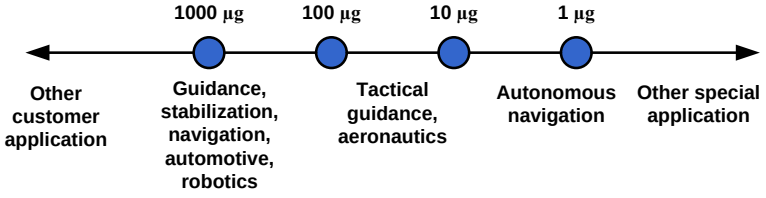

Fig. 2 - Required precision of sensed acceleration according to specified applications [2.1]

For aircraft navigation it is, according to Fig. 1 and Fig. 2, required to employ ARS/gyros with the precision better than 1 deg/h and ACC not more than 10 μg. The higher precision, the more expensive the device is. The other aspect, which has to be taken in account, is if a particular device is solid-state or is using moving parts. According to Fig. 3 and Fig. 4, one can see that mechanical gyros and ACCs satisfy requirements on precision the most; nevertheless, there is a trend to replace them with solid-state devices for their better reliability, stability, and MTBF (Mean-Time-Before-Failure) parameter. Therefore, in the following text there will be preferred solid-state devices.

The most precise device for angular rate measurements is a ring laser gyroscope (RLG), which has the stability better than 0.1 deg/h and the resolution better than 10^{-6} deg/s. In the case of ACC, the most precise existing device is a servo ACC with the resolution about 1 μg. These devices would have been ideal for all applications, if they were not so expensive. Due to this reason other systems, such as Micro-Electro-Mechanical-Systems (MEMSs), have been used in cost-effective applications, such as in UAVs or small aircrafts. MEMSs are typically defined as microscopic devices designed, processed, and used to interact or produce changes within a local environment. MEMSs offer reduced power consumption, weight, manufacturing and assembly costs, and increased system design flexibility. Reducing the size and weight of a device allows multiple MEMS components to be used to increase functionality, device capability, and reliability. In contrast, MEMS performance has many weak aspects, such as for precise navigation purposes low resolution, noisy output, worse bias

stability, temperature dependence and so on. Nevertheless, their applicability in navigation is wide due to fast technology improvements, applied data processing algorithms, and used aiding systems. In a navigation area aiding systems are commonly used to provide corrections for position or attitude evaluation both coming from ACCs and ARSs. Those systems might be based on for instance GNSS, electrolytic tilt sensors, pressure based altimeter or speedometer.

A near-term gyro technology from a scale factor and bias stability point of view is depicted in Fig. 3. It compares the performance of cost-effective MEMS sensors with fiber optic gyros (FOG), ring laser gyros (RLG), and mechanical gyros with a high-speed rotating inner fly-wheel. It has been a big progress in MEMS technology recently to increase the capability of MEMS based ARS to be sensitive even to the Earth rate. Therefore, it is possible to find such devices on market and use them in applications, in which FOG has been previously dominant. However, FOG devices still fulfill the gap between RLG and MEMS ARS technology and still provide better solution in applications, in which a higher stability is required, higher than MEMS based ARS can provide.

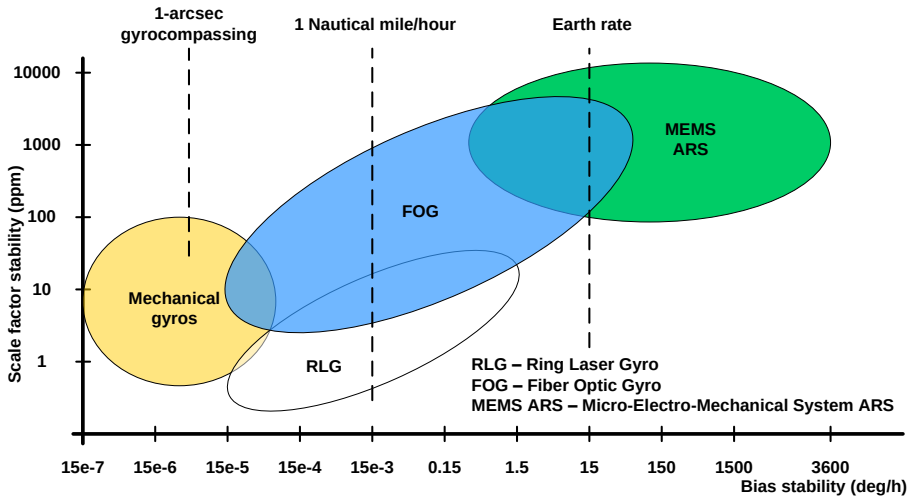

Fig. 3 – Near-term gyro technology [2.2]

A similar comparison for a current and near-term ACC technology is shown in Fig. 4. MEMS based ACC enables wide range of applications, in which requirements on resolution and precision are not so tough, e.g. high-g ACC in airbags, 1-mg resolution for stabilization purposes. It has become very popular to use quartz-resonator ACC in more accurate applications due to its costs. If higher accuracy is still required, only mechanical pendulous rebalance (servo) ACC has to be utilized.

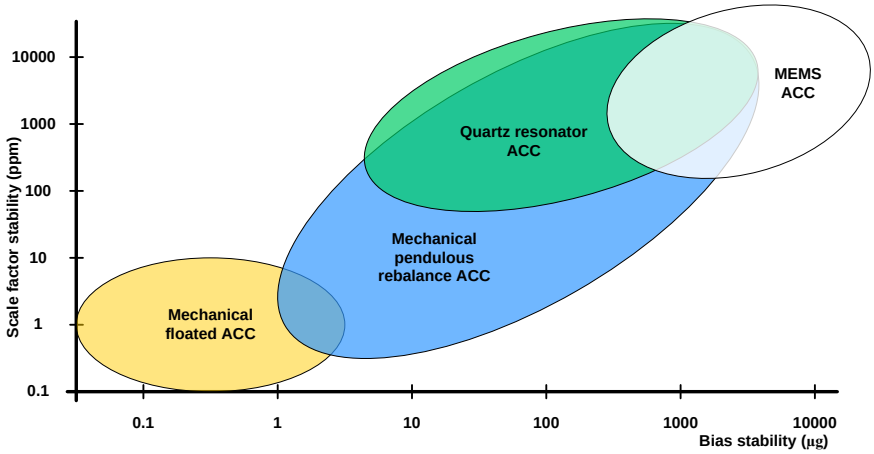

Fig. 4 - Accelerometer types and their performances [2]

In cost-effective applications MEMS based devices are preferred. Therefore, their usage has to be accompanied by modern methods of signal and data processing, algorithms for their calibration, parameters identification, and fusion. Only this can thus provide stable solution for a particular application with required accuracy.

2.2. INERTIAL SENSORS AND THEIR MEASUREMENT FRAMES

This chapter is about to introduce basic parameters and characteristics of MEMS technology based inertial sensors which fall into the applicant major interest. It aims to provide the overview of MEMS inertial sensor technology, its current stage, and difficulties which have to be dealt with.

2.2.1. GYROS/ANGULAR RATE SENSORS

Among basic parameters generally provided in product datasheets there belong a dynamic range, initial sensitivity, nonlinearity, alignment error, initial bias error, in-run bias instability, angular random walk, linear acceleration effect on bias, and rate noise density. According to these parameters there can be defined following types of gyros: low-cost, moderate-cost, and high-performance gyros. When looking at datasheets an in-run bias stability provides the information about the best sensor performance corresponding to the gyro resolution floor. Unfortunately, there are other exhibiting error factors which affect a gyro performance. In all cases a gyro noise and its frequency dependency have to be taken into account and handled. Methods for stochastic sensor parameters estimation and handling are closely described in chapters 4.2, 4.5, and 4.6. In the case of low and moderate-cost gyros scale factor, alignment error, and null bias errors accompanied by parameters variation over a temperature range highly decrease the gyro performance. To minimize their impacts it is required to perform the calibration within which a correction table or polynomial correction function is acquired. Calibration methods are dealt with in chapter 4.1.

The other perspectives of the gyro performance are produced by the fact that it does not measure just a rotational rate but also its sensitive element has linear acceleration and g^2 sensitivities. It is caused by the asymmetry of a mechanical design and/or micromachining inaccuracies and it can vary design to design. Due to Earth's 1 g field of gravity, according to [2.3], it can suffer from large errors when uncompensated. In the case of low-cost gyros the g and g^2 sensitivities are not specified because their design is not optimized for a vibration rejection. They can have g sensitivity about 0.3°/s/g. Therefore, looking at a bias instability in these cases is almost pointless due to a high effect of this vibration behavior. Higher performance gyros improve the vibration rectification by a design so the g-sensitivity goes down to 0.1°/s/g. To further decrease this sensitivity anti-vibration mounts might be applied. Nevertheless, these anti-vibration mounts are very difficult to design, because they do not have a flat response over a wide frequency range and they work particularly poorly at low frequencies. Moreover, their vibration reduction characteristics change over the temperature and life-cycle.

Analog Devices, Inc. (ADI) [2.3] introduced in 2011 new high-performance, low-power iMEMS® gyros specifically for angular rate (rotational) sensing in harsh environments. They employ differential quad-sensor technology, which rejects the influence of linear acceleration and vibration very efficiently. Therefore they offer exceptionally accurate and reliable rate sensing even when shocks and vibrations are applied. Their g-sensitivity is as low as 0.015°/s/g.

2.2.2. ACCELEROMETERS

MEMS technology based accelerometers in the navigation area measure linear acceleration mainly on a capacitive principle. Among their basic parameters there can be included a measurement range, nonlinearity, sensitivity, initial bias error, in-run bias instability, noise density, bandwidth of frequency response, alignment error, and cross-axis sensitivity. In the case of multi-axis accelerometers z-axis often has a different noise and bias performance. Unlike the gyros, accelerometers are affected by vibrations in principle and if the frequency spectrum is adequate for the application no problem arises from this point of view. A current technology of MEMS accelerometers cannot compete with high-performance types and cannot be implemented to stand-alone inertial navigation systems due to their low resolution and insufficient noise level reduction. Generally, this type of accelerometers is used in navigation systems in which GPS receiver is also implemented to compensate position errors or in attitude and heading reference systems in which the position is not required and thus accelerometers are used just for an attitude compensation done according to Earth's field 1g sensing.

2.2.3. INERTIAL MEASUREMENT FRAMES

To provide navigation in 3D it is obligatory to use at least 3 gyros for rotational rate sensing and 3 accelerometers for linear transitional motion sensing. These two triads compose an inertial measurement unit (IMU). The gyro frame and accelerometer frame generally coincide and their sensitive axes correspond to vehicle main axes as shown in Fig. 5. The framework structure is defined with respect to the international orders ISO 1151-1 and 1151-2.

Fig. 5 – Typical framework of the vehicle (left), of the measurement unit (right)

There exist modifications of IMU configuration, for instance for a gyro-free measurement unit, but this modification is suitable just for particular applications where attitude is evaluated according to accelerometers measurements and Earth field 1g sensing, which does not work properly under dynamics. It is, however, also possible to modify the framework structure and its orientation. These modifications can be applied to increase precision of acquisition data process, for details see chapters 4.3, 5.1.

2.3. DATA PROCESSING IN NAVIGATION SYSTEMS

Navigation systems are primary supposed to provide position, velocity, and attitude outcomes. These navigation data are typically estimated by a chain of processes schematically shown in Fig. 6. A detailed description of particular processes follows.

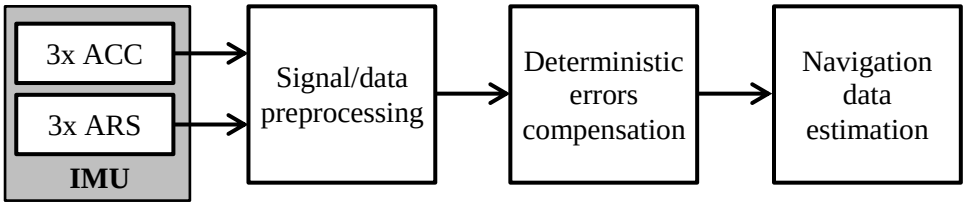

Fig. 6 – Block scheme of processes required for position, velocity, and attitude estimation
(ACC – accelerometer, ARS – angular rate sensor/gyro, IMU – inertial measurement unit)

2.3.1. SIGNAL/DATA PREPROCESSING

Signal/data preprocessing can differ according to types of sensors utilized. The sensors might have analog as well as digital outputs. In the case of analog outputs the preprocessing requires A/D conversion with an analog low-pass filter applied. The low-pass filter is then used for both high-frequency components reduction and as an anti-aliasing filter. When the outputs are in digital form then a digital low-pass filter is utilized alone. It is very important to choose a cut-off frequency correctly plus observe a group delay. Usually, the sensors' bandwidth is about 300 Hz up to 800 Hz depending on the sensors' type. If high rate navigation solution is required, which is generally intended for airborne applications, the frequency bandwidth can be reduced down to 50 or 40 Hz. In some applications it can go lower down to 20 or 10 Hz, but it is not a common case. A main

challenge is related with a spectrum and amplitude of vehicle vibrations coming from its propeller and structure. The character of vibrations is closely discussed in chapter 4.5; however, the vibration influence also drops all the way down to 1 Hz as well and can then go up to tens of Hz. Higher frequencies are not so complicated to recognize in data and treat them by low-pass filtering; nevertheless, so low frequencies cannot be distinguished in data from vehicle dynamic maneuvers. This aspect is crucial and also makes a big difference from robotic-grounded applications in which the vibration spectrum differs in principle. A proper signal/data filtering helps to reduce vibration and noise components in sensors' readings and makes easier following data processing and fusion. The easiest design of a low-pass filter is the 1st order one with its transfer function defined as

$$H(s) = \frac{y(s)}{u(s)} = \frac{1}{1+s\tau}, \tag{2.3.1}$$

where τ is a time constant, *y(s)* denotes the Laplace transform of the filter output, and *u(s)* corresponds to the input.

This kind of the filter is advantageous for its small group delay; however, its efficiency is generally low. Therefore, other types with higher orders are used; common types correspond to windowed FIR filters, for example the Bartlett window is used in ADI smart inertial sensors. Other possibilities were also studied, such as wavelet multi-resolution filter in its real-time form, for details see chapter 4.5.

2.3.2. DETERMINISTIC ERROR COMPENSATION

In the field of navigation the estimation of inertial sensor deterministic errors plays a key role. Mainly multi-axial non-orthogonalities/misalignment and scale factor errors have to be identified and estimated within a calibration process and then compensated. There exist many approaches to calibrate the sensor; however, their applicability is strongly influenced by the approach time consumption and by the equipment which is needed for the calibration purposes. These two factors mainly affect the price which is the factor all manufactures consider the most. According to required precision and price a method is determined and applied. The calibration methods differ according to used equipment with its motion frame control and measurement frame, where knowledge of the reference information is or is not required for all measured values or for their combination. Platforms with a precise measurement frame are very expensive. The more the precision is needed, the more they are expensive. More details about different calibration methods are presented in chapter 4.1.

2.3.3. NAVIGATION DATA ESTIMATION

Navigation data generally inform about position, velocity, and attitude, all defined in 3D coordinate frame. This coordinate frame can be defined with different origins and axes; however, in the navigation field according to [2.4] there are used:

- Inertial frame (I-frame),
- Earth-Centered-Earth-Fixed frame (ECEF frame),
- Navigation frame (N-frame) often corresponding to the Local-level frame,
- Body frame (B-frame) assumed to correspond to the vehicle frame,
- Sensors' frame forcing to align with the B-frame.

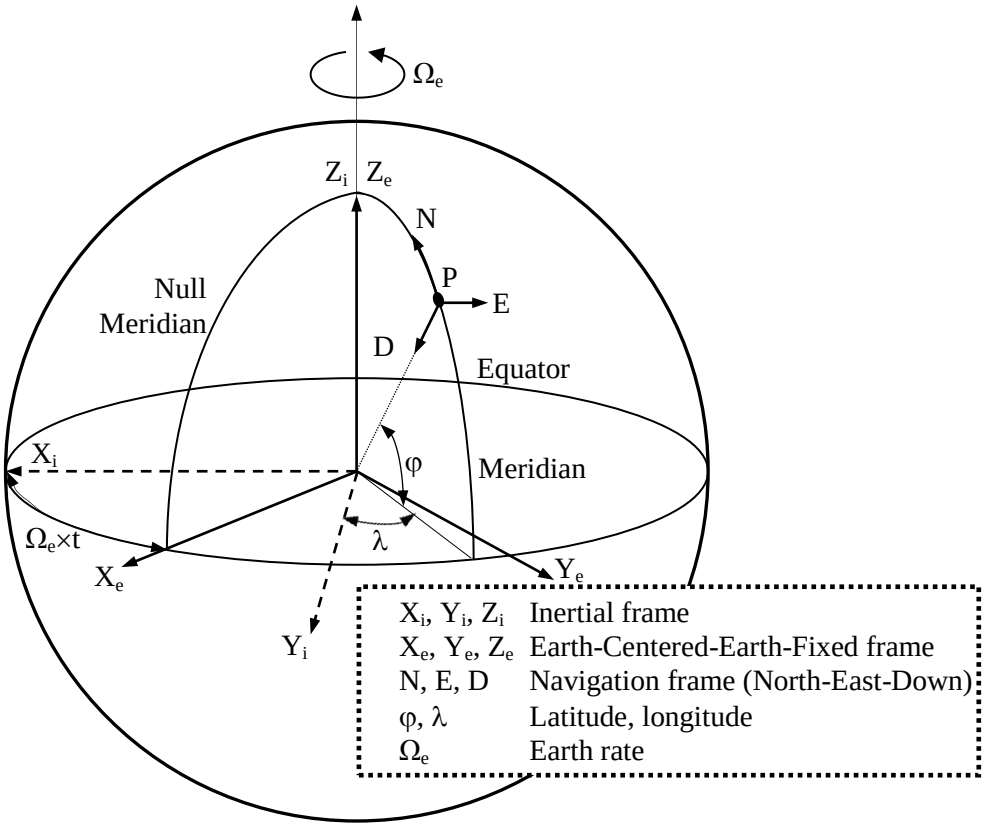

Fig. 7 – Coordinate frames overview

Navigation data are primary provided by so called inertial navigation system which is formed by a combination of an inertial measurement unit and a computer running estimation of navigation equations. This approach can be find in more details in [2.4-2.8] etc. The approach is defined as a strapdown mechanization (or INS mechanization) and is processing raw inertial sensors' data in differential equations. These equations have a form with respect to [2.8] as follows

$$\dot{\boldsymbol{v}}^n = \boldsymbol{C}_b^n \boldsymbol{a}^b + \boldsymbol{g}^n - (2\boldsymbol{\omega}_{ie}^n + \boldsymbol{\omega}_{en}^n) \times \boldsymbol{v}^n, \tag{2.3.2}$$

$$\dot{\boldsymbol{C}}_n^e = \boldsymbol{C}_n^e(\boldsymbol{\omega}_{en}^n \times), \tag{2.3.3}$$

$$\dot{h} = -v_D, \tag{2.3.4}$$

$$\dot{\boldsymbol{C}}_b^n = \boldsymbol{C}_b^n\big(\boldsymbol{\omega}_{ib}^b \times\big) - (\boldsymbol{\omega}_{in}^n \times)\boldsymbol{C}_b^n, \tag{2.3.5}$$

where low-letter indices indicate the frame (***n*** – N-frame, ***e*** – ECEF frame, ***i*** – I-frame, ***b*** – B-frame, ***en*** – N-frame with respect to ECEF, ***ie*** - ECEF frame with respect to I-frame, ***ib*** – B-frame with respect to I-frame),
upper indices define in which frame the vector is expressed,
low indices express in which frame the vector is measured or obtained
v_D corresponds to "D" component of the velocity vector $\boldsymbol{v}^n$ defined in N-frame (N, E, D),
$\boldsymbol{C}_b^n$ is a transformation matrix transforming the very next vector from B-frame to N-frame,
$\boldsymbol{a}^b$ notes a vector of accelerations measured and expressed in B-frame,
$\boldsymbol{g}^n$ is a vector of gravitational acceleration defined in N-frame,
$\boldsymbol{\omega}$ notes a vector of angular rates,
$\boldsymbol{\omega}_{in}^n = \boldsymbol{\omega}_{ie}^n + \boldsymbol{\omega}_{en}^n$.

The ECEF frame is needed for the expression of the gravity vector, vector of the Corriolis and the centrifugal force and their compensation in a data processing chain. To do so, transformations from ECEF frame to N-frame and reversely are needed. The reference ellipsoid used to approximate the Earth surface is called WGS 84 with following parameters: semi-major axis a = 6378137.0 m and

semi-minor axis b = 6356752.3 m. This reference ellipsoid is given by the radius of curvature in the prime vertical R_N and by the meridian radius of curvature R_M, which both depend on the latitude φ [2.7 p. 54] as follows

$$R_M = \frac{a(1-\varepsilon^2)}{\sqrt{(1-\varepsilon^2 sin^2(\varphi))^3}} = a\left[1+\varepsilon^2\left(\frac{2}{3}sin^2(\varphi)-1\right)\right], \tag{2.3.6}$$

$$R_N = \frac{a}{\sqrt{1-\varepsilon^2 sin^2(\varphi)}} = a\left[1+\frac{\varepsilon^2}{2}sin^2(\varphi)\right], \tag{2.3.7}$$

$$\varepsilon = \sqrt{1-\frac{b^2}{a^2}}\ . \tag{2.3.8}$$

The position vector is then defined as

$$r^e = \begin{bmatrix} (R_N+h)cos(\varphi)cos(\lambda) \\ (R_N+h)cos(\varphi)sin(\lambda) \\ (R_N(1-\varepsilon^2)+h)sin(\varphi) \end{bmatrix}, \tag{2.3.9}$$

where φ, λ, h denote latitude, longitude, and height above the surface.

For the transport rate between I-frame and ECEF frame it is needed to define

$$\omega_{ie}^e = \begin{bmatrix} 0 \\ 0 \\ \Omega_e \end{bmatrix}, \text{ where } \Omega_e = 7.2921158 \times 10^{-5}\text{rad/s}. \tag{2.3.10}$$

The proceeding of INS mechanization can be done by two-speed or single-speed approach [2.4-2.6], [8]. The two-speed approach can be comprehended as a predecessor of the single-speed approach and was used before high-computation-load computers were available. It divided the full calculation cycle into two parts with different update rates. Generally, it was caused by the fact that not all variables were not necessary to calculate with the high rate. In the case of the single-speed all is calculated with the same rate.

Equations (2.3.2-2.3.5) can be applied in the principle scheme depicted in Fig. 8. Blocks corresponding to ACC and ARS frames include compensation of sensors' frames deterministic errors, which is closely described in chapters 2.3.2, 4.1.

The INS mechanization algorithm consists of following steps running in an infinite cycle. Those steps are:

1. numerical integration,
2. velocity update,
3. position update,
4. attitude update.

A numerical integration is about to get increments of attitude angles and velocity from measured angular rates and acceleration. It comes from the continuous form [2.7] defined as

$$\Delta\boldsymbol{\theta}_k = \int_{t_{k-1}}^{t_k} \widetilde{\boldsymbol{\omega}}_{ib}^b \, dt, \quad \Delta\boldsymbol{v}_k^b = \int_{t_{k-1}}^{t_k} \widetilde{\boldsymbol{a}}^b \, dt, \tag{2.3.11}$$

where $\widetilde{\boldsymbol{\omega}}_{ib}^b$ and $\widetilde{\boldsymbol{a}}^b$ are vectors of measured angular rates and accelerations in B-frame.

To proceed a numerical integration it is sufficient according to [2.4] to apply 2nd order Runge-Kutta method defined as

$$\Delta\theta_k = \frac{1}{2}\big(\omega(t_k)+\omega(t_{k-1})\big)\Delta t, \tag{2.3.12}$$

where Δt corresponds to a difference of the time instances, which is to a sampling period.

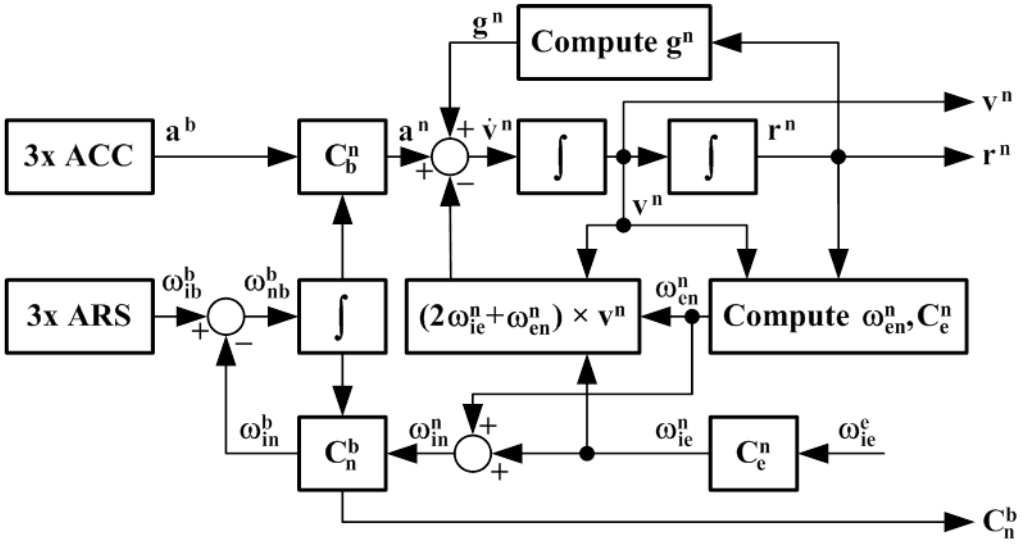

Fig. 8 – Principle scheme of the INS mechanization [2.8]

Eq. (2.3.12) can be also used for velocity increments from accelerations. Before other steps of INS mechanization are described two aspects affecting the INS precision have to be learnt. Those are:

- Coning effect (gyros): *Coning effect is the apparent drift rate caused by motion of an input axis in a manner that generally describes a cone. This usually results from a combination of oscillatory motions about the gyro principal axes. The apparent drift rate is a function of the amplitudes and frequencies of oscillations present and the phase angles between them, and is equal to the net solid angle swept out by the input axis per unit time* [2.9].
- Sculling effect (accelerometer): *Sculling effect is the apparent acceleration resulting from the combined inputs of linear vibration along one axis, and angular oscillation at the same frequency around a perpendicular axis. The magnitude of the effect depends on the amplitudes and relative phase of these inputs, and appears on the axis perpendicular to both inputs* [2.9].

After a numerical integration is processed velocity, position, and attitude updates take place. Mathematical procedure provided below is primary related to [2.5-2.7], [2.10]. The subscript *k* denotes a current time instance; other subscripts are described at (2.3.2-2.3.12). To simplify the report of equations the vectors are not marked differently; however, except Δt all is three-dimensional.

1) Velocity update

a) Approximation of the rotational and sculling motion

$$\Delta v_k^{b,k-1} = \Delta v_k^b + \frac{1}{2}\Delta\theta_k \times \Delta v_k^b + \frac{1}{12}\left(\Delta\theta_{k-1} \times \Delta v_k^b + \Delta v_{k-1}^b \times \Delta\theta_k\right). \tag{2.3.13}$$

b) Extrapolation of the height

$$h_{k-1/2} = h_{k-1} - v_{D,k-1}\Delta t/2. \tag{2.3.14}$$

c) Extrapolation of the longitude and latitude

I. Computation of the N-frame rotation vector ζ

$$\zeta_{k-1/2} = \left(\omega_{ie,k-1}^n + \omega_{en,k-1}^n\right)\Delta t/2. \tag{2.3.15}$$

II. Computation of the ECEF frame rotation vector ξ

$$\xi_{k-1/2} = \omega_{ie}^e \Delta t/2. \tag{2.3.16}$$

III. Computation of the quaternions

$$q_{n,k-1/2}^{n,k-1} = \begin{bmatrix} cos\left\|0.5\zeta_{k-1/2}\right\| \\ \frac{cos\left\|0.5\zeta_{k-1/2}\right\|}{\left\|0.5\zeta_{k-1/2}\right\|}\left\|0.5\zeta_{k-1/2}\right\| \end{bmatrix}, \tag{2.3.17}$$

$$q_{e,k-1}^{e,k-1/2} = \begin{bmatrix} cos\left\|0.5\xi_{k-1/2}\right\| \\ -\frac{cos\left\|0.5\xi_{k-1/2}\right\|}{\left\|0.5\xi_{k-1/2}\right\|}\left\|0.5\xi_{k-1/2}\right\| \end{bmatrix}, \tag{2.3.18}$$

IV. Computation of the quaternion for the N-frame extrapolation to ECEF frame

$$q_{n,k-1/2}^{e,k-1} = q_{n,k-1}^{e,k-1} * q_{n,k-1/2}^{n,k-1}, \tag{2.3.19}$$

$$q_{n,k-1/2}^{e,k-1/2} = q_{e,k-1}^{e,k-1/2} * q_{n,k-1/2}^{e,k-1} \tag{2.3.20}$$

$$C_{n,k-1/2}^{e,k-1/2} = \begin{bmatrix} (q_1^2+q_2^2-q_3^2-q_4^2) & 2(q_2q_3-q_1q_4) & 2(q_2q_4+q_1q_3) \\ 2(q_2q_3+q_1q_4) & (q_1^2-q_2^2+q_3^2-q_4^2) & 2(q_3q_4-q_1q_2) \\ 2(q_2q_4+q_1q_3) & 2(q_3q_4+q_1q_2) & (q_1^2-q_2^2-q_3^2+q_4^2) \end{bmatrix},$$

in this case $q = q_{n,k-1/2}^{e,k-1/2}$. (2.3.21)

d) Extrapolation of the velocity using the increments of velocity from measured acceleration and calculated gravity vector compensated for a Corriolis effect

$$v_{k-1/2}^n = v_{k-1}^n + \frac{1}{2}\left(\Delta v_{k-1}^n + \Delta v_{g/Cor,k-1}^n\right). \tag{2.3.22}$$

e) Update of angular rates using extrapolated latitude

$$\omega_{ie}^n = C_e^n \omega_{ie}^e = \begin{bmatrix} \Omega_e \cos(\varphi) \\ 0 \\ -\Omega_e \sin(\varphi) \end{bmatrix}, \quad \omega_{en}^n = \begin{bmatrix} v_E/(R_N+h) \\ -v_N/(R_M+h) \\ -v_E \tan(\varphi)/(R_N+h) \end{bmatrix}. \tag{2.3.23}$$

f) Re-computation of the N-frame rotation vector

$$\zeta_k = \left(\omega_{ie,k-1/2}^n + \omega_{en,k-1/2}^n\right)\Delta t. \tag{2.3.24}$$

g) Velocity update

I. Transformation of the velocity increment from B-frame to N-frame

$$\Delta v_k^n = [I - (0.5\zeta_k \times)] C_{b,k-1}^{n,k-1} \Delta v_k^{b,k-1}, \tag{2.3.25}$$

where $\left(0.5\begin{bmatrix}\zeta_1 \\ \zeta_2 \\ \zeta_3\end{bmatrix}\times\right) = 0.5\begin{bmatrix} 0 & -\zeta_3 & \zeta_2 \\ \zeta_3 & 0 & -\zeta_1 \\ -\zeta_2 & \zeta_1 & 0 \end{bmatrix}$.

II. Computation of the velocity increment caused by gravity/Corriolis vector

$$\Delta v_{g/Cor,k}^n = \left[g_{k-1/2}^n - \left(2\omega_{ie,k-1/2}^n + \omega_{en,k-1/2}^n\right) \times v_{k-1/2}^n\right]\Delta t. \tag{2.3.26}$$

III. Velocity computation by composing the velocity increments

$$v_k^n = v_{k-1}^n + \Delta v_k^n + \Delta v_{g/Cor,k}^n. \tag{2.3.27}$$

2) Position update

a) Interpolation of the true half interval velocity defined in N-frame

$$v_{k-1/2}^n = 0.5(v_{k-1}^n + v_k^n). \tag{2.3.28}$$

b) Extrapolation of the height

$$h_k = h_{k-1} - v_{D,k-1/2}\Delta t. \tag{2.3.29}$$

c) Interpolation of the longitude and latitude

I. Re-computation of the N-frame rotation vector

$$\zeta_k = \left(\omega_{ie,k-1/2}^n + \omega_{en,k-1/2}^n\right)\Delta t. \tag{2.3.30}$$

II. Re-computation of the ECEF frame rotation vector

$$\xi_k = \omega_{ie}^e \Delta t. \tag{2.3.31}$$

III. Computation of the quaternions $q_{n,k}^{n,k-1}$ and $q_{e,k-1}^{e,k}$ for the N-frame and ECEF frame using ζ_k and ξ_k and the same principle as in velocity update part.

IV. Computation of the quaternion for the N-frame extrapolation to ECEF frame

$$q_{n,k}^{e,k-1} = q_{n,k-1}^{e,k-1} * q_{n,k}^{n,k-1}, \tag{2.3.32}$$

$$q_{n,k}^{e,k} = q_{e,k-1}^{e,k} * q_{n,k}^{e,k-1}, \tag{2.3.33}$$

$$C_{n,k}^{e,k} = \begin{bmatrix} (q_1^2 + q_2^2 - q_3^2 - q_4^2) & 2(q_2q_3 - q_1q_4) & 2(q_2q_4 + q_1q_3) \\ 2(q_2q_3 + q_1q_4) & (q_1^2 - q_2^2 + q_3^2 - q_4^2) & 2(q_3q_4 - q_1q_2) \\ 2(q_2q_4 + q_1q_3) & 2(q_3q_4 + q_1q_2) & (q_1^2 - q_2^2 - q_3^2 + q_4^2) \end{bmatrix},$$

in this case $q = q_{n,k}^{e,k}$. (2.3.34)

d) Position update - in this case there exist several approaches using direct velocity integration or quaternion proceedings. The first case has a form

$$r_k^n = r_{k-1}^n + v_k^n \Delta t. \tag{2.3.35}$$

e) Update of ω_{ie}^n and ω_{en}^n goes from the change of $q_{n,k}^{e,k}$ as well as updated latitude and longitude.

3) Attitude update

1. Correction of the interpolated values of longitude and latitude

$$\begin{bmatrix} \varphi_{k-1/2} \\ \lambda_{k-1/2} \\ h_{k-1/2} \end{bmatrix} = \frac{1}{2}\left(\begin{bmatrix} \varphi_{k-1} \\ \lambda_{k-1} \\ h_{k-1} \end{bmatrix} + \begin{bmatrix} \varphi_k \\ \lambda_k \\ h_k \end{bmatrix} \right). \tag{2.3.36}$$

2. Correction of the N-frame rotation vector ζ_k using (2.3.30) with modified $\omega_{ie,k-1/2}^n$ and $\omega_{en,k-1/2}^n$ with respect to $[\varphi_{k-1/2},\ \lambda_{k-1/2},\ h_{k-1/2}]$ applied in (2.3.23).

3. Approximation of the B-frame rotation vector ϕ_k with a compensation of the coning effect

$$\phi_k = \Delta\theta_k + \frac{1}{12}\Delta\theta_{k-1} \times \Delta\theta_k. \tag{2.3.37}$$

4. Attitude update

$$q_{b,k}^{b,k-1} = \begin{bmatrix} cos\|0.5\phi_k\| \\ \frac{cos\|0.5\phi_k\|}{\|0.5\phi_k\|}\|0.5\phi_k\| \end{bmatrix}, \tag{2.3.38}$$

$$q_{n,k-1}^{n,k} = \begin{bmatrix} cos\|0.5\zeta_k\| \\ -\frac{cos\|0.5\zeta_k\|}{\|0.5\zeta_k\|}\|0.5\zeta_k\| \end{bmatrix}, \tag{2.3.39}$$

$$q_{b,k}^{n,k-1} = q_{b,k-1}^{n,k-1} * q_{b,k}^{b,k-1}, \tag{2.3.40}$$

$$q_{b,k}^{n,k} = q_{n,k-1}^{n,k} * q_{b,k}^{n,k-1}. \tag{2.3.41}$$

The quaternion $q_{b,k}^{n,k}$ contains the information about actual Euler angles and also is used to calculate an actual form of the transformation matrix $C_{b,k}^{n,k}$.

INS mechanization has been known for a long time and has been verified in many applications. However, it still works with just raw inertial data passed through a low-pass filter and extracted from deterministic sensors' errors. To further improve the performance and precision of the navigation solution there is commonly used a Kalman filter fusing results of INS mechanization with aiding systems. These aiding systems can vary based on a particular application having a different form and can use variable integration scheme as presented in chapter 4.6.

The Kalman filtering (KF) will not be described further in details in this thesis because the first mention about the KF was referred by Rudolf E. Kálmán in 1960 and since that time this filtering has become an approach widely used for data processing and fusion. Details can be found for example in [2.7], [2.11], chapter 4.6 and in many other publications. The KF originally was aimed for linear systems; nevertheless, it has been modified for non-linear solutions as well. It has many modifications which use different approaches to solve and optimize mathematical equations and their calculation load in a data process performed in the KF cycle. Another extension of the KF is an unscented Kalman filter and a particle filter. These filters are often used for highly non-linear solutions and are highly computation loaded. Nevertheless, these types of the filters are not often used in real-time navigation. The KF implementation has also several forms depended on its coupling. It can be operated in loosely-coupled, tightly-coupled, or ultra-tightly-coupled as well as in centralized or decentralized scheme; details can be found in [2.10], [2.12]. Other modifications of the scheme can go from the close-loop or open-loop integration design. The choice of a particular design depends always on a designer and the application.

Other possibility for the inertial data processing is the utilization of complementary filters. Their structure and design go from analogue regulation circuits as shown in Fig. 9. The feedback is provided by proportional and integral controllers with their gains K_I and K_P. A practical application can be found in chapter 4.6. According to the scheme from Fig. 9 the estimated angles $\hat{\phi}_c$ is defined in Laplace form as follows [2.13]

$$\hat{\phi}_c = \frac{1}{s}\dot{\phi} + \frac{K_P}{s}\Delta + \frac{K_I}{s^2}\Delta, \tag{2.3.42}$$

where $\Delta = \hat{\phi}_c - \hat{\phi}_{acc}$.

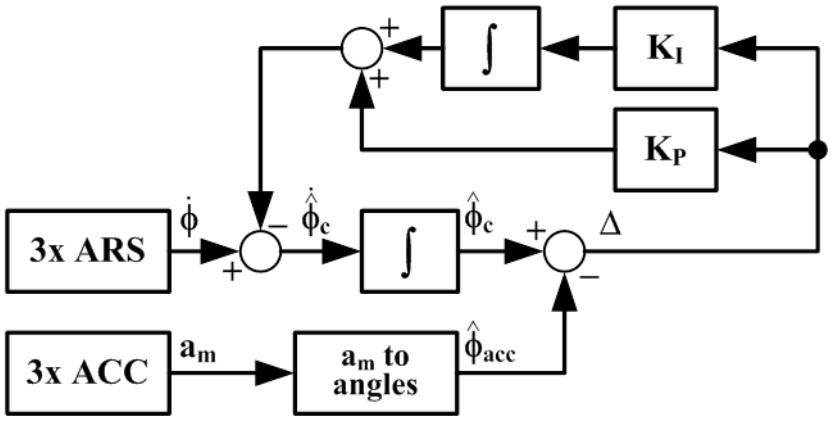

Fig. 9 – Principle scheme of a complementary filter [2.13]

2.4. INERTIAL SENSORS AND THEIR PARAMETERS ESTIMATION

In the case of stochastic errors estimation and modeling there also exist various methods using for example PSD (Power Spectral Density) and ACF (Auto Correlation Function) which are straightforward; however, these methods cannot clearly distinguish different characters of noise error sources inside the data without understanding of a sensor model and its state-space representation [2.14]. Unlikely, Allan VARiance analysis (AVAR) is a time-domain approach to analyze time series of data from noise terms point of view. The AVAR was introduced by D. W. Allan in 1966 in [2.15]. Originally it was oriented at the study of oscillator stability; however, after its first publication this kind of analysis was adopted for general noisy data characterization. Because of the close analogies to inertial sensors the AVAR has been also included in IEEE Standard [2.16-2.18] and that is the reason why AVAR became a standard tool for inertial sensors' noise analyzing. As described in [2.19] the AVAR technique provides several significant advantages over the others. Traditional approaches, such as computing the sampled mean and variance from a measured data set, do not reveal the underlying error sources. Although the combined PSD/ACF approach provides a complete description of error sources, the results are difficult to interpret [2.20].

The AVAR estimates the variance of averaged data in a cluster of a certain length, which is defined by interval τ, moving through the whole data set. The AVAR characterizes Allan deviation that can vary based on the cluster length τ and analyzed data set y. A basic equation can be defined as [2.21]

$$\sigma_y^2 = f(\tau, y) \tag{2.4.1}$$

The AVAR has some modifications and based on the shift of clusters in the data set and corresponding AVAR calculations (for details see [2.21]) it is possible to distinguish three basic types of AVAR: non-overlapped (original), overlapped, and modified. There also exists another type called dynamic AVAR, for details see [2.22-2.23]. The original non-overlapped AVAR is defined as [2.21]

$$\sigma_y^2(\tau) = \frac{1}{2(M-1)} \sum_{i=1}^{M-1} \left(\bar{y}_{i+1} - \bar{y}_i\right) \tag{2.4.2}$$

where M – the number of clusters in the data set, $M=floor(N/m)$, N – the total number of samples in the data set, m – the number of samples in the cluster, τ – the time length of the cluster, $\boldsymbol{\tau = m \times T_s}$, $\boldsymbol{T_s}$– the sampling period, $\boldsymbol{\bar{y}_i, \bar{y}_{i+1}}$ – mean values of certain cluster corresponding to $\boldsymbol{i}$ and $i+1$ cluster.

In cases of short intervals τ there is a large number of used clusters which leads to small errors in estimation and large confidence. On the contrary, a small number of clusters in case of long τ leads to large errors in estimation and small confidence. The usage of the overlapped AVAR improves the confidence of the result estimate and its stability mainly in cases of long clusters where M comes close to value 2. However, the applicability and suitability of the overlapped AVAR for long data sets are questionable mainly for its high computational load. The confidence of the AVAR result corresponds to the estimate error defined as [2.14]:

$$\boldsymbol{\delta_\sigma(\tau) = \frac{1}{\sqrt{2\left(\frac{N}{m}-1\right)}}} \tag{2.4.3}$$

where all variables are denoted at (2.4.2).

The AVAR and its results are related to seven noise terms, whose typical performance can be seen in Fig. 10, that can be identified in inertial sensors output and whose estimation can lead to errors suppression in the data [2.18], [2.24]. The five basic noise terms correspond to the following random processes: angle/velocity random walk, rate/acceleration random walk, bias instability, quantization noise, and drift rate ramp. Furthermore, this basic set of random processes is extended by the sinusoidal noise and exponentially correlated (Markov) noise [2.24]. In most cases different noise processes appear in different length of time interval τ with different slopes or shapes. Due to this aspect long data set should be measured to be capable to cover all noise terms presented in it. It can be assumed that if the existing random processes are all statistically independent then AVAR allows easy identification of various random processes based on their influences within the time interval τ. Generally, the total error can be classified as a sum of individual independent noise errors [2.18] and the total variance can be expressed as:

$$\sigma_{total}^2 = \sigma_Q^2 + \sigma_{ARW}^2 + \sigma_{BIN}^2 + \sigma_{RRW}^2 + \sigma_{RR}^2 \tag{2.4.4}$$

where all abbreviations correspond to Table 1.

Type of the noise	Abb.	Curve slope	Value of the coefficients
Quantization noise	Q	-1	$Q = \sigma(\sqrt{3})$
Angular/velocity random walk	ARW	-1/2	$N = \sigma(1)$
Flicker noise/bias instability	BIN	0	$B = \sigma_{min}/0.664$
Rate/acceleration random walk	RRW	+1/2	$K = \sigma(3)$
Rate ramp noise	RR	+1	$R = \sigma(\sqrt{2})$

Table 1 - Summary of error sources and their characterization

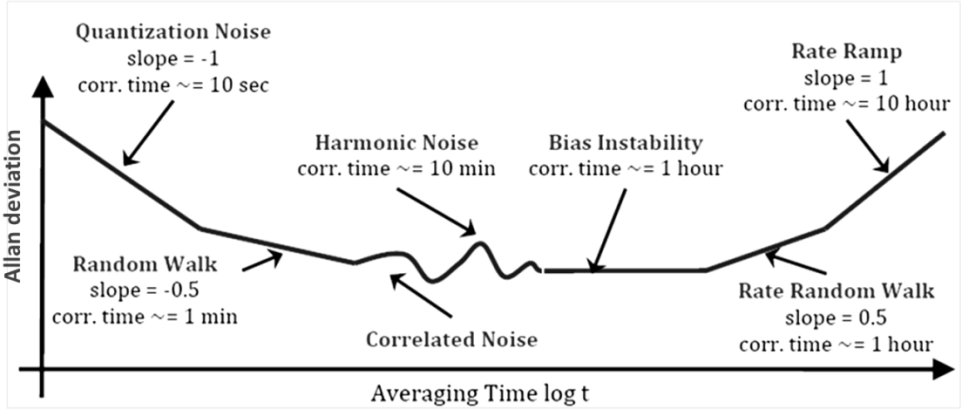

Fig. 10 - Allan variance/deviation plot [2.18].

In guidance and navigation applications the integrated velocities and integrated angles are also often used as observables instead of accelerations and angular rates. Therefore, when a quantization noise can be characterized by a white noise in integrated observables [2.16], it can be done the same way in measured accelerations and angular rates. A white noise can also be applied for the angular/velocity random walk modeling in measured quantities due its random walk effect in integrated observables [2.14]. Furthermore, the rest of the noise sources have to be considered and included in the model if their influences are not negligible and their shapes are visible in a log-log Allan deviation plot. For this kind of analysis long data (more than 1 hour) should be preferred. Basic mathematical description for the error sources are stated in Table 2.

Types of error source	Basis for the model	Mathematical description
Q + ARW	white noise	–
BIN	1st order Gauss-Markov process	$\dot{e}(t) + \beta e(t) = \beta B w(t)$
RRW	random walk	$\dot{e}(t) = K w(t)$
RR	2nd order Gauss-Markov process	$\ddot{e}(t) + \sqrt{2}\omega_0 \dot{e}(t) + \omega_0^2 e(t) = R w(t)$

Table 2 - Model definitions of five basic noise error sources,
(β represents a correlation time, B&K correspond to the noise terms estimated from AVAR, w is a white noise)

Based on (4) the total error of terms needed for modeling can be expressed as [2.25]:

$$e_{total} = e_{BIN} + e_{RRW} + e_{RR} \tag{2.4.5}$$

Individual models based on Table 2 can be defined with differential operator as:

$$e_{BIN} = \frac{\beta B w}{D+\beta}, \quad e_{RRW} = \frac{K w}{D}, e_{RR} = \frac{R w}{D^2+\sqrt{2}\omega_0 D+\omega_0^2} \tag{2.4.6}$$

The substitution of (2.4.6) in (2.4.5) gives

$$e_{total} = \frac{\beta B w}{D+\beta} + \frac{K w}{D} + \frac{R w}{D^2+\sqrt{2}\omega_0 D+\omega_0^2} \tag{2.4.7}$$

By rearranging (2.4.7) it leads to

$$D(D+\beta)\left(D^2+\sqrt{2}\omega_0 D+\omega_0^2\right)e_{total} = \tag{2.4.8}$$
$$= K(D+\beta)\left(D^2+\sqrt{2}\omega_0 D+\omega_0^2\right)w + \beta B D\left(D^2+\sqrt{2}\omega_0 D+\omega_0^2\right)w + R D(D+\beta)w$$

Eq. (2.4.8) can be also expressed in a general form

$$a_4 e^{(4)} + a_3 e^{(3)} + a_2 e^{(2)} + a_1 e = b_3 w^{(3)} + b_2 w^{(2)} + b_1 w + b_0, \tag{2.4.9}$$

which leads to coefficients definition as

$$a_4 = 1;\ a_3 = \sqrt{2}\omega_0 + \beta;\ a_2 = \sqrt{2}\omega_0\beta + \omega_0^2;\ a_1 = \beta\omega_0^2 \tag{2.4.10}$$

$b_3 = K + \beta B;\ \ b_2 = \sqrt{2}\omega_0(K + \beta B) + \beta K + R;\ b_1 = \sqrt{2}\omega_0\beta K + \omega_0^2(K + \beta B) + \beta R;\ \ b_0 = \omega_0^2\beta K$

In majority cases AVAR plot includes only RRW and BIN parts, so (2.4.7) has a form

$$e_{total} = \frac{\beta B w}{D+\beta} + \frac{K w}{D} \ |_{\mathrm{RR}\,=\,0,} \tag{2.4.11}$$

Subsequently rearranging (2.4.11) differential equation can be constructed as

$$D^2 e_{total} + \beta D e_{total} = (K + \beta B) D w + K\beta w; \tag{2.4.12}$$

and its state space model in continuous domain and one channel has a form as

$$\begin{aligned} \dot{x} &= \begin{bmatrix} 0 & 0 \\ 1 & -\beta \end{bmatrix} x + \begin{bmatrix} b_1 \\ b_2 \end{bmatrix} w = \begin{bmatrix} 0 & 0 \\ 1 & -\beta \end{bmatrix} x + \begin{bmatrix} K + \beta B \\ K\beta \end{bmatrix} w. \\ y &= [0 \quad 1] x \end{aligned} \tag{2.4.13}$$

Eq. (2.4.13) can be rewrite into the form of a discrete state space model as

$$\begin{aligned} x_{k+1} &= \begin{bmatrix} 1 & 0 \\ T_s & 1 - \beta T_s \end{bmatrix} x_k, \\ y_k &= [0 \quad 1] x_k, \end{aligned} \tag{2.4.14}$$

where T_s is a sampling period.

Covariance matrix of the discrete model Q_d can then be in form

$$Q_d \approx Q T_s = \begin{bmatrix} b_1^2 & b_1 b_2 \\ b_1 b_2 & b_2^2 \end{bmatrix} T_s = \begin{bmatrix} (K + \beta B)^2 & \beta K (K + \beta B) \\ \beta K (K + \beta B) & \beta^2 K^2 \end{bmatrix} T_s \tag{2.4.15}$$

where Q represents covariance matrix of the continuous model.

To design and develop a perfect model for each sensor to cover as many sources of errors as possible is one side of the modeling problem. The AVAR can analyze and evaluate a part of it from the noise point of view when long data under static conditions are available. For this case more than 5 hours of the observation is sufficient; however, more than 10 hours is recommended. The other part comes from the deterministic parameter estimation within which random behavior of the sensor has to be considered as well. Example of the single ACC model equation can be found in [2.16 p. 192]. It is rather complicated to cover all errors because special calibration equipment should be used. Even when the sensor was calibrated and its model evaluated, it would be also complicated to implement it. In all cases the model observability and stability should be assured and it addresses the main problem. Therefore, involving smaller number of errors into the model generally is preferred. The model is then called sub-optimal and often it provides the only solution of the observability and stability problem. Nevertheless, in the case of MEMS based navigation means so deep modeling seems faint. When noise perspectives are the only concern, it is commonly enough to include only white noise and exponentially correlated noise or just one of them, because of the aiding systems presence. The model should treat the noise just in the time range corresponding to a time interval when no data from the aiding system are available. That leads to the time range about 1 to 3 minutes, no more. For each sensor this range can be estimated based on the evaluated AVAR plot.

The simplification of the model provides another advantage in a reduction of a computation load. As all aspects for modeling are considered it is clear that sub-optimal solution in a MEMS based application is rather optimal from the implementation point of view.

2.5. REFERENCES

[2.1] Barbour Neil M. Inertial Navigation Sensors – NATO. USA: Charles Stark Draper Laboratory, Cambridge, RTO-EN-SET-116(2011)
[2.2] Schmidt George T. INS/GPS Technology Trends - NATO. USA: Massachusetts Institute of Technology, Lexington, RTO-EN-SET-116(2011)
[2.3] Analog Devices, Inc. web pages www.analog.com
[2.4] Salychev, O. Applied Inertial Navigation:Problems and Solutions. ISBN 5-7038-2395-1 : Bauman MSTU Press, 2004.
[2.5] Savage, P. G. Strapdown Inertial Navigation Integration Algorithm Design Part 1: Attitude Algorithms. Journal of Guidance, Control, and Dynamics. 1998, Vol. 21, No.1, pp. 19 - 28.
[2.6] Savage, P. G. Strapdown Inertial Navigation Integration Algorithm Design Part 2: Velocity and Position Algorithms. Journal of Guidance, Control, an Dynamics. 1998, Vol. 21, No. 2, pp. 208 - 221.
[2.7] Titterton, D. H. and Weston, J. L. Strapdown Inertial Navigation Technology. Lavenham, UK : The Lavenham Press ltd, 1997. ISBN 0 86341 260 2.
[2.8] Shin, E-H. Estimation Techniques for Low-Cost Inertial Navigation. PhD Thesis. Calgary, Canada: Department of Geomatics Engineering, University of Calgary, 2005. Vol. UCGE Reports Number 20219.
[2.9] IEEE Std. 528-2001, *IEEE Standard for Inertial Sensor Terminology.* [PDF] New York : IEEE Aerospace and Electronic Systems Society, 29 November 2001. ISBN 0-7381-3022-2 SS94961.
[2.10] Reinštein, M. - Draxler, K. (supervisor): Use of Adaptive Filtering Methods in Inertial Navigation Systems. [PhD Thesis]. Praha: České vysoké učení technické v Praze, 2011. 140 p.
[2.11] Grewal, M. S. and Andrews, A. P. Kalman Filtering - Theory and Practice using Matlab. New York: Wiley-Interscience, 2001.
[2.12] Abdel-Hamid, W. Accuracy Enhancement of Integrated MEMS-IMU/GPS Systems for Land Vehicular Navigation Applications. PhD Thesis. Calgary, Canada : Department of Geomatics Engineering, University of Calgary, 2005. Vol. UCEG Reports Number 20207.
[2.13] Tae Suk Yoo et al. Gain-Scheduled Complementary Filter Design for a MEMS Based Attitude and Heading Reference System, Sensors 2011, 11(4), 3816-3830; doi:10.3390/s110403816
[2.14] El-Sheimy, N., Hou, H. and Niu, X. (2008) 'Analysis and Modeling of Inertial Sensors Using Allan Variance', *IEEE Transactions on Instrumentation and Measurement*, vol. 57, No. 1, January, pp. 140-149, Available: 0018-9456.
[2.15] Allan, D.W. (1966) 'Statistics of Atomic Frequency Standards', *Proceedings of the IEEE*, vol. 2, no. 54, February, pp. 221-230.
[2.16] 'IEEE Std. 1293', *IEEE Standard Specification Format Guide and Test Procedure for Linear Single-Axis, Nongyroscopic Accelerometers*, Available: ISBN 0-7381-1430-8 SS94679.
[2.17] 'IEEE Std. 528', *IEEE Standard for Inertial Sensor Terminology*, Available: ISBN 0-7381-3022-2.
[2.18] 'IEEE Std. 647', *IEEE Standard Specification Format Guide and Test Procedure for Single-Axis Laser Gyros*, pp. 68-80.
[2.19] Lawrence, C.N. (1993) 'On The Application of Allan Variance Method for Ring Laser Gyro Performance Characterization.', Available: UCRL-ID-115695.
[2.20] Reinstein M., Sipos M., Rohac J., Error Analyses of Attitude and Heading Reference Systems, Przeglad Elektrotechniczny, 85 (2009), No. 8, 114-118
[2.21] Riley, W.J. (2007) Handbook of Frequency Stability Analysis, Hamilton Technical Services.
[2.22] Galleani L., Tavella P.: The Dynamic Allan Variance, "IEEE Transaction on Ultrasonics, Ferroelectrics, and Frequency Control", vol. 56, no. 3, March 2009
[2.23] Galleani L.: The Dynamic Allan Variance II: A Fast Computational Algorithm, "IEEE Transaction on Ultrasonics, Ferroelectrics, and Frequency Control", vol. 57, no. 1, January 2010
[2.24] Sotak, M. (2009) 'Determining Stochastic Parameters Using an Unified Method', vol. 9, no. 2, pp. 59-63, Available: ISSN 1335-8243.
[2.25] Han S., et al: Using Allan Variance to Determine the Calibration Model of Inertial Sensors for GPS/INS Integration, "6th Symposium on Mobile Mapping Technology", Brazil 2009

3. FIELDS OF THE APPLICANT INTEREST IN AREAS OF NAVIGATION SYSTEMS

A main applicant interest aims at applications of MEMS based inertial sensors to provide navigation data. It is caused by the fact that high performance sensors, such as ring laser gyros and servo-accelerometers, are not commonly available due to their price as well as these sensors implementation changes the character of a final application. The applicant's interest is mainly put to technology applicable in light or small aircrafts or unmanned aerial vehicles. When these applications are considered many challenges in signal/data processing and data validation occur. Even though the processing of the navigation equation is theoretically well-known, it is a big challenge to implement and verify a full navigation equation and observe its long-distance behavior. However, the core of the applicant activities is in a local-matter applications in which a simplified navigation equation is more suitable. It goes from a character and time range of the navigation solution in which under these circumstances particular aspects can be considered negligible, e.g. Corriolis effect. As MEMS based sensors are cheaper and thus more suitable for a wider range of applications, it has to be considered that this kind of navigation unit is not generally stand-alone. Thus the utilization of aiding systems, such as GPS receiver, tilt sensors, magnetometers, distance sensors etc., has to take place. Even if aiding systems are implemented, inertial sensors should play a primary role. Therefore, one of main applicant activities is aimed at increasing the sensitivity and signal to noise ratio of sensors by increasing their numbers and by the modification of their sensitive axes. It is followed by a study of measuring unit calibration procedures and special data treatment by data validation, preprocessing and fusion.

A following part formed by chapters 4 and 5 provides the overview of the applicant activities and work which have been done. Chapter 4 summarizes theory and practical considerations accompanied by results in selected published papers. Chapter 5 informs about other resent activities which have not been published yet.

3.1. THE APPLICANT CONTRIBUTION

The applicant has aimed primary at MEMS based navigation system design so his main contribution can be summarized and structured in the following areas and points:

a) estimation of deterministic sensor parameters and calibration procedures

- The selected paper
  Šipoš, M. - Pačes, P. - Roháč, J. - Nováček, P.: Analyses of Triaxial Accelerometer Calibration Algorithms. IEEE Sensors Journal. 2012, vol. 12, no. 5, p. 1157-1165. ISSN 1530-437X. (IF: 1.520),
  presented in chapter 4.1, provides the overview about different up-to-date approaches to calibration processes, parameters identification, and consecutive sensor error compensation. It is accompanied by a proposal of new approaches to a calibration procedure; it analyzes and compares them in various manners.
- Other applicant papers concerning this area are listed in chapter 3.4 in [3.1 – 3.6].

b) estimation of the stochastic sensor parameter and modeling

- The selected paper
  Roháč, J. - Šipoš, M. - Šimánek, J. - Tereň, O.: Inertial Reference Unit in a Directional Gyro Mode of Operation. In IEEE SENSORS 2012 - Proceedings [CD-ROM]. Piscataway: IEEE Service Center , 2012, p. 1356-1359. ISBN 978-1-4577-1765-9. (IF: --),
  presented in chapter 4.2, deals with a design of an inertial reference unit in which AVAR was used for analyses of sensors' noise parameters. It was supplemented by another signal processing methods, calibration, models for data fusion, and the system verification.
- Other applicant papers concerning this area are listed in chapter 3.4 in [3.7 – 3.8].

c) measurement frames modification

- The selected paper
  Roháč, J.: Accelerometers and an Aircraft Attitude Evaluation. In IEEE Sensors 2005 – The 4-th IEEE Conference on Sensors [CD-ROM]. Irvine, CA: IEEE Sensors, 2005, p. 784-788. ISBN 0-7803-9057-1. (IF: --),
  presented in chapter 4.3, is the original paper about the ACC measurement frame modifications and their advantages against a usual configuration.
- Other applicant papers concerning this area are listed in chapter 3.4 in [3.9 – 3.11].

d) navigation data evaluation and their fusion

- The selected paper
  Reinštein, M. - Roháč, J. - Šipoš, M.: Algorithms for Heading Determination using Inertial Sensors. Przeglad Elektrotechniczny. 2010, vol. 86, no. 9, p. 243-246. ISSN 0033-2097. (IF: 0.244),
  presented in chapter 4.4, provides the way of data evaluation and addresses the advantages of data fusion in navigation systems. It presents the model of data fusion and its application in the Kalman filter.
- Other applicant papers concerning this area are listed in chapter 3.4 in [3.12 – 3.21].

e) data pre-processing and validation

- The selected paper
  Roháč, J. - Ďaďo, S.: Environmental Vibration Impact on Inertial Sensors' Output. In: Sensors & Transducers. 2012, In Press. ISSN 1726-5479. (IF: --),
  presented in chapter 4.5, proposes a solution for data pre-processing in harsh-environment conditions when aircraft vibrations affect the data in a wide frequency range. There was proposed a real-time application of the wavelet multi-resolution denoising approach.
- Other applicant papers concerning this area are listed in chapter 3.4 in [3.22 – 3.25].

f) aiding systems and their integration

- The selected paper
  Roháč, J. - Šipoš, M.: Sensors and Data Processing Methods Used in Navigation Systems. In Proceedings of the International Scientific Conference Modern Safety Technologies in Transportation. Košice: SUPREMA Ltd., 2011, p. 342-348. ISBN 978-80-970772-0-4. (IF: --),
  presented in chapter 4.6, makes the overview of aiding systems possible to be implemented in navigation systems of UAVs. Furthermore, it deals with and compares several possible methods suitable for data fusion and processing.
- Other applicant papers concerning this area are listed in chapter 3.4 in [3.26 – 3.38].

g) implementation of navigation means in non-aerial applications

- The selected paper
  Nováček, P. - Roháč, J. - Ripka, P.: Complex Markers for a Mine Detector. IEEE Transactions on Magnetics. 2012, vol. 48, no. 4, p. 1489-1492. ISSN 0018-9464. (IF: 1.363),
  presented in chapter 4.7, informs about other possible applications for navigation systems, particularly in this case it was in the system of a hand-held mine detector whose head positioning was required. The paper proposes an alternative solution suitable for aiding.
- Other applicant papers concerning this area are listed in chapter 3.4 in [3.39 – 3.41].

h) aerospace related topics

- Other applicant papers concerning none of above mentioned areas are listed in chapter 3.4 in [3.42 – 3.47].

The applicant is also one of authors of the book "Inertial Systems Navigation" pressed in 2006 (ISBN 80-969619-9-3). The book is written in Slovak language, so it cannot be found in international databases. Nevertheless, it was meant to be a handbook introducing the area of inertial navigation systems with their sensors, data acquisition and evaluation methodology. It is the only recent book about this topic written in Slovak or Czech with this wide range of cover. Moreover, he is a coauthor of the book "Aircraft Maintenance Technician" pressed by CERM in 2006. The handbook is determined for aircraft technicians and provides the overview of current aircraft systems.

3.2. List of Research Projects

1. 2012-2014 Technology Agency of the Czech Republic - grant No. TA02011092 "Research and development of technologies for radiolocation mapping and navigation systems"
2. 2012-2015 Ministry of the Interior of the Czech Republic - grant No. VG2VS/243 "Two survey points range-finding system utilization for perimeter security"
3. 2010-2012 Grant Agency of the Czech Technical University in Prague - grant No. SGS10/288/OHK3/3T/13 "Modular system for precise attitude and position estimation".

3.3. OVERVIEW OF SENSORS STUDIED AND APPLIED

As was previously mentioned a target kind of inertial sensors belongs to the group of cost-effective ones and thus MEMS based sensors have been generally used in the research. However, lately the applicant has started dealing with a fiber optic gyro and quartz accelerometers.

In the applicant research there has been studied a behavior of the following sensors or multi-axis measurement units:

- ADIS16355, ADIS16405 are IMU units consisting of 3-axis ACC and 3-axis ARS from Analog Devices, Inc. In the case of ADIS16405 the composition is supplemented by 3-axis magnetometer, which we did not use for its strong dependency on surrounding environment.
- AHRS M3, 3DM-GX2 units are Attitude and Heading Reference Systems also evaluating all three Euler angles. The units include all sensors as was mentioned at ADIS16405. Nevertheless, in this case we used only sensors raw data. The manufacturer is Innalabs International, and MicroStrain respectively.
- CLX02LF3 is a 3-axis ACC from the Crossbow manufacturer.
- ADIS16136 is a single axis tactical grade gyro from Analog Devices, Inc.
- *DSP-3100 is a single axis fiber optic gyro from the KVH manufacturer.*
- *INN-204 is a single axis accelerometer from the Innalabs manufacturer.*

3.4. REFERENCES

[3.1] Roháč, J.: Calibration of an Artificial Horizon Unit. In Nové trendy rozvoja letectva - Zborník 7. medzinárodnej vedeckej konferencie [CD-ROM]. Košice: Slovenský letecký inštitút a. s., 2006, ISBN 80-8073-520-4. (in Czech).

[3.2] Roháč, J.: Calibration and Its Effect on Precision of a Low-Cost Artificial Unit. In ICIT 2006 International Conference on Industrial Technology [CD-ROM]. Kolkata: Cygnus Advertising, 2006, p. 1777-1781. ISBN 1-4244-0726-5.

[3.3] Šipoš, M. - Reinštein, M. - Roháč, J.: Levenberg-Marquardt Algorithm for Accelerometers Calibration. In Sborník z 8. mezinárodní vědecké konference Měření, diagnostika a spolehlivost palubních soustav letadel. Brno: Univerzita obrany, Fakulta vojenských technologií, 2008, p. 39-45. ISBN 978-80-7231-555-0.

[3.4] Šipoš, M. - Roháč, J.: Calibration of Tri-axial Angular Rate Sensors. In MDS - Měření, diagnostika, spolehlivost palubních soustav letadel 2010. Brno: Univerzita obrany, 2010, p. 148-152. ISBN 978-80-7231-741-7.

[3.5] Šipoš, M. - Roháč, J. - Nováček, P.: Improvement of Electronic Compass Accuracy Based on Magnetometer and Accelerometer Calibration. Acta Physica Polonica A. 2012, vol. 121, no. 4, p. 945-949. ISSN 0587-4246.

[3.6] Šipoš, M. - Roháč, J.: Improvement of Electronic Compass Accuracy Based on Magnetometer and Accelerometer Calibration. In SPM 2011 - X Symposium of Magnetic Measurements. Czestochowa Branch: Polish Society of Theoretical and Applied Electrical Engineering, 2011, p. 33.

[3.7] Reinštein, M. - Roháč, J.: Modelling and Evaluation of Inertial Sensors. In MDS - Měření, diagnostika, spolehlivost palubních soustav letadel - 7. mezinárodní vědecká konference. Brno: Univerzita obrany, Fakulta vojenských technologií, 2007, p. 97-105. ISBN 978-80-7231-281-8.

[3.8] Roháč, J. - Šipoš, M.: Practical Usage of Allan Variance in Inertial Sensor Parameters Estimation and Modeling. In New Trends in Civil Aviation 2011. Praha: ČVUT v Praze a OSL ČR, 2011, p. 107-112. ISBN 978-80-01-04893-1

[3.9] Roháč, J.: Accelerometers and their Usage in an Aircraft Attitude Evaluation . In Applied Electronics 2005 - International Conference Pilsen. Pilsen: University of West Bohemia, 2005, p. 285-288. ISBN 80-7043-369-8.

[3.10] Roháč, J.: Artificial Horizon with a Modified Low-Cost IMU. In The Navigation Conference and Exhibition ARE WE THERE NOW? [CD-ROM]. London: Royal Institute of Navigation, 2007, p. 1-16.

[3.11] Roháč, J. - Šipoš, M.: Measurement Unit of an Artificial Horizon. Užitný vzor Úřad průmyslového vlastnictví, 23268. 2012-01-16.

[3.12] Roháč, J.: Low-Cost System of an Artificial Horizon. In MOSATT 2005 - Modern Safety Technologies in Transportation. Košice: Slovak Transport Society at the Slovak Academy of Sciences, 2005, p. 343-347. ISBN 80-969106-1-2.

[3.13] Roháč, J.: Accelerometers and their Usage in Angular Rate Evaluation. In MDS palubních soustav letadel - 6. odborný seminář. Brno: Univerzita obrany, Fakulta vojenských technologií, 2006, s. 8-12. ISBN 80-7231-155-7. (in Czech).

[3.14] Reinštein, M. - Roháč, J.: System for Verification of Adaptive Algorithms Enhancing the Precision of Low Cost Inertial Sensors. In MOSATT 2007, Proceedings of the International Scientific Conference "Modern Safety Technologies in Transportation". Košice: Slovak Transport Society at the Slovak Academy of Sciences, 2007, p. 224-230. ISBN 978-80-969760-2-7.

[3.15] Roháč, J.: Primary Sensors Used in Navigation. In Integrácia navigačných systémov. Košice: Bréda Róbert, 2006, s. 85-130. ISBN 80-969619-9-3. (in Slovak).

[3.16] Reinštein, M. - Pačes, P. - Roháč, J. - Šipoš, M.: Advanced Implementations Techniques in Kalman Filtering. In 2008 PEGASUS-AIAA Student Conference [CD-ROM]. Prague: Czech Technical University, 2008,

[3.17] Roháč, J. - Reinštein, M.: New Trends in Angular Rate Sensing and Attitude Evaluation. In Nové trendy v civilním letectví. Praha: ČVUT, Fakulta dopravní, 2008, p. 155-161. ISBN 978-80-7204-604-1.

[3.18] Reinštein, M. - Šipoš, M. - Roháč, J.: Error Analyses of Attitude and Heading Reference Systems. Przeglad Elektrotechniczny. 2009, vol. 85, no. 8, p. 114-118. ISSN 0033-2097.

[3.19] Reinštein, M. - Roháč, J. - Šipoš, M.: Algorithms for Heading Determination using Inertial Sensors. Przeglad Elektrotechniczny. 2010, vol. 86, no. 9, p. 243-246. ISSN 0033-2097.

[3.20] Roháč, J.: Artificial Horizon without Kalman Filter Applied. In ICMT'11 International Conference on Miltary Technologies 2011 [CD-ROM]. Brno: Univerzita obrany, 2011, p. 679-684. ISBN 978-80-7231-788-2.

[3.21] Roháč, J. - Šipoš, M.: Sensors and Data Processing Methods Used in Navigation Systems. In Proceedings of the International Scientific Conference Modern Safety Technologies in Transportation. Košice: SUPREMA Ltd., 2011, p. 342-348. ISBN 978-80-970772-0-4.

[3.22] Reinštein, M. - Roháč, J.: Signal Processing and Data Transfer Concerning Angular Rate Sensors. In The third AIAA-Pegasus Student Conference [CD-ROM]. Napoli: Universita degli Studi di Napoli "Federico II", 2007,

[3.23] Reinštein, M. - Roháč, J.: Measuring System for Angular Rate Sensors. In POSTER 2007 [CD-ROM]. Prague: CTU, Faculty of Electrical Engineering, 2007,

[3.24] Roháč, J.: Navigation Data Denoising. In MDS - Měření, diagnostika, spolehlivost palubních soustav letadel 2010. Brno: Univerzita obrany, 2010, p. 133-140. ISBN 978-80-7231-741-7.

[3.25] Roháč, J. - Reinštein, M. - Draxler, K.: Data Processing of Inertial Sensors in Strong-Vibration Environment. In Intelligent Data Acquisition and Advanced Computing Systems (IDAACS). Piscataway: IEEE, 2011, vol. 1, p. 71-75. ISBN 978-1-4577-1426-9.

[3.26] Roháč, J. - Pačes, P. - Draxler, K. - Jakl, P.: Air Speed Measurement by Low-cost Sensors. In MDS palubních soustav letadel - 6. odborný seminář. Brno: Univerzita obrany, Fakulta vojenských technologií, 2006, s. 68-74. ISBN 80-7231-155-7. (in Czech).

[3.27] Roháč, J.: GPS and its Usage in Attitude Evaluation. In MOSATT 2007, Proceedings of the International Scientific Conference "Modern Safety Technologies in Transportation". Košice: Slovak Transport Society at the Slovak Academy of Sciences, 2007, p. 237-244. ISBN 978-80-969760-2-7.

[3.28] Šipoš, M. - Roháč, J. - Reinštein, M.: Measurement with Electrolytic Tilt Sensor. In 2008 PEGASUS-AIAA Student Conference [CD-ROM]. Prague: Czech Technical University, 2008,

[3.29] Šipoš, M. - Reinštein, M. - Roháč, J.: System for Measuring Tilt-Angle. In New Development Trends In Aeronautics. Košice: Technical University of Košice, 2008, p. 120-121. ISBN 978-80-553-0067-2.

[3.30] Reinštein, M. - Roháč, J. - Šipoš, M.: Improving Performance of a Low-cost AHRS. Acta Avionica. 2008, vol. X, no. 16, p. 132-137. ISSN 1335-9479.

[3.31] Šipoš, M. - Roháč, J.: Integration of Low-cost Inertial Navigation Unit with Secondary Navigation Systems. In Workshop 2010 [CD-ROM]. Praha: České vysoké učení technické v Praze, 2010, p. 146-147. ISBN 978-80-01-04513-8.

[3.32] Roháč, J.: Aided Navigation Systems for UAVs. In 2nd Conference for Unmanned Aerial Systems. Praha: FSI ČVUT, 2010, . ISBN 978-80-86059-53-2.

[3.33] Nováček, P. - Roháč, J.: GPS Based Attitude Estimation. In 2nd Conference for Unmanned Aerial Systems [CD-ROM]. Praha: FSI ČVUT, 2010, p. 1-8. ISBN 978-80-86059-53-2.

[3.34] Roháč, J. - Šipoš, M. - Nováček, P. - Pačes, P. - Reinštein, M.: Modular System for Attitude and Position Estimation. In Workshop 2011 [CD-ROM]. Praha: České vysoké učení technické v Praze, 2011, p. 1-4.

[3.35] Draxler, K. - Pačes, P. - Roháč, J. - Fetr, M.: Use of Differential Air Pressure Sensor for Barometric Difference Altitude and Vertical Speed Measurement. In ICMT'11 International Conference on Miltary Technologies 2011 [CD-ROM]. Brno: Univerzita obrany, 2011, p. 605-610. ISBN 978-80-7231-788-2.

[3.36] Šipoš, M. - Roháč, J.: Usage of Electrolytic Tilt Sensor for Initial Alignment of Tri-axial Accelerometer. In ICMT'11 International Conference on Miltary Technologies 2011 [CD-ROM]. Brno: Univerzita obrany, 2011, p. 685-691. ISBN 978-80-7231-788-2.

[3.37] Šipoš, M. - Roháč, J. - Nováček, P.: Analyses of Electronic Inclinometer Data for Tri-axial Accelerometer's Initial Alignment. Przeglad Elektrotechniczny. 2012, vol. 88, no. 01a, p. 286-290. ISSN 0033-2097.

[3.38] Roháč, J. - Šipoš, M. - Nováček, P.: Azimuth Determination Based on Magnetometer Measurements. In MDS - Měření, diagnostika, spolehlivost palubních soustav letadel 2011 - Sborník příspěvků z 11.mezinárodní vědecké konference. Brno: Univerzita obrany, Fakulta vojenských technologií, 2011, p. 11-17. ISBN 978-80-7231-828-5.

[3.39] Ripka, P. - Nováček, P. - Reinštein, M. - Roháč, J.: Position Sensing System for Eddy-current Mine Imager. In EUROSENSORS XXIV - Proceedings [CD-ROM]. Linz: Elsevier BV, 2010, p. 276-279. ISSN 1877-7058.

[3.40] Nováček, P. - Ripka, P. - Roháč, J. - Paroulek, L.: Explosive Remnants of Wars Differentiation. In SPM 2011 - X Symposium of Magnetic Measurements. Czestochowa Branch: Polish Society of Theoretical and Applied Electrical Engineering, 2011, p. 28.

[3.41] Nováček, P. - Roháč, J.: Inertial Sensors Utilization in Humanitarian Demining. In MDS - Měření, diagnostika, spolehlivost palubních soustav letadel 2011 - Sborník příspěvků z 11.mezinárodní vědecké konference. Brno: Univerzita obrany, Fakulta vojenských technologií, 2011, s. 138-144. ISBN 978-80-7231-828-5.

[3.42] Reinštein, M. - Roháč, J. - Šipoš, M.: Turbulence Modelling for Attitude Evaluation Purposes. In Sborník z 8. mezinárodní vědecké konference Měření, diagnostika a spolehlivost palubních soustav letadel. Brno: Univerzita obrany, Fakulta vojenských technologií, 2008, p. 46-54. ISBN 978-80-7231-555-0.

[3.43] Pačes, P. - Roháč, J. - Ramos, H.: Intelligent Sensing in a Design of a Distributed Engine Control Unit. In ICST 2007 - The 2nd International Conference on Sensing Technology [CD-ROM]. Palmerston North: Massey University, Institute of Information Sciences and Technology, 2007, p. 205-210. ISBN 978-0-473-12432-8.

[3.44] Pačes, P. - Šipoš, M. - Reinštein, M. - Roháč, J.: Sensors of Air Data Computers - Usability and Environmental Effects. In ICMT'09 - Proceedings of the International Conference on Military Technologies. Brno: Univerzita obrany, 2009, p. 401-409. ISBN 978-80-7231-649-6.

[3.45] Šipoš, M. - Pačes, P. - Reinštein, M. - Roháč, J.: Flight Attitude Track Reconstruction Using Two AHRS Units under Laboratory Conditions. In IEEE SENSORS 2009 - The Eighth IEEE Conference on Sensors [CD-ROM]. Christchurch: IEEE Sensors Council, 2009, p. 675-678. ISBN 978-1-4244-5335-1.

[3.46] Roháč, J. - Řeřábek, M. - Hudec, R.: Multi-Functional Star Tracker - Future Perspectives. Acta Polytechnica. 2011, vol. 51, no. 6, p. 61-64. ISSN 1210-2709.

[3.47] Šipoš, M. - Roháč, J. - Stach, M.: System for Vibration Testing. In MDS - Měření, diagnostika, spolehlivost palubních soustav letadel 2011 - Sborník příspěvků z 11.mezinárodní vědecké konference. Brno: Univerzita obrany, Fakulta vojenských technologií, 2011, p. 213-225. ISBN 978-80-7231-828-5.

4. METHODS USED IN NAVIGATION SYSTEMS – PUBLISHED PAPERS

4.1. ESTIMATION OF DETERMINISTIC SENSOR PARAMETERS, CALIBRATION

Šipoš, M. - Pačes, P. - Roháč, J. - Nováček, P.: Analyses of Triaxial Accelerometer Calibration Algorithms. IEEE Sensors Journal. 2012, vol. 12, no. 5, p. 1157-1165. ISSN 1530-437X. (IF: 1.520)

IEEE SENSORS JOURNAL, VOL. 12, NO. 5, MAY 2012 1157

Analyses of Triaxial Accelerometer Calibration Algorithms

Martin Šipoš, Pavel Pačes, *Member, IEEE*, Jan Roháč, and Petr Nováček

***Abstract*—This paper proposes a calibration procedure in order to minimize the process time and cost. It relies on the suggestion of optimal positions, in which the calibration procedure takes place, and on position number optimization. Furthermore, this paper describes and compares three useful calibration algorithms applicable on triaxial accelerometer to determine its mathematical error model without a need to use an expensive and precise calibration means, which is commonly required. The sensor error model (SEM) of triaxial accelerometer consists of three scale-factor errors, three nonorthogonality angles, and three offsets. For purposes of calibration, two algorithms were tested—the Levenberg–Marquardt and the Thin-Shell algorithm. Both were then related to algorithm based on Matlab *fminunc* function to analyze their efficiency and results. The proposed calibration procedure and applied algorithms were experimentally verified on accelerometers available on market. We performed various analyses of proposed procedure and proved its capability to estimate the parameters of SEM without a need of precise calibration means, with minimum number of iteration, both saving time, workload, and costs.**

***Index Terms*—Accelerometers, calibration, error analysis, inertial navigation.**

I. INTRODUCTION

OVER the last decades technological progress in the precision and reliability of Micro-Electro-Mechanical-Systems (MEMS) has enabled the usage of inertial sensors based on MEMS in a wide range of military and commercial applications, e.g., in Unmanned Aircraft Systems (UASs), indoor and personal navigation, human motion tracking, and attitude-control systems [1]–[5].

The Inertial Measurement Unit (IMU), which forms a basic part of Inertial Navigation System (INS), primarily contains only inertial sensors-accelerometers and angular rate sensors or gyroscopes to provide inertial data, and additionally magnetometers. The major errors of electronically-gimbaled navigation systems with accelerometers and magnetometers are caused by sensor triplet deviations (mutual misalignment) [6], and therefore, a calibration has to take a place for their proper function. The calibration is necessary to be performed to estimate sensor errors like nonorthogonalities (misalignment) and scale factor errors for their compensation. Factory based sensor calibration is an expensive and time-consuming process, which is typically done for specific high-grade IMUs. For low-cost inertial sensors, such as MEMS based ones, manufacturers perform only basic calibration [7] which is very often insufficient, because even small uncompensated imperfections can cause position deviation growth and also inaccuracy in tilt angle evaluation [8], [9].

There are already known different sensor error models (SEMs) [10] and calibration methods based on different principles, but they have limitations such as the necessity of precise position system or a platform providing precise alignment. This requirement increases manufacturing costs, and therefore, there is a need for investigating alternatives.

One example of a commonly used calibration procedure described by Titterton and Weston in ([11] p. 238) and by Won in [8] uses six static positions, in which the sensors' axes are consecutively aligned up and down along the vertical axis of the local level frame. The calibration is capable to determine only offsets and scale factor errors, not nonorthogonalities. The calibration accuracy strongly depends on the alignment precision [7]. To increase the precision of alignment an accurate reference system is usually used, as presented in [10], [11]. In the first case a 3-D optical tracking system and nonlinear least squares algorithm were applied, the other case used an *fminunc* Matlab function as a minimizing algorithm and a robotic arm. In both cases the calibration is capable to estimate sensor' axes misalignments, offsets, and electrical gains/scale factors, which define nine-parameter-error model. The same model for a triaxial accelerometer can be estimated by an iterative calibration procedure described by Petrucha *et al.* in [12] using an automated nonmagnetic system, or the one described by Syed *et al.* in [7], in which offset and scale factor initial values are required for a modified multiposition method. Other method for an accelerometer calibration, presented by Skog and Händel in [13], is based on the cost function formulation and its minimization with respect to unknown model parameters using Newton's method. The cost function can reach several local optima, and therefore, the initial starting values have to be determined. Automatic adaptive method of a 3-D field sensor based on a linearized version of an ellipsoid fitting problem has been published in [14]. It relies on a procedure that fits an ellipsoid to data using linear regression. Based on estimated ellipsoid parameters the unknown model parameters can be evaluated. An alternative to this method using modified ellipsoidal-fitting procedure has

Manuscript received May 13, 2011; revised August 01, 2011; accepted August 24, 2011. Date of publication September 08, 2011; date of current version April 11, 2012. This work was supported in part by the Czech Science Foundation project 102/09/H082; in part by the Research Program No. MSM6840770015 "Research of Methods and Systems for Measurement of Physical Quantities and Measured Data Processing" of the CTU in Prague sponsored by the Ministry of Education, Youth, and Sports of the Czech Republic; and in part by the Grant Agency of the Czech Technical University in Prague under Grant SGS10/288/OHK3/3T/13. The associate editor coordinating the review of this paper and approving it for publication was Prof. Boris Stoeber.

The authors are with the Department of Measurement, Faculty of Electrical Engineering, Czech Technical University in Prague, Technicka 2, 166 27 Prague, Czech Republic (e-mail: siposmar@fel.cvut.cz; pacesp@fel.cvut.cz; xrohac@fel.cvut.cz; petr.novacek@fel.cvut.cz).

Digital Object Identifier 10.1109/JSEN.2011.2167319

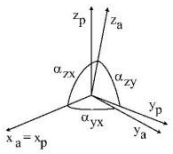

Fig. 1. Orthogonalization of sensor frame; a—nonorthogonal sensor frame; p—orthogonal sensor frame.

been described by Bonnet *et al.* in [15]. He proved that an ellipsoid fitting using either linear optimization (Merayo's algorithm) or nonlinear optimization (Quasi-Newton factorization algorithm) is robust with data sets from static positions obtained within free rotations along a vertical axis in case of accelerometers and free rotations along East-West axis in case of magnetometers.

In Section II, the SEM of triaxial accelerometer is described. We present three algorithms for its calibration in Section III; the Levenberg–Marquardt algorithm, the Thin-Shell algorithm, and an algorithm based on Matlab *fminunc* function. First two algorithms were related to third one, which was used as a reference, in order to have a means for the comparison of algorithms efficiency. In Section IV, we shortly present the most important parameters of calibrated sensors and used measurement setup. To compare a calibration effect on measured and evaluated data based on applied algorithms and SEMs we used a Rotational-Tilt Platform with precise positioning capability to provide precise tilt angles. The experiments, analyses, and result accuracy are provided in Section V.

II. Sensor Error Model

For triaxial accelerometer calibration we considered the sensor error model (SEM), which consisted of nine unknown parameters—three scale factor corrections, three angles of nonorthogonality, and three offsets. The SEM can be defined as (1). Offset forms a stochastic part of biases and can be modeled as a random constant. The time variant part of the bias is drift, which changes based on environmental and other sensor conditions. The calibration process is supposed to be performed during short-time period; therefore, drift can be considered as zero

$$\begin{aligned} a_p &= T_a^p \mathrm{SF}_a (a_m - b_a) \\ &= \begin{pmatrix} 1 & 0 & 0 \\ \alpha_{yx} & 1 & 0 \\ \alpha_{zx} & \alpha_{zy} & 1 \end{pmatrix} \begin{pmatrix} \mathrm{SF}_{ax} & 0 & 0 \\ 0 & \mathrm{SF}_{ay} & 0 \\ 0 & 0 & \mathrm{SF}_{az} \end{pmatrix} \\ &\quad \times \left(\begin{pmatrix} a_{mx} \\ a_{my} \\ a_{mz} \end{pmatrix} - \begin{pmatrix} b_{ax} \\ b_{ay} \\ b_{az} \end{pmatrix} \right) \end{aligned} \tag{1}$$

where $a_p = [a_{px}, a_{py}, a_{pz}]^T$ is the compensated vector of a measured acceleration defined in the orthogonal system (platform frame); T_a^p denotes matrix providing transformation from nonorthogonal frame to orthogonal one with nondiagonal terms $\alpha_{yx}, \alpha_{zx}, \alpha_{zy}$ that correspond to the axes misalignment (nonorthogonality angles) (Fig. 1); SF_a represents a scale factor matrix; $b_a = [b_{ax}, b_{ay}, b_{az}]^T$ is the vector of sensor offsets; $a_m = [a_{mx}, a_{my}, a_{mz}]^T$ denotes the vector of measured accelerations. The SEM and its derivation are described in more detail in [13] and [16].

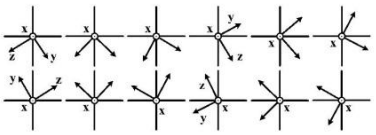

Fig. 2. Positions for calibration; rotation around x axis.

III. Calibration Algorithms

This section briefly describes the algorithms for triaxial accelerometer calibration—Levenberg–Marquardt (LM) algorithm, Thin-Shell (TS) algorithm, and algorithm based on Matlab *fminunc* function. The fundamental principle of the proposed calibration procedure is based on the fact that the magnitude of measured acceleration should be equal to the gravity magnitude, which is ensured by static conditions (2). It corresponds to "scalar field calibration" used in [17]. The proposed procedure uses only general knowledge about the applied quantity, which is in contrast to the case when precise positioning system is available, and thus, the knowledge about precise tilt angle is also provided in all steps of iteration

$$g_x^2 + g_y^2 + g_z^2 = |g|^2 \tag{2}$$

where g_i denotes sensed acceleration in direction of i axis and $|g|$ is the magnitude of gravity vector, ideally equal to $1g$.

To obtain the most accurate estimation without the need of having a precise positioning system, the sensor should be consecutively placed to positions in manner to cover the whole globe surface and the sensor should be influenced only by gravity. In practice, it is not possible to do so, because the number of measurements would be infinite. Therefore, in the proposed procedure, the number of positions is optimized and suggested their orientation, in which a high influence of all errors is expected. Only 36 positions are used, 3 times 12 positions along x, y, z axis. The positions along x axis are shown in Fig. 2. Precise knowledge of their orientations is not required, only 3 positions per quadrant are recommended.

A. Principle of Levenberg–Marquardt Algorithm

The Levenberg–Marquardt (LM) algorithm is one of the most efficient and popular algorithms. It has better convergence than the other ones for nonlinear minimization. The LM algorithm is widely utilized in software applications, neural networks, and curve-fitting problems [18]–[21]. The LM algorithm combines two algorithms: the Gradient Descent (GD) and the Gauss–Newton (GN) algorithm [22]. The LM algorithm can be described by (3)

$$S(\beta) = \sum_{i=1}^{m} [y_i - f(x_i, \beta)]^2 = \sum_{i=1}^{m} q_i(\beta)^2 \tag{3}$$

where $S(\beta)$ denotes the sum of residuals $q_i(\beta)^2; m$ is the number of measurements; x_i are measured data; y_i are the reference values, and β is a vector of parameters being estimated

and forming the SEM defined in (1). The LM algorithm is iterative algorithm reducing $S(\beta)$ with respect to the parameters in vector β.

1) Gradient Descent Algorithm: The Gradient Descent (GD) algorithm is a minimization algorithm updating the estimated parameters in the direction opposite to the gradient of the cost function. The GD algorithm is highly convergent and can be used for problems with thousands of parameters forming the cost function. The h_{GD} modifies the GD algorithm step to reduce $S(\beta)$ in the direction of steepest descent and is defined by (4) [22]

$$h_{\mathrm{GD}} = \alpha J^T W(y_i - f(x_i, \beta)) \tag{4}$$

where α is a parameter corresponding to the length of step in the steepest descent direction; J is the Jacobian related to the vector β; W is the weighting diagonal matrix [22].

2) Gauss–Newton Algorithm: A main advantage of Gauss–Newton (GN) algorithm is its rapid convergence; however, it depends on the initial conditions. The GN algorithm does not require the calculation of second-order derivatives [21]. The equation for GN algorithm reducing $S(\beta)$ is given by (5)

$$\lfloor J^T W J \rfloor h_{\mathrm{GN}} = J^T W(y_i - f(x_i, \beta)) \tag{5}$$

where h_{GN} denotes the GN algorithm update of estimated parameter leading to a minimization of $S(\beta)$.

3) Levenberg–Marquardt Algorithm: As was mentioned, the Levenberg–Marquardt (LM) algorithm combines both the GD and GN algorithm. In the LM algorithm, the parameter h_{LM} is adaptively weighted with respect to h_{GD} and h_{GN} to reach optimal progress in $S(\beta)$ minimization, and thus, the LM algorithm equation is given by (6)

$$\lfloor J^T W J + \lambda \operatorname{diag}(J^T W J) \rfloor h_{\mathrm{LM}} = J^T W(y_i - f(x_i, \beta)) \tag{6}$$

where λ is a damping parameter and h_{LM} is the LM algorithm update. The parameter λ has several characteristics [23]:

- for all $\lambda > 0$, the coefficient matrix $(J^T W J + \lambda \operatorname{diag}(J^T W J))$ is positive definite, and this fact ensures that h_{LM} is descent directional;
- for large values of λ the iteration step (parameter modification) is in the steepest descent direction, which is good when the current stage is far from required solution;
- for small values of λ, the $h_{\mathrm{LM}} \cong h_{\mathrm{GN}}$ and it is good for final phases of iteration, when estimated parameters are close to required solution.

In other words, if the iteration step decreases the error, it implies that quadratic assumption $f(x_i)$ is working and λ can be reduced (usually by a factor of 10) to decrease the influence of GD. On the other hand, if $S(\beta)$ increases, λ is increased by the same factor increasing GD influence and the iteration step is repeated.

B. Thin-Shell Algorithm

The Thin-Shell (TS) algorithm is based on an estimation of Linear Minimum Mean Square Error, which is applied on SEM

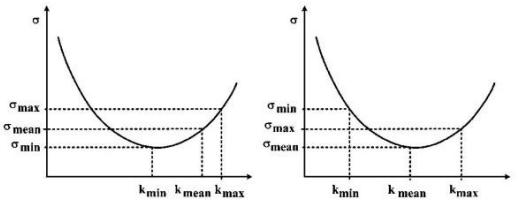

Fig. 3. Criterions for halving the interval, for which the estimated parameters are searched.

(1) of calibrated sensor. According to (1) nine parameters have to be estimated. The iteration is based on successive halving of intervals, in which the estimated parameter is searched for. The intervals are halved based on a standard deviation defined by (7) and if-conditions related to Fig. 3

$$\sigma = \sqrt{\frac{\sum_{i=1}^{m} \left(\widehat{a}_{xi}^2 + \widehat{a}_{yi}^2 + \widehat{a}_{zi}^2 - |g|^2 \right)^2}{m-1}} \tag{7}$$

where σ is the standard deviation; m is the number of positions; $\widehat{a}_{xi}, \widehat{a}_{yi}, \widehat{a}_{zi}$ are estimations of compensated measured gravity vector components and $|g|$ is the magnitude of gravity vector corresponding to the reference value.

At the beginning of the algorithm, the minimal and maximal values of each parameter must be set (it defines the interval, in which the unknown parameter is searched for); the mean value is computed as an average of them. Each iteration cycle can be divided into three steps:

1) Min, max, and mean values of the parameter being searched for ($\mathrm{k_{min}}, \mathrm{k_{mean}}$, and $\mathrm{k_{max}}$) are used for the estimation of compensated accelerations in all positions.
2) Three corresponding standard deviations ($\sigma_{\mathrm{min}}, \sigma_{\mathrm{mean}}$, and σ_{max}) are then obtained based on (7). Other parameters are set to their mean values.
3) Based on $\sigma_{\mathrm{min}}, \sigma_{\mathrm{mean}}$, and σ_{max} the interval, in which estimated parameter should be, is halved according to Fig. 3 and following conditions:
   - if $(\sigma_{\mathrm{min}} > \sigma_{\mathrm{mean}})$ and $(\sigma_{\mathrm{max}} > \sigma_{\mathrm{mean}})$, the interval is reduced to a half around the mean value k_{mean}.
   - if $(\sigma_{\mathrm{min}} < \sigma_{\mathrm{mean}})$ and $(\sigma_{\mathrm{mean}} < \sigma_{\mathrm{max}})$ the true value of the parameter should be in the interval $(k_{\mathrm{min}}, k_{\mathrm{mean}})$; for the following iteration cycle $k_{\mathrm{max}} = k_{\mathrm{mean}}$ and k_{mean} is computed as a mean value of k_{min} and new k_{max}.
   - if $(\sigma_{\mathrm{max}} < \sigma_{\mathrm{mean}})$ and $(\sigma_{\mathrm{mean}} < \sigma_{\mathrm{min}})$ the true value of the parameter should be in the interval $(k_{\mathrm{mean}}, k_{\mathrm{max}})$; for the following iteration cycle $k_{\mathrm{min}} = k_{\mathrm{mean}}$ and k_{mean} is computed as a mean value of new k_{min} and k_{max}.

The steps described above are repeated until the computed standard deviation is less than the required value or required number of iteration cycles is reached. Consequently the rest of the parameters are estimated in the same manner. The final value of standard deviation defines the calibration algorithm accuracy. This algorithm is described in more detail in [24].

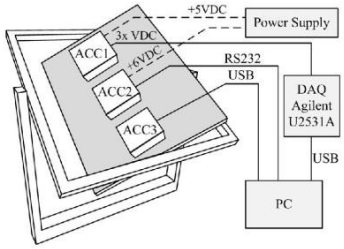

Fig. 4. Measurement setup for triaxial accelerometer calibration; ACC1—CXL02LF3; ACC2—AHRS M3; ACC3—ADIS16405.

(a) (b)

Fig. 5. (a) Calibrated systems (from left): ADIS16405; AHRS M3; CXL02LF3; (b) Rotational-tilt platform.

C. Algorithm Based on Fminunc Matlab Function

To evaluate the efficiency of Levenberg–Marquardt (LM) and Thin-Shell (TS) algorithms with respect to minimum required number of iterations and reached accuracy Matlab functions *fminunc, lsqnonlin*, and *fminsearch* were tested. Based on their performances the function *fminunc* was chosen as a reference and a means for LM and TS algorithm evaluation. Function *fminunc* is based on quasi-Newton minimization with numerical gradients [25]. Its description is not the subject of this paper and can be found [26].

IV. Calibrated Sensors and Measurement Setup

In this section, we briefly present the systems used for the calibration and measurement setup (Fig. 4) which uses a simple platform enabling to measure accelerometer data in the static positions defined approximately as shown in Fig. 2. Furthermore, we used a Rotational-Tilt Platform (RoTiP), see Fig. 5(b), as a reference for analyses needed to verify the results of the proposed calibration procedure according to applied algorithms. The RoTiP parameters are shown in Table I. Although we evaluated five sensors in sum, such as AHRS M3's accelerometer (Innalabs [27]), ADIS16405's accelerometer (Analog Devices [28]), CXL02LF3 accelerometer (Crossbow [29]), 3DM-GX2's accelerometer (MicroStrain [30]), and STEVAL-MKI062V2's accelerometer (STMicroelectronics [31]), we present the results of analyses only from first three accelerometers of calibrated systems [see Fig. 5(a)]. The analyses of last two sensors were very similar.

TABLE I
Parameters of Rotational-Tilt Platform

Parameter	Range	Speed of Motion	Resolution
Pitch	±45 deg	±42 deg/s	0.00033 deg
Roll	±25 deg	±60 deg/s	0.00065 deg
Heading	0 to 360 deg	±310 deg/s	0.00074 deg

V. Calibration Analyses

Three aforementioned algorithms were used to estimate SEMs of three triaxial accelerometers described in Section IV according to measured data in suggested positions. It helped to decrease the influence of manufacturing imperfection on the sensor precision. As said in [32] other problematic errors can show up with incorrect determination of sensor error parameters; therefore, for results, a comparison Root Mean Square Error (RMSE) defined by (8) was used

$$\mathrm{RMSE}(p,g) = \sqrt{\frac{\sum_{i=1}^{n}(x_i - g)^2}{n}}$$
$$x_i = \sqrt{g_{xi}^2 + g_{yi}^2 + g_{zi}^2} \tag{8}$$

where $p = (x_1, \ldots, x_n)^T$ is n-dimensional vector; n—number of evaluated positions; g is an ideal magnitude of the gravity vector equal to $1g$; g_{xi}, g_{yi}, g_{zi} are components of the estimated gravity vector.

For the calibration purposes and consecutive analyses we measured the raw data from sensors and evaluated data in 364 positions. The number was chosen with respect to the number of suggested positions in Section III multiplied by 10 and modified to have uniformly spaced data along all axes. The analyses included the observation of estimated parameters of SEM with respect to algorithms applied, the RMSE dependence on the number of taken positions and the number of iterations, and the observation of a long-period permutation of estimated SEMs. Furthermore, the calibration effect on the precision of evaluated tilt angles and the calibration effect from the sensors' drift point of view were performed.

A. Sensor Error Models

We estimated Sensor Errors Models (SEMs) of three accelerometers. Results are listed for LM and TS algorithms in Table II. Although we estimated the SEMs using three algorithms, only LM and TS algorithms' results are listed due to the fact that the results estimated by LM algorithm were identical to the ones from algorithm based on *fminunc* function. From Table II, it can be seen that SEMs estimated by LM and TS algorithms are comparable for all tested units, which also proves the values of RMSE. The effect of SEM applying on measured data is shown in Fig. 6, where magnitude of compensated acceleration vector has approximately 100 times smaller deviation from $1g$ than the one before calibration.

B. Dependence of RMSE on Evaluated Data Positions

To prove that only 36 static positions are sufficient for the calibration purposes, we measured 364 positions uniformly spaced, and analyzed the variation of RMSE for the different number of

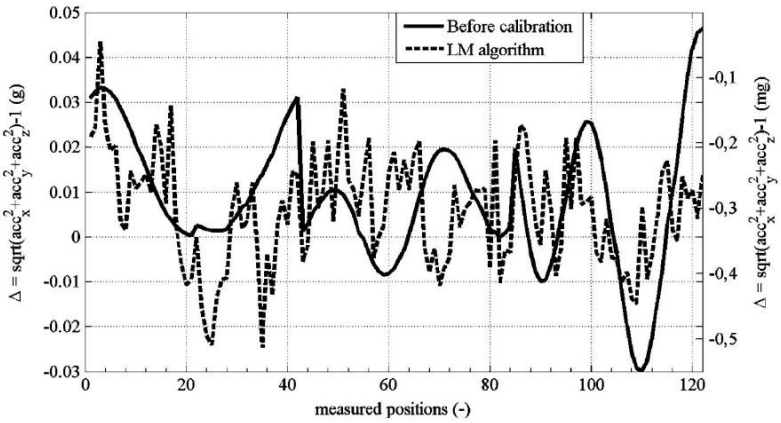

Fig. 6. Dependence of deviations of measured accelerations before (left vertical axis) and after (right vertical axis) calibration using LM algorithm applied on AHRS M3's accelerometer data in evaluated different positions.

TABLE II
SENSOR ERROR MODELS OBTAINED USING LEVENBERG–MARQUARDT (LM) AND THIN-SHELL (TS) ALGORITHM FOR ACCELEROMETERS OF AHRS M3'S (AHRS) AND ADIS16405'S (ADIS) AND CXL02LF3 (CXL) ACCELEROMETER

Par	LM AHRS	LM ADIS	LM CXL	TS AHRS	TS ADIS	TS CXL
α_{yx} (deg)	-0.8758	-0.0230	1.0237	-0.8760	-0.0227	1.0235
α_{zx} (deg)	3.0286	0.0351	-0.5217	3.0229	0.0350	-0.4476
α_{zy} (deg)	0.1765	-0.1639	-1.4939	0.1784	-0.1639	-1.4829
SF_{ax} (-)	0.99865	0.99956	1.05591	0.99866	0.99957	1.05664
SF_{ay} (-)	0.98946	1.00194	1.06517	0.98946	1.00194	1.06508
SF_{az} (-)	0.98611	0.99828	1.06144	0.98608	0.99828	1.06128
b_{ax} (g)	0.00173	-0.01354	-0.00255	0.00172	-0.01353	-0.00272
b_{ay} (g)	-0.00602	-0.00671	-0.03445	-0.00598	-0.00678	-0.03675
b_{az} (g)	0.01440	-0.00402	0.03690	0.01427	-0.00400	0.04003
RMSE [1]	0.01810	0.00948	0.06628	0.01810	0.00948	0.06628
RMSE [2]	0.00015	0.00252	0.01527	0.00017	0.00252	0.01545

Superscript 1 denotes RMSE before calibration and 2 after calibration.

positions (NoP) in intervals from 12 to 364. NoP can be seen in Table III, where N represents the relationship between Figs. 7–9 horizontal axes and the NoP used for calculation. In each static position, an average of 100 measured data samples was calculated to reduce noise. The dependence between RMSE defined in (8) and NoP is shown in Fig. 7 for AHRS M3, in Fig. 8 for ADIS16405, and in Fig. 9 for CXL02LF3. The RMSE was evaluated between an ideal magnitude of gravity vector and the magnitude of compensated measured gravity. The compensated measured gravity obtained from the measured data multiplication with SEM is further notified as a compensated result. The left vertical axes of Figs. 7–9 correspond to RMSE before calibration and right vertical axes correspond to RMSE after calibration. As a criterion for the evaluation of RMSE dependence on the number of evaluated positions we considered a maximum deviation of RMSE from RMSE in $N = 1$ position to be equal or less than 1 mg, which corresponds to sensor resolutions. From Figs. 7–9 it can be seen, that 21 positions and more satisfy desired limitation no matter which algorithm was used. This means that the variation of the compensated results in the case of usage

TABLE III
RELATIONSHIP BETWEEN THE NUMBER OF EVALUATED POSITIONS (NOP) AND NOTATION OF FIGS. 7–9 HORIZONTAL AXES (N)

N	NoP	N	NoP	N	NoP	N	NoP	N	NoP
1	364	7	52	13	28	19	20	25	14
2	182	8	46	14	26	20	19	26	13
3	122	9	41	15	25	21	18	27	12
4	91	10	36	16	23	22	17		
5	73	11	34	17	22	23	16		
6	61	12	31	18	21	24	15		

21 positions or more (up to 364) differs under the required value; therefore, further differences are considered as negligible. Because having 7 positions in 360 deg and also in 4 quadrants does not have a uniform distribution with a constant number of positions per quadrant, it is suitable to increase the number to 12. This leads to having 36 positions covering all axes, which was the number we used in Section III-A. The result optimizes the number of positions needed for the calibration with respect to a workload and precision.

C. Dependence of RMSE on Number of Iterations

Based on the data measured in 36 positions as described in Section III and proven in Section V-B, we analyzed the dependency of RMSE calculated between compensated results and an ideal gravity vector on the number of iterations for LM and TS algorithms. The iteration denotes a calibration cycle, in which all measured data (in our case in 36 positions) are used for an unknown SEM parameter estimation. This analysis relied on the progress of RMSE with respect to the number of iteration. When the deviation from the steady-state value was less than 1 mg we considered the accuracy of calibration to be sufficient. Fig. 10 shows the RMSE dependency on number of iterations for TS algorithm applied on AHRS M3 accelerometer. The comparison between LM and TS algorithms from the number of iterations point of view is presented in Table IV.

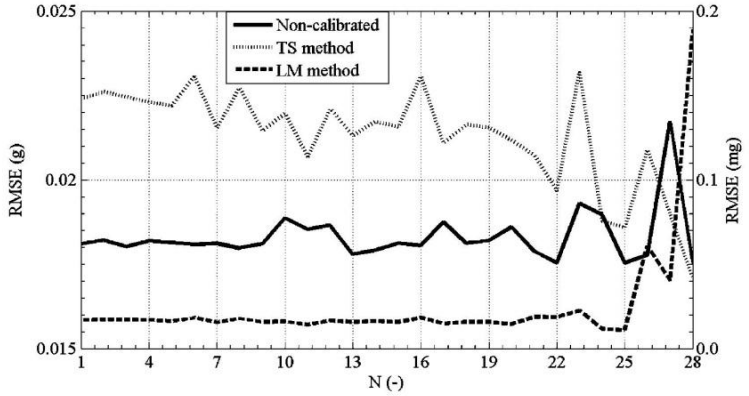

Fig. 7. Dependence of RMSE before (left axis) and after (right axis) calibration on the number of positions using AHRS M3's accelerometer.

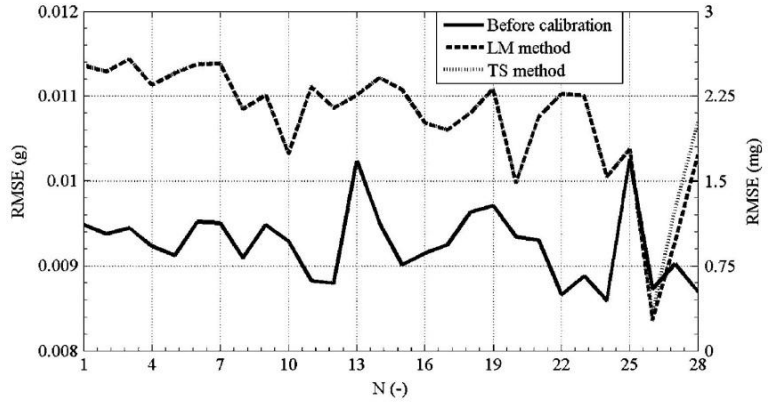

Fig. 8. Dependence of RMSE before (left axis) and after (right axis) calibration on the number of positions using ADIS16405's accelerometer.

D. Comparison of SEM During Time Period

We analyzed the variation of SEMs obtained by LM and TS algorithms during a longer time period corresponding to one and half years (the first measurement was taken in April 2009 and the second one was taken in November 2010). We measured 122 positions in both cases with different distributions as shown in Fig. 11. We analyzed the SEMs permutation and their accuracy. The SEMs evaluated based on two data sets using LM and TS calibration algorithms are presented in Table V. In each position the average of 100 data samples was used as in previous analyses.

From Table V it can be seen that parameters are slightly different, which we think was caused by reaching the resolution of the method applied. The influence of different distribution of evaluated positions shown in Fig. 11 is considered as negligible, because the number of evaluated positions was always higher than 21.

E. Comparison of Tilt Angles Before and After Calibration

To see the effect of calibration, we performed another analysis in which the tilt angles estimated based on calibration results were compared to the reference ones measured by Rotational-Tilt Platform (RoTiP).

We mounted the accelerometers on RoTiP and tilted them along two axes. A tilt corresponded to pitch (θ) and roll (ϕ) angles. Specification of RoTiP is listed in Section IV. The pitch angle calculation is defined as (9) and roll angle calculation as (10)

$$\theta = \operatorname{arctg}\left(-f_{by} \Big/ \sqrt{f_{bx}^2 + f_{bz}^2}\right) \tag{9}$$

$$\phi = \operatorname{arctg}(f_{bx}/-f_{bz}) \tag{10}$$

where θ is the pitch angle; ϕ is the roll angle; f_{bx}, f_{by}, f_{bz} are measured accelerations. For computation of *arctg* function, the Matlab function *atan2*, which returns the four-quadrant invert tangent (arctangent) of real parts x and y. [2], was used.

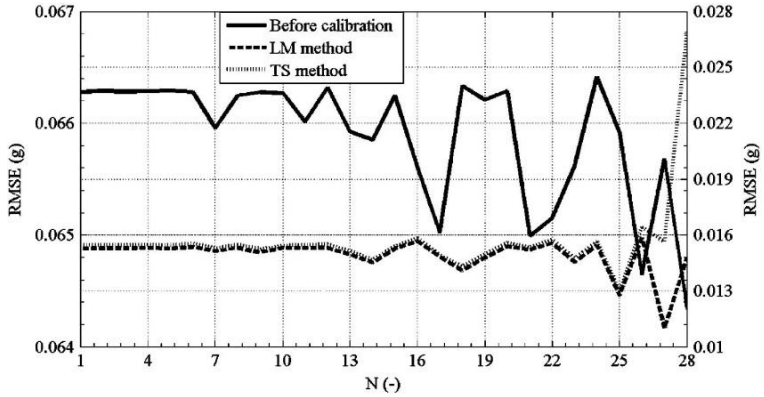

Fig. 9. Dependence of RMSE before (left axis) and after (right axis) calibration on the number of positions using CXL02LF3 accelerometer.

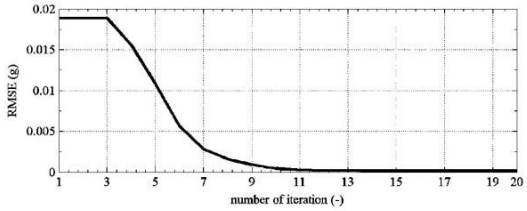

Fig. 10. Dependence of RMSE on the number of iterations for AHRS M3's accelerometer using TS calibration algorithm.

TABLE IV
NUMBER OF ITERATIONS FOR LM AND TS CALIBRATION ALGORITHMS

	AHRS M3	ADIS16405	CXL02LF3
LM Algorithm	2	1	1
TS Algorithm	9	7	6

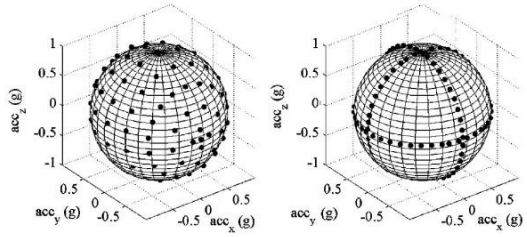

Fig. 11. Evaluated positions in April 2009 (left) and in November 2010 (right).

We analyzed the variation of results when LM and TS algorithms had been applied. The last column of Tables VI–VIII (AHRS M3, ADIS16405, CXL02LF3) describes an Error Percentage Improvement (EPI) which corresponds to the difference between particular deviations (relative errors) related to the maximum angle, i.e., 20 deg. From these tables it can be seen that due to the calibration the tilt angles are more accurate than

TABLE V
SENSOR ERROR MODELS OBTAINED USING LM ALGORITHM (LM) AND TS ALGORITHM (TS) DURING TIME INTERVAL OF ONE AND HALF YEARS FOR ACCELEROMETER CONTAINED IN AHRS M3

Parameter	LM Apr 2009	LM Nov 2010	TS Apr 2009	TS Nov 2010
α_{yx} (deg)	-0.8769	-0.8758	-0.8830	-0.8760
α_{zx} (deg)	3.0261	3.0286	3.0253	3.0229
α_{zy} (deg)	0.1794	0.1765	0.1818	0.1784
SF_{ax} (-)	0.99868	0.99865	0.99902	0.99866
SF_{ay} (-)	0.98951	0.98946	0.98828	0.98946
SF_{az} (-)	0.98609	0.98611	0.98640	0.98608
b_{ax} (g)	0.00153	0.00173	0.00156	0.00172
b_{ay} (g)	-0.00541	-0.00602	-0.00527	-0.00598
b_{az} (g)	0.01461	0.01440	0.01448	0.01427
RMSE [1]	0.01957	0.01810	0.01957	0.01810
RMSE [2]	0.00014	0.00015	0.00055	0.00017

Superscript 1 denotes RMSE before calibration and 2 after calibration.

TABLE VI
COMPARISON OF TILT ANGLES BEFORE AND AFTER CALIBRATION USING LM AND TS ALGORITHMS FOR AHRS M3; θ—PITCH, ϕ—ROLL

Reference Angle θ; ϕ (deg)	Without Calibration θ; ϕ (deg)	LM Algorithm θ; ϕ (deg)	TS Algorithm θ; ϕ (deg)	LM EPI θ; ϕ (%)
0; 0	-0.77; -0.59	-0.70; -0.30	-0.68; -0.26	0.4; 1.5
10; 0	9.18; -0.62	9.61; -0.16	9.62; -0.12	2.2; 2.3
20; 0	19.18; -0.63	20.13; 0.01	20.14; 0.05	3.4; 3.1
0; -10	-0.96; -10.83	-0.90; -10.72	-0.89; -10.69	0.3; 0.6
0; -20	-0.83; -21.10	-0.76; -21.00	-0.75; -21.06	0.4; 0.5
10; -10	9.31; -10.98	9.76; -10.82	9.77; -10.79	2.3; 0.8
20; -20	19.00; -19.62	19.98; -19.76	19.99; -19.72	4.9; 0.7

in case without calibration for all tested sensors and tilt angles.

F. Position Determination With and Without Calibration

Furthermore, we analyzed the drift influence on the accuracy of position determination when a compensated model was used. The accelerations were measured for 200 s in a static position with different tilt angles and then two times integrated to get the position. The effect of compensation applied on an

TABLE VII
COMPARISON OF TILT ANGLES BEFORE AND AFTER CALIBRATION USING LM AND TS ALGORITHMS FOR ADIS16405; θ—PITCH, ϕ—ROLL

Reference Angle θ; ϕ (deg)	Without Calibration θ; ϕ (deg)	LM Algorithm θ; ϕ (deg)	TS Algorithm θ; ϕ (deg)	LM EPI θ; ϕ (%)
0; 0	0.85; -0.29	0.07; 0.10	0.07; 0.10	3.9; 1.0
10; 0	10.80; -0.46	10.09; -0.07	10.09; -0.07	3.6; 2
20; 0	20.66; -0.36	20.04; 0.05	20.04; 0.05	3.1; 1.6
0; -10	1.11; -10.51	0.34; -10.22	0.34; -10.22	3.9; 1.5
0; -20	1.07; -20.35	0.31; -20.15	0.31; -20.15	3.8; 1.5
10; -10	10.92; -10.51	10.23; -10.20	10.23; -10.20	3.5; 1.0
20; -20	20.73; -20.21	20.16; -19.99	20.16; -19.97	2.9; 1.0

TABLE VIII
COMPARISON OF TILT ANGLES BEFORE AND AFTER CALIBRATION USING LM AND TS ALGORITHMS FOR CXL02LF3; θ—PITCH, ϕ—ROLL

Reference Angle θ; ϕ (deg)	Without Calibration θ; ϕ (deg)	LM Algorithm θ; ϕ (deg)	TS Algorithm θ; ϕ (deg)	LM EPI θ; ϕ (%)
0; 0	4.69; -3.84	-0.43; -0.92	-0.37; -0.75	21.3; 14.6
10; 0	13.48; -3.76	10.71; 0.29	10.54; 0.24	13.9; 17.4
20; 0	21.37; -3.78	20.47; 0.15	20.47; 0.09	4.6; 18.2
0; -10	4.56; -13.25	0.90; 10.37	0.71; -10.31	18.3; 9.4
0; -20	4.63; -22.52	0.94; -20.30	0.74; -20.24	18.5; 11.1
10; -10	13.67; -13.30	10.25; -10.92	10.19; -10.73	17.1; 11.9
20; -20	22.12; -22.37	18.82; -20.75	18.76; -20.54	4.9; 8.2

TABLE IX
POSITION DETERMINATION IN PLATFORM FRAME BEFORE AND AFTER CALIBRATION USING SEMS GOT FROM LM AND TS ALGORITHMS FOR AHRS M3'S ACCELEROMETER; $\delta_X, \delta_Y, \delta_Z$—DEVIATIONS IN X, Y, Z AXES

Reference Angle θ; ϕ (deg)	Without Calibration δ_X; δ_Y; δ_Z (m)	LM Algorithm δ_X, δ_Y, δ_Z (m)	TS Algorithm δ_X, δ_Y, δ_Z (m)
0; 0	-239; -56; 5867	7; 2; -160	5; 9; -160
10; 0	-1516; -36; 7224	27; 1; -116	22; 9; -117
20; 0	-3105; 51; 7987	20; -30; -50	10; -22;- 54
0; -10	-350; -1078; 6061	-121; 40; -88	-123; 44; -87
0; -20	-721; -2116; 5921	-508; 85; -67	-507; 84; -67
10; -10	-2299; -635; 7555	-674; 828; -30	-680; 832; -31
20; -20	-7555; 1618; 7981	-4553; 5026; 64	-4561; 5025; 22

TABLE X
POSITION DETERMINATION IN PLATFORM FRAME BEFORE AND AFTER CALIBRATION USING SEMS GOT FROM LM AND TS ALGORITHMS FOR ADIS16405'S ACCELEROMETER; $\delta_X, \delta_Y, \delta_Z$—DEVIATIONS IN X, Y, Z AXES

Reference Angle θ; ϕ (deg)	Without Calibration δ_X; δ_Y; δ_Z (m)	LM Algorithm δ_X, δ_Y, δ_Z (m)	TS Algorithm δ_X, δ_Y, δ_Z (m)
0; 0	-679; -107; -1825	-30; -1; 136	-27; -4; 135
10; 0	-420; 66; -2403	93; 62; 222	95; 60; 222
20; 0	-2366; 93; -6110	-1157; -70; -3050	-1156; -72; 3051
0; -10	-171; 296; 1618	-44; 156; 821	-42; 153; 821
0; -20	-693; -1492; -4065	-328; -497; -1447	-327; -501; -1423
10; -10	-1629; -548; -2659	-933; 1005; 193	-931; 1002; 194
20; -20	-8276; -1733; -2077	-7422; 6714; -1015	-7120; 6710; -1015

AHRS M3's accelerometer, ADIS16405's accelerometer, and CXL02LF3 can be seen in Tables IX–XI.

Results from Tables IX–XI show that, in most cases, the deviations in position decreased due to the calibration. The deviations in position can be partially caused by imprecise alignment of the compensated sensor frame with respect to the platform frame which lies along main axes of the moving object. Due to imprecise sensor-platform, the alignment measured acceleration deviates from the true one and causes a deviation in position as well. This can be reduced by a successive alignment procedure which was not the subject of this analysis.

TABLE XI
POSITION DETERMINATION IN PLATFORM FRAME BEFORE AND AFTER CALIBRATION USING SEMS GOT FROM LM AND TS ALGORITHMS FOR CXL02LF3 ACCELEROMETER; $\delta_X, \delta_Y, \delta_Z$—DEVIATIONS IN X, Y, Z AXES

Reference Angle θ; ϕ (deg)	Without Calibration δ_X; δ_Y; δ_Z (m)	LM Algorithm δ_x, δ_y, δ_z (m)	TS Algorithm δ_x, δ_y, δ_z (m)
0; 0	-2951; -339; -586	1668; -169; 15	1683; -190; 40
10; 0	-5867; -3609; -804	-3487; -3541; 32	-3628; -3561; 44
20; 0	-8388; -6863; -794	-6479; -6863; 162	-6534; -6824; 179
0; -10	-6187; 2908; -796	-3224; 3226; 103	-3773; 3198; 164
0; -20	-9345; 5971; 942	-6485; 5481; 210	-7059; -6455; 153
10; -10	-9140; -393; -1022	-1585; -158; 136	-1265; -184; 305
20; -20	-14242; -547; -1202	-1314; -182; 336	-1273; -205; 610

VI. CONCLUSION

The main aim of this paper was to prove the effectiveness of the calibration approach, which does not need to use precise positioning devices and thus is not expensive and time-consuming. These characteristics are the main benefits of the proposed approach. Based on Levenberg–Marquardt (LM) and Thin-Shell (TS) algorithms we evaluated sensor error models (SEMs) for accelerometers of AHRS M3, ADIS16405, CXL02LF3 units and compared them with ones obtained from a Matlab *fminunc* function, which was used as a reference. We provided various analyses to show different aspects of the calibration such as reached values of SEM when LM or TS algorithm was applied, how many taken positions had to be used and how many iterations had to be performed to reach the required precision, or how greatly SEMs changed when they were compared with long-period perspectives. In all cases, the calibration had significant effect on results, e.g., according to Fig. 6 they were approx. 100 times improved. All results proved the suitability of the proposed calibration approach.

REFERENCES

[1] D. Jurman, M. Jankovec, R. Kamnik, and M. Topic, "Calibration and data fusion solution for the miniature attitude and heading reference system," *Sens. Actuators A, Phys.*, vol. 138, no. 2, pp. 411–420, Aug. 2007.

[2] M. Soták, "Coarse alignment algorithm for ADIS16405," *Przegląd elektrotechniczny*, vol. 86, no. 9, pp. 247–251, 2010.

[3] M. Sipos, P. Paces, M. Reinstein, and J. Rohac, "Flight attitude track reconstruction using two AHRS units under laboratory conditions," in *Proc. IEEE Sensors*, Nov. 2009, vol. 1–3, pp. 630–633.

[4] M. Reinstein, J. Rohac, and M. Sipos, "Algorithms for heading determination using inertial sensors," *Przeglad Elektrotechniczny*, vol. 86, no. 9, pp. 243–246, 2010.

[5] N. Barbour and G. Schmidt, "Inertial sensor technology trends," *IEEE Sensors J.*, vol. 1, no. 4, pp. 332–339, Dec. 2001.

[6] J. Včelák, P. Ripka, J. Kubik, A. Platil, and P. Kašpar:, "AMR navigation systems and methods of their calibration," *Sens. Actuators A, Phys.*, vol. 123–124, pp. 122–128, 2005.

[7] Z. Syed, P. Aggarwal, C. Goodall, X. Niu, and N. El-Sheimy, "A new multi-position calibration method for MEMS inertial navigation systems," *Meas., Sci., Technol.*, vol. 18, no. 7, pp. 1897–1907, Jun. 2007.

[8] S. P. Won and F. Golnaraghi, "A triaxial accelerometer calibration method using a mathematical model," *IEEE Trans. Instrum. Meas.*, vol. 59, no. 8, pp. 2144–2153, Aug. 2010.
[9] S. Luczak, W. Oleksiuk, and M. Bodnicki, "Sensing tilt with MEMS accelerometers," *IEEE Sensors J.*, vol. 6, no. 6, pp. 1669–1675, Dec. 2006.
[10] A. Kim and M. F. Golnaraghi, "Initial calibration of an inertial measurement unit using optical position tracking system," in *Proc. PLANS 2004: Position Location and Navigation Symp.*, 2007, pp. 96–101.
[11] D. H. Titterton and J. L. Weston, *Strapdown Inertial Navigation Technology*. London, U.K.: Peter Peregrinis, 1997, p. 238.
[12] V. Petrucha, P. Kaspar, P. Ripka, and J. M. G. Merayo, "Automated system for the calibration of magnetometers," *J. Appl. Phys.*, vol. 105, no. 7, 2009.
[13] I. Skog and P. Händel, "Calibration of a MEMS inertial measurement unit," presented at the XVII IMEKO World Congr., Rio de Janeiro, Brazil, 2006.
[14] T. Pylvanainen, "Automatic and adaptive calibration of 3D field sensors," *Appl. Math. Model.*, vol. 32, no. 4, pp. 575–587, Apr. 2008.
[15] S. Bonnet, C. Bassompierre, C. Godin, S. Lesecq, and A. Barraud, "Calibration methods for inertial and magnetic sensors," *Sens. Actuators A, Phys.*, vol. 156, no. 2, pp. 302–311, Dec. 2009.
[16] M. Reinstein, M. Sipos, and J. Rohac, "Error analyses of attitude and heading reference systems," *Przeglad Elektrotechniczny*, vol. 85, no. 8, pp. 114–118, 2009.
[17] J. Včelák, V. Petrucha, and P. Kašpar, "Electronic compass with miniature fluxgate sensors," *Sensor Lett.*, vol. 5, no. 1, pp. 279–282, 2007.
[18] B. M. Wilamowski and H. Yu, "Improved computation for Levenberg & Marquardt training," *IEEE Trans. Neural Netw.*, vol. 21, no. 6, pp. 930–937, Jun., 2010.
[19] L. S. H. Ngia and J. Sjoberg, "Efficient training of neural nets for nonlinear adaptive filtering using a recursive Levenberg–Marquardt algorithm," *IEEE Trans. Signal Process.*, vol. 48, no. 7, pp. 1915–1927, Jul. 2000.
[20] A. Ranganathan, The Levenberg–Marquardt Algorithm. Atlanta, GA, College of Computing, Georgia Inst. Technol., 2004.
[21] L. M. Saini and M. K. Soni, "Artificial neural network based peak load forecasting using Levenberg–Marquardt and quasi-Newton methods," *Proc. IEEE Proc.*, vol. 149, no. 5, pp. 578–584, 2002, Generation, Transmission and Distribution.
[22] H. Gavin, "The Levenberg–Marquardt method for nonlinear least squares curve-fitting problems," Dept. Civil and Environmental Engineering, Duke Univ. Durham, NC, 2011.
[23] K. Madsen, H. B. Nielsen, and O. Tingleff, *Methods for Non-Linear Least Squares Problems*, 2nd ed. Lyngby, Denmark: Tech. Univ. Denmark, 2004, Informatics and Mathematical Modelling.
[24] M. Soták, M. Sopata, R. Bréda, J. Roháč, and L. Váci, Navigation System Integration, Košice: Robert Breda. Kosice, Slovak Republic, 2006.
[25] E. L. Renk, W. Collins, M. Rizzo, F. Lee, and D. S. Bernstein, "Calibrating a triaxial accelerometer-magnetometer—Using robotic actuation for sensor reorientation during data collection," *IEEE Control Syst. Mag.*, vol. 25, no. 6, pp. 86–95, Jun. 2005.
[26] Find Minimum of Unconstrained Multivariable Function—MATLAB [Online]. Available: http://www.mathworks.com/help/toolbox/optim/ug/fminunc.html [Accessed: 29-Apr-2011].
[27] Attitude and Heading Reference System, Innalabs AHRS M3, Datasheet [Online]. Available: http://www.galaxynav.com/AHRS_M3_datasheet_2008.10.08.pdf [Accessed: 29-Apr-2011].
[28] ADIS16405 | High Precision Tri-Axis Gyroscope, Accelerometer, Magnetometer | Inertial Sensors | Sensors | Analog Devices [Online]. Available: http://www.analog.com/en/sensors/inertial-sensors/adis16405/products/product.html [Accessed: 24-Apr-2011].
[29] Crossbow Accelerometers, High Sensitivity, LF Series [Online]. Available: http://www.datasheetarchive.com/cxl-datasheet.html [Accessed: 29-Apr-2011].
[30] MicroStrain: Inertial Systems—3DM-GX2® [Online]. Available: http://www.microstrain.com/3dm-gx2.aspx [Accessed: 29-Apr-2011].
[31] STEVAL-MKI062V2—STMicroelectronics [Online]. Available: http://www.st.com/internet/evalboard/product/250367.jsp [Accessed: 29-Apr-2011].
[32] J. Vcelak, P. Ripka, A. Platil, J. Kubik, and P. Kaspar, "Errors of AMR compass and methods of their compensation," *Sens. Actuators A, Phys.*, vol. 129, no. 1–2, pp. 53–57, 2006.

Martin Šipoš was born in Prague, Czech Republic, in 1983. He received the Engineering degree (M.Sc. equivalent) with a specialization in aeronautical instrumentation systems from the Department of Measurement, Faculty of Electrical Engineering, Czech Technical University, Prague, in 2008, where he is currently pursuing the Ph.D. degree in the Laboratory of Aeronautical Information Systems with a dissertation titled "Improvement of INS accuracy using alternative sensors."

His main research activity is INS, GPS, Earth's magnetic field navigation, and adaptive filtering.

Pavel Pačes (M'09) was born in Prague, Czech Republic, in 1978. He received the M.Sc. degree in aerospace engineering from the Faculty of Electrical Engineering, Czech Technical University, Prague, in 2005, and the Ph.D. degree from the air traffic control program with two patent applications in 2011.

He gained industrial experience as a programmer and tester of avionics instruments at DevCom, as an HW and SW developer for the Aircraft Research Institute of the Czech Republic, etc.

Dr. Pačes is member of the IEEE Aerospace and Electronic Systems Society and the American Institute of Aeronautics and Astronautics. Currently, he is a National Point of Contact for the Space Generation Advisory Council in support of the United Nations Program on Space Applications.

Jan Roháč received the Ing. degree (M.Sc. equivalent) and the Ph.D. degree from the Faculty of Electrical Engineering (FEE), Czech Technical University (CTU), Prague, Czech Republic, in 2000 and 2005, respectively.

He is an Assistant Professor and Researcher with the Department of Measurement, FEE, CTU. He teaches courses concerning aircraft and space systems. His main research interests are in avionics, space technologies, inertial navigation systems, GNSS, AOCS, sensors and their modeling, and data processing methods.

Dr. Roháč is a member of the Czech Aeronautical Society and one of the representatives of the CTU in the PEGASUS Network.

Petr Nováček was born in 1983 in Prague, Czech Republic. He received an Ing. degree (M.Sc. equivalent) with a specialization in aeronautical instrumentation systems from the Department of Measurement, Faculty of Electrical Engineering (FEE) Czech Technical University (CTU), Prague, in January 2010. He is currently pursuing the Ph.D. degree under Prof. P. Ripka at the FEE, CTU.

His research interests include sensors (magnetometers and accelerometers), electronics of sensors, digital signal processing, and microcontroller design for low-cost precise navigation systems.

4.2. ESTIMATION OF STOCHASTIC SENSOR PARAMETERS

Roháč, J. - Šipoš, M. - Šimánek, J. - Tereň, O.: Inertial Reference Unit in a Directional Gyro Mode of Operation. In IEEE SENSORS 2012 - Proceedings [CD-ROM]. Piscataway: IEEE Service Center, 2012, p. 1356-1359. ISBN 978-1-4577-1765-9. (IF: --)

Inertial Reference Unit in a Directional Gyro Mode of Operation

Jan Rohac[1], Martin Sipos[2], Jakub Simanek[3], Ondrej Teren[4]
Department of Measurement, Faculty of Electrical Engineering
Czech Technical University in Prague
Prague, Czech Republic
E-mail: xrohac@fel.cvut.cz[1], martin.sipos@fel.cvut.cz[2], simanjak@fel.cvut.cz[3], terenond@fel.cvut.cz[4]

***Abstract*—This paper deals with a cost effective inertial reference unit design providing both MEMS based navigation unit calibration means and an attitude and heading measurement system in a directional gyro mode of operation. A main contribution of this paper is a novel design of such a universal system not primary relying on a magnetometer (MAG) or GPS aiding. Generally, without this aiding Attitude and Heading Reference Systems (AHRSs) are not directionally stable. Also, having precise reference in a calibration process is crucial and in most cases the solution is expensive. We thus replaced an expensive solution of both applications with the cost effective one suiting mentioned purposes using only one single axis fiber optic gyro supported by an inertial MEMS based aiding system. We also proposed a calibration procedure and blended solution to provide both stable and reliable navigation data with accuracy better than 5 deg/h specified by the TSO-C5e.**

I. INTRODUCTION

A rapid proliferation of low-cost inertial sensors based on MEMS (Micro-Electro-Mechanical Systems) technology in recent years enables low-cost MEMS based navigation systems application in many areas, e.g. in robotics, aeronautics as well as in automotive industry. MEMS sensors have numerous advantages such as small size, weight, price, and power consumption [1]. On the other hand, they suffer from a high drift rate, noise, misalignment, low sensitivity, etc., which have to be dealt with via calibration, sensor error modeling, and data fusion processes [2]. Our previous work has included the research of suitable calibration methods for both accelerometers (ACCs) [3, 4] and angular rate sensors (ARSs). For calibration purposes a precise reference is required. For ACC calibration the gravitational force is generally used; however, in the case of ARSs expensive turntables are commonly used. In our previous work we aimed at cheap solutions and thus we used only a theodolite as the reference [5]. Nevertheless, this solution was not universal. Therefore, our motivation was to propose a new design providing all-in-one calibration procedure, in which all sensors (ACCs, ARSs, and MAGs) could be calibrated at once. The other motivation for our research was to design a cost-effective AHRS directionally stable in certain boundaries primary dependent just on inertial sensors and not on supportive MAGs or GPS, which are generally used for yaw angle stabilization and compensation. Therefore, yaw angle evaluation is a main concern of this paper.

This research has been partially supported by the research program TA CR Alfa No. TA02011092 "Research and development of technologies for radiolocation mapping and navigation systems", partially by Grant Agency of the Czech Technical University in Prague grant No. SGS10/288/OHK3/3T/13, and partially by Czech Science Foundation project 102/09/H082.

II. CONCEPT OF THE INERTIAL REFERENCE UNIT

A proposed Inertial Reference Unit (IRU) was designed for two purposes. The first one was to have a means for MEMS based angular rate sensors calibration. This task could be fulfilled by utilization of only a Fiber Optic Gyro (FOG) KVH DSP3100 supplemented by an electrolytic tilt module (ETM) EZ-TILT-2000; nevertheless, the IRU further consisted of additional Inertial Measurement Unit (IMU) formed by 3 axial accelerometer and angular rate sensor. In this case we used ADIS16355 from Analog Devices Ltd. The reason for the IMU implementation was mainly because of the other application using the IRU as a navigation unit for a real-time attitude and heading estimation.

All implemented measurement systems were connected with a main control unit which synchronized data flow, processed the data, and via CAN bus transmitted them out. The IRU realization and its principle scheme are shown in Fig. 1 and Fig. 2. The IRU was also capable to link a GPS receiver and magnetometer via RS232 when full navigation with attitude, speed, and position estimation was required. Even if IRU algorithms were autonomously modified according to linked measurement systems, the basis and obligatory set of systems was FOG, ETM, IMU, and CU.

Figure 1. The system for calibration purposes and real-time attitude and heading estimation: (FOG-fibre optic gyro, ETM-electrolytic tilt module, IMU-inertial measurement unit, CU-control unit).

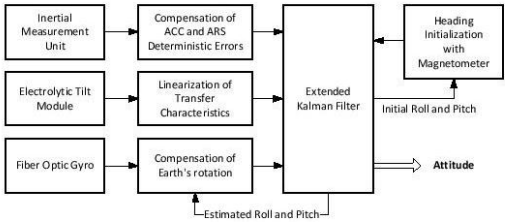

Figure 2. Principle scheme of the proposed inertial reference unit

A. Sensors' Noise Parameter Estimation

From a stochastic point of view we compared the FOG performance with other representatives MEMS based angular rate sensors via Allan Variance analysis (AVAR), see Fig. 3. It is a time-domain approach to analyze long time data series from noise terms point of view. The AVAR was introduced by D. W. Allan in 1966 in [6] originally analyzing clock stability; however, later on it became useful in inertial sensors' parameter estimation and also included in IEEE Standards [7, 8]. Generally, the total error can be classified as a sum of individual independent noise errors [8] and the total variance can be expressed as

$$\sigma^2_{total} = \sigma^2_Q + \sigma^2_{ARW} + \sigma^2_{BIN} + \sigma^2_{RRW} + \sigma^2_{RR} \qquad (1)$$

where lower indices denote: *Q*-quantization noise, *ARW*-angular/velocity random walk, *BIN*-bias instability, *RRW*-rate/acceleration random walk, and *RR*-rate ramp.

B. Unit Calibration and Deterministic Error Estimation

Deterministic errors are those, which can be considered constant in time. Because the IMU is formed by orthogonal three-axis accelerometer and angular rate sensor frame we had to take into account angles of the frame misalignment as well as scale factor (SF) errors. In [3, 9] the methodology of calibration procedures can be found in more details; however, in this case for the IMU calibration we used 9-state error model for the acceleration frame. In the case of angular rate sensors no scale factor and misalignment compensations were applied due to the fact that a stand-alone integration process in the attitude estimation would have caused unbound error if the attitude correction coming from ETM and accelerometers were not applied.

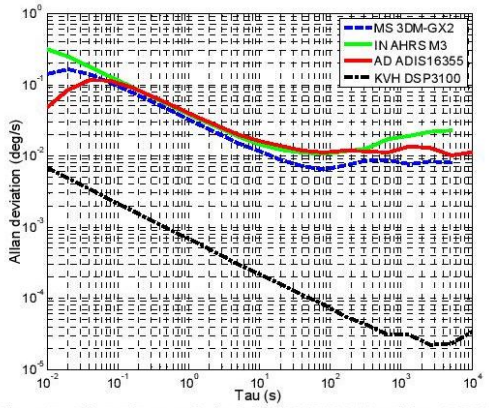

Figure 3. Allan variance analysis of the KVH DSP3100 and three MEMS gyros forming a part of AHRS M3, 3DM-GX2, and ADIS16355 unit.

In the case of the ETM calibration we used precise MEMS base inclinometer Clinotronic PLUS as a reference. The calibration was done in the range of ±25 deg. For the best fitting procedure we divided the whole range on three parts according to the deviation progress, as shown in Fig. 4, and then we made an approximation by three-ordered polynomials. The deviation progress of θ angle after SF compensation is also shown in Fig. 4. The results are summarized in Table I.

TABLE I. ETM DEVIATION BEFORE AND AFTER SF COMPENSATION

	Before compensation		After compensation	
	Max. dev (deg) range ±10 deg	Max. dev (deg) range ±25 deg	Max. dev (deg) range ±10 deg	Max. dev (deg) range ±25deg
φ	1.45	5.00	0.03	0.15
θ	0.83	4.68	0.04	0.16

Since the manufacturer of the FOG states only the uncertainty in the linearity of the scale factor, we performed several multiple-turns experiments exploiting the horizontally aligned FOG mounted on a theodolite and we estimated a scale factor. Using a precise reference angle from the theodolite and the FOG angle integrated during turns, we estimated the FOG scale factor (SF) as an optimized average value for all performed experiments keeping a rate range of ±150 deg/s. After SF compensation we reached resulting error for all experiments being less than 0.05%. Table II shows two different results for clockwise (CW) and counter-clockwise (CCW) experiments and original and estimated scale factor.

III. PERFORMANCE OF THE INERTIAL REFERENCE UNIT

A. Initialization

Initial attitude, defined by Euler angles as roll φ and pitch θ, was determined as a weighted average of results of a leveling algorithm using measured angles by ETM and measured acceleration, see (2).

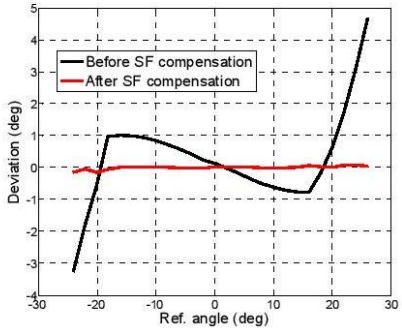

Figure 4. ETM deviation of θ angle before and after SF compensation.

TABLE II. FOG CALIBRATION USING THEODOLITE

Experiment *Duration*	SF orig. SF estimated	Ref. angle (deg)	FOG angle (deg)	Error (%)
CW 15 turns *204 s*	1	5407.97	5350.43	1.06
	1.011	5407.97	5409.29	0.03
CCW 30 turns *315 s*	1	10794.48	10680.06	1.06
	1.011	10794.48	10797.53	0.03

$$\varphi = \operatorname{atan}(a_x, -a_z)w + \varphi_{ETM}(1-w),$$
$$\theta = \operatorname{atan}\left(-a_y, \sqrt{a_x^2 + a_z^2}\right)w + \theta_{ETM}(1-w), \quad (2)$$

where a_x, a_y, a_z are measured accelerations, φ_{ETM}, θ_{ETM} denote the angles measured by the ETM, and w is the weighting coefficient.

B. System Model and Signal processing

First of all, it was required to define the vector of angular rates. Our system utilized only one FOG whose sensitive axis was vertical. Along the other axes the IMU sensors were used. The vector was excluded by Earth rotation determined based on actual geographical latitude, which can be done as

$$\boldsymbol{\omega}_{nb}^b = \begin{bmatrix} \omega_{ARS_x} \\ \omega_{ARS_y} \\ \omega_{FOG_z} \end{bmatrix} - \boldsymbol{C}_n^b \begin{bmatrix} \omega_{ie}\cos\phi \\ 0 \\ -\omega_{ie}\sin\phi \end{bmatrix}, \quad (3)$$

where ω_{ARS_x}, ω_{ARS_y} are angular rates measured by the IMU, ω_{FOGz} is an angular rate along z axis measured by the FOG, ω_{ie} represents the Earth rotation rate. Transformation matrix defined as

$$\boldsymbol{C}_n^b = \begin{bmatrix} c_\theta c_\psi & -c_\varphi s_\psi + s_\varphi s_\theta c_\psi & s_\varphi s_\psi + c_\varphi s_\theta c_\psi \\ c_\theta s_\psi & c_\varphi c_\psi + s_\varphi s_\theta s_\psi & -s_\varphi c_\psi + c_\varphi s_\theta s_\psi \\ -s_\theta & s_\varphi c_\theta & c_\varphi c_\theta \end{bmatrix}^T, \quad (4)$$

where $c_\varphi = \cos\varphi$, $s_\varphi = \sin\varphi$, transforms the Earth rate from the navigation frame into the body frame.

The attitude estimation propagated in discrete time steps as follows

$$\begin{bmatrix} \varphi \\ \theta \\ \psi \end{bmatrix}_k = \begin{bmatrix} \varphi \\ \theta \\ \psi \end{bmatrix}_{k-1} + T_s \begin{bmatrix} 1 & \sin\varphi\tan\theta & \cos\varphi\tan\theta \\ 0 & \cos\varphi & \sin\varphi \\ 0 & \sin\varphi\sec\theta & \cos\varphi\sec\theta \end{bmatrix} \boldsymbol{\omega}_{nb}^b \quad (5)$$

where T_s is the sampling period.

The Eq. (5) was used under dynamic conditions which were recognized according to the norm of the angular rate vector and comparing its value with a preset limit. When null or slow dynamics was recognized for a period of at least 5 seconds we used Euler angles evaluated from (2) as a new attitude value.

Since we utilized a suboptimal Kalman filter (KF) for data acquisition and fusion, we applied first-order low-pass filter (LPF) for all data to restrict the dynamics and a noise. A continuous-time transfer function of LPF can be defined as

$$H(s) = \frac{y(s)}{u(s)} = \frac{1}{1+s\tau} \quad (6)$$

where τ is a time constant, $y(s)$ denotes the Laplace transform of the filter output, and $u(s)$ corresponds to the input. The time constant of the LPF is related to its cut-off frequency f_m defined as

$$f_m = \frac{1}{2\pi\tau} \quad (7)$$

A discrete form of the LPF can be derived from (6) using difference equation and can be written as

$$y(k) = (1-a)\,y(k-1) + a\,u(k) \quad (8)$$

where parameter $a = T_s/(T_s+\tau)$, k denotes the count of time steps, and T_s is a sampling period.

IV. MEASUREMENTS AND RESULTS

The calibration platform is still in a construction process, and therefore we present only results related to the other application of IRU, which is a navigation unit providing attitude and heading evaluation.

To verify the accuracy of the IRU in a navigation unit function we performed several experiments. These experiments were supposed to test the IRU under different conditions. The first experiment lasted 72 minutes and we used a small four-wheel bubble car driven by hands as a carrier of the IRU. The experiment consisted in round trip movement (15 turns/measurements in CCW direction), in which before each turn steady conditions were held for 120 s. In these steady conditions we estimated the reference yaw angle with a laser pointing device. The accuracy of this reference was 0.024 deg. Fig. 5 shows the deviation progress of estimated FOG based yaw angle related to initial angle after each turn performed with the IRU. The leveling of IRU was done by ACC, ACC fused with ETM, or ETM alone. It corresponded to cases when into (2) the parameter w equaled to 1, 0.5, and 0. The inaccuracy of IRU yaw angle after one hour of the experiment was in the case of ACC leveling was-1.982 deg, in the case of ACC/ETM leveling -1.319 deg, and when only ETM was used -0.747 deg. According to reached results the usage of only ETM for leveling had the best accuracy; however, we still had to use ACC to extend the ETM range of angles, which was only ± 25 deg along both axes, as well as to quicken a reaction time of algorithms detecting the dynamic conditions and affecting the attitude evaluation process. We had to handle a slow reaction of ETM, whose electrolyte in comparison to the standard one had increased density about 15%, which provided better immunity to vibration but also slower reaction on attitude changes.

The second experiment was supposed to verify the IRU immunity to vibration when the IRU was mounted in a car. The car was static, only an engine RPM (revolution per minute) was changing. The impact of vibration on FOG angular rate measurements and consecutively on evaluated yaw angle is shown in Fig. 6. It shows three intervals in which the engine was switched on. At the beginning of each interval a high impact of engine ignition was observed. Within the first interval the RPM was held at the level about 1200, within the second one it was in the range of (500-800) RPM, and within the third one about 3200 RPM.

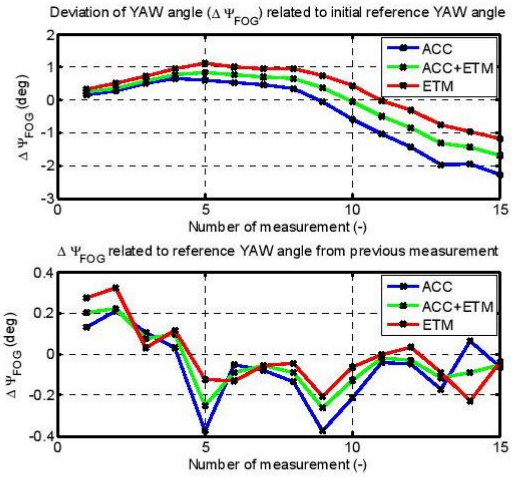

Figure 5. Deviations of yaw angle from the reference related to initial reference yaw angle (top figure) and related to previous measurement (bottom figure). The ACC, ACC+ETM and ETM denote the sensors' data used for leveling and correction of roll and pitch angles determined by the integration of angular rates.

The last experiment was performed under real traffic conditions and we observed the IRU yaw angle progress and compared it with the azimuth of straightaway laps of the streets determined from Google maps. The comparison is summarized in Tab. III. The first column specifies time intervals in which the azimuth of street laps was approximately constant. The speed was kept under the speed limit which was 50 km/h. The relative error was calculated as a difference between the map azimuth and an evaluated yaw angle all divided by 180 deg, which would correspond to 100 % error.

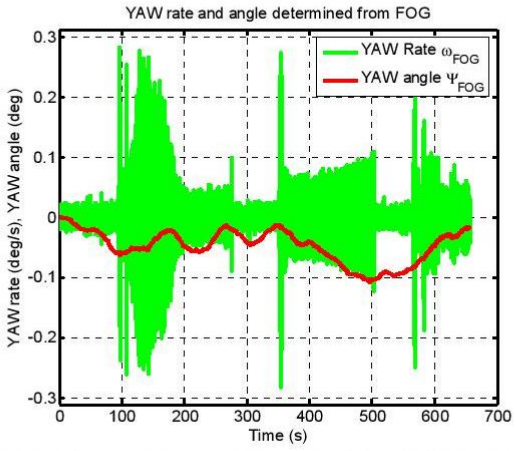

Figure 6. The FOG yaw rate measured during car vibration test and corrected according to (5); the yaw angle obtained by numerical integration of FOG yaw rate.

TABLE III. FOG YAW VERSUS MAP AZIMUTH (PERSONAL CAR EXPERIMENT)

Time (min)	Map azimuth (deg)	FOG yaw (deg)	Error (%)
3.0-4.3	174.0	172.5	0.8
4.9-6.0	265.4	264.5	0.3
9.6-11.5	254.4	252.6	0.7
16.3-18.2	273.5	271.6	0.7
16.2-21.6	137.2	135.6	1.1
28.8-23.0	239.7	237.6	0.9

V. CONCLUSIONS

We designed a cost effective system suitable for both calibration purposes and real-time attitude and heading estimation. The calibration platform was still in construction process, and therefore we focused on the system calibration and its verification when attitude and heading were required. In this system the evaluation of yaw angle corresponding to azimuth was challenging mainly because GPS or magnetometer was not used. The functionality thus primary relied on a vertically orientated fiber optic gyro KVH DSP3100 supplemented by an inertial measurement unit ADIS16355 and dual axis electrolytic tilt module EZ-TILT-2000. All data readings were synchronized and processed by a control unit utilizing a STM32F407 microcontroller. To prove the suitability of the fiber optic gyro we used Allan variance analysis and we compared reached results with other commercially available MEMS based gyros. To determine deterministic system errors we calibrated all subparts of the system and evaluated scale factor and misalignment compensation parameters. Then we performed three types of experiments to verify the whole system performance. According to reached results we can say that the proposed inertial reference unit satisfied the requirements of TSO-C5e with inaccuracy better than 5 deg/h.

REFERENCES

[1] N. Barbour and G. Schmidt, "Inertial sensor technology trends", IEEE Sensors Journal, vol. 1, no. 4, pp. 332-339, Dec. 2001.

[2] M. Soták, "Coarse alignment algorithm for ADIS16405", Przegląd elektrotechniczny, vol. 9, no. 86, pp. 247-251, 2010.

[3] M. Šipoš, P. Pačes, J. Roháč and P. Nováček, "Analyses of Triaxial Accelerometer Calibration Algorithms", IEEE Sensors Journal, vol. 12, no. 5, pp. 1157-1165, May 2012.

[4] M. Šipoš, J. Roháč and P. Nováček, "Improvement of Electronic Compass Accuracy Based on Magnetometer and Accelerometer Calibration", Acta Physica Polonica A, vol. 121, no. 4, pp. 945-949, Apr. 2012.

[5] M. Šipoš and J. Roháč, "Calibration of Tri-axial Angular Rate Sensors", Measurement, Diagnostics, Dependability of Aircraft Systems 2010, University of Defence, Brno, Czech Republic, pp. 148-152, 2010.

[6] Allan, D.W. (1966) 'Statistics of Atomic Frequency Standards', Proceedings of the IEEE, vol. 2, no. 54, February, pp. 221-230.

[7] 'IEEE Std. 528', IEEE Standard for Inertial Sensor Terminology, Available: ISBN 0-7381-3022-2.

[8] 'IEEE Std. 647', IEEE Standard Specification Format Guide and Test Procedure for Single-Axis Laser Gyros, pp. 68-80.

[9] M. Šipoš, J. Roháč and P. Nováček, "Analyses of Electronic Inclinometer Data for Tri-axial Accelerometer's Initial Alignment", Przeglad Elektrotechniczny, vol. 88, no. 01a, pp. 286-290, Jan. 2012.

4.3. NAVIGATION AND ITS RELATION WITH MEASUREMENT FRAMES

Roháč, J.: Accelerometers and an Aircraft Attitude Evaluation. In IEEE Sensors 2005 - The 4-th IEEE Conference on Sensors. Irvine, CA: IEEE Sensors, 2005, p. 784-788. ISBN 0-7803-9057-1.

Accelerometers and an aircraft attitude evaluation

Jan ROHAC
Dept. of Measurement, Faculty of Electrical Engineering
Czech Technical University in Prague
Prague, Czech Republic
xrohac@fel.cvut.cz

***Abstract* - The paper describes a method that enables a usage of low-cost inertial sensors, such as angular rate sensors and accelerometers, in a system of aircraft attitude evaluation. The method depicts a suitability of using accelerometers to restrict an influence of angular rates' integration on a precision of the attitude assessment. The method was verified with a simulation in MATLAB-Simulink environment and with various measurements. The method principles, simulation and measurement results are presented.**

I. INTRODUCTION

There exists a traditional approach to evaluate an aircraft attitude. The evaluation is based on an angular rates sensing, its subsequent recalculation into the reference framework to get derivative of Euler angles, see equations (1) to (3), and finally on those angles integration.

$$\dot{\varphi} = \omega_x + \omega_y \sin\varphi \tan\theta - \omega_z \cos\varphi \tan\theta \quad (1)$$

$$\dot{\theta} = \omega_y \cos\varphi - \omega_z \sin\varphi \quad (2)$$

$$\dot{\psi} = -\omega_y \frac{\sin\varphi}{\cos\theta} + \omega_z \frac{\cos\varphi}{\cos\theta} \quad (3)$$

Mentioned procedure is useful only if very precise and time-steady measurement is available, for instance if laser or dynamic-tuned gyros are utilized. A drift of these sensors is approximately 10^{-2} deg/hour. In case of using low-cost sensors, the integration causes time invariant and growing error, because of a low sensors' resolution and their drifts. Particularly, a measured drift of an angular rate sensor ENV-05D, from MURATA manufacturer, is 4×10^{-5} deg/s. In accordance with the simulated motion with 60 m/s of forward speed and an drift of angular rate sensor, that is placed in vertical axis, whose value is 4×10^{-5} deg/s, it is possible to declare that the drift causes the error of velocity in y-axis, whose value reaches 20 m/s in less than 17 minutes. It implies the error of position in the same axis of 7500 m. In x-axis the error of velocity reaches 4 m/s in the same time duration and it evokes the error of position in x-axis of 800 m. The axes x and y correspond to a reference frame where the simulation was realized (see Fig. 1). In the same time the drift causes an error in angle evaluation of 20 degrees. These errors are unacceptable.

However, a question is if there is possible to use any alternative information source to make corrections. Of course, there exists a method which uses GPS receivers to correct the attitude and the position. The position can be determined with not permanent growing error [7]. Unlikely, in attitude evaluation there are some restrictions, such as a wing length to provide enough distance among GPS receivers specially placed on an aircraft fuselage. Other way, the attitude can be evaluated with magnetometer as well. However, the method has also many restrictions and can be influenced by other quantities that do not correspond to aircraft motion. Therefore, there was an effort to search for an untraditional approach in an aircraft attitude evaluation which would use only inertial sensors and would be accurate with an error less than 1 deg. with no regard to time of a flight.

II. THE METHOD PRINCIPLES

The main idea of the method is to use accelerometers for the attitude evaluation. The evaluation is based on a distribution of gravitational acceleration into accelerometers framework. The distribution changes accordingly to an aircraft attitude. To optimize sensitive axes of accelerometers for low-cost sensors usage with a resolution up to 1 mg there is convenient to change an orientation of accelerometers' framework as well. The proposed accelerometers framework has two alternatives, see Fig. 2b,c. In Fig. 2a there is shown a traditional configuration. Fig. 2b shows an accelerometers' frame transformation for 3-axis accelerometer and Fig. 2c depicts the cluster configuration for two 2-axis accelerometers. A purpose of the transformation is to reach better accelerometers' framework parameters in the attitude evaluation in horizontal flight and in its close states. Those parameters are:

- A lower sensitivity of the attitude evaluation on accelerometers' drifts. See Fig. 3, where horizontal axes correspond to a sensor reference voltage, which is an output voltage for a zero influence of a sensing quantity. For the sensor CLX02LF

0-7803-9056-3/05/$20.00 © 2005 IEEE.

the value is 2.5 V, but it can change in a range of ±0.1 V. Vertical axes correspond to the evaluated attitude. Graphs in Fig. 3 show that the attitude errors are smaller in modified frameworks than in the traditional configuration.

- A resolution increase of an accelerometer that is placed in a vertical axis of the traditional framework orientation (Fig. 2a). A reason is based on the fact that an accelerometer in that axis is influenced by a gravitational force with dependence on cosine function of the attitude. For small angles there are very small differences in sensed acceleration and in that way low-cost sensor with low resolution could not be able to sense those changes.

$$\theta = \sin^{-1}\left(\frac{0.7071(a_y + a_z) - a_x}{g\sqrt{2}}\right) \tag{4}$$

$$\varphi = \tan^{-1}\left(\frac{a_y - a_z}{0.7071(a_y + a_z) + a_x}\right), \tag{5}$$

where a_x, a_y, a_z correspond to gravitational acceleration in defined axes orientations.

The second transformation, based on Fig. 2c, consists of "x-z" plane rotation about -45 deg. along y-axis and "y-z" plane rotation about 45 deg. along x-axis. This configuration is more suitable for its easier mounting realization, but it is non-orthogonal. For this cluster configuration the pitch and roll angle can be evaluated accordingly to:

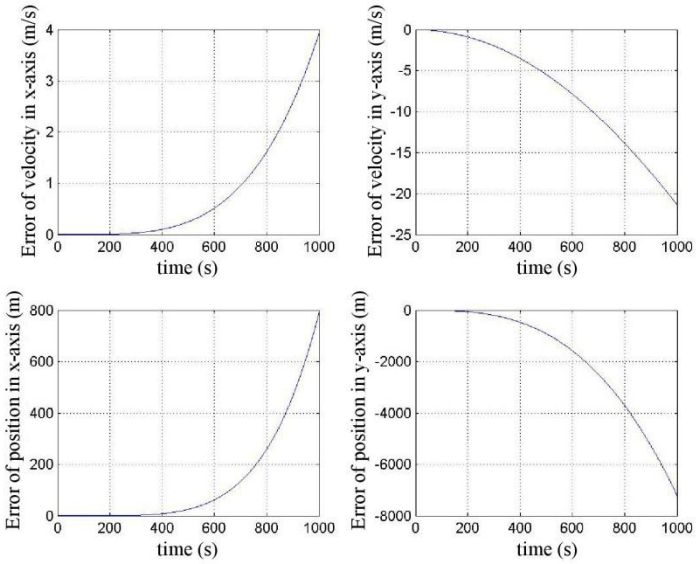

Figure 1. Simulated data of the errors caused by a drift of an angular rate sensor

Of course, accelerometers sense not just a gravitational acceleration, but a composition of gravitational, forward and centrifugal acceleration and acceleration caused by a wind impact. All of these, except the gravitational one, must be deducted from the total sensed acceleration before the attitude evaluation is processed. The attitude evaluation depends on an accelerometers configuration. The transformation which is determined for 3-axis accelerometer (Fig. 2b) consists of two rotations. The first one is along y-axis about -45 deg. and the other one along a new established x'-axis about 45 deg. For this configuration the pitch and roll angle can be evaluated accordingly to:

$$\theta = \sin^{-1}\left(\frac{x_2' - x_1'}{g\sqrt{2}}\right), \tag{6}$$

$$\varphi = \tan^{-1}\left(\frac{y' - z'}{x_1' + x_2'}\right), \tag{7}$$

where x_1', x_2', y', z' correspond to gravitational acceleration in defined axes orientations,
g is a magnitude of a vector of gravitational acceleration.

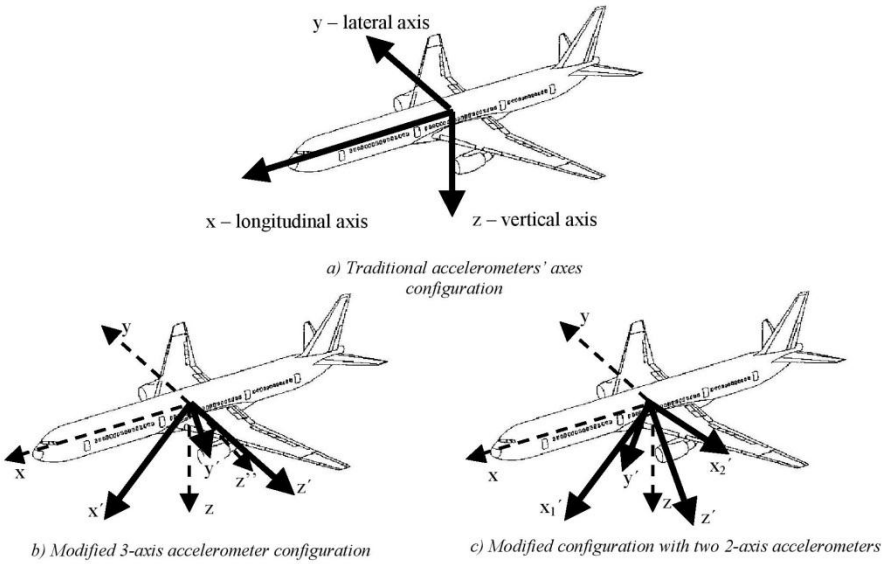

a) Traditional accelerometers' axes configuration

b) Modified 3-axis accelerometer configuration

c) Modified configuration with two 2-axis accelerometers

Figure 2. Accelerometers' framework orientation

The proposed method does not enable to determine yaw angle, which corresponds to a course of flight. This angle can be calculated via angular rate integration, sensed in vertical axis, or there must be used other source of information, for instance GPS receiver or a magnetometer. This feature predestinates the usage of this procedure only in systems of artificial horizon, because originally there was a task to design an autonomous unit which uses only primary inertial sensors, accelerometers and angular rate sensors. Angular rate sensors can not be omitted from the evaluation procedure, but the method tries to minimize a usage of angular velocities integration to get the attitude. The framework of these sensors lies in compliance with the main airplane framework, unlike the accelerometers' one.

The main part of the method relies on estimation of forward, centrifugal and wind impact acceleration. All these influences must be estimated before the attitude evaluation is processed. Centrifugal acceleration can be calculated as a vector multiplication of angular velocities and speed of motion and then deducted from the total sensed acceleration as the first in a row. Forward and wind impact acceleration can be evaluated under presumption that wind has null effect on an airplane in its longitudinal axis. The evaluation procedure traces acceleration changes in modified accelerometer framework and simultaneously calculates derivatives of forward and wind impact acceleration defined in the reference frame. These derivatives are integrated and converted into modified framework. Results are then deducted from the total sensed acceleration that is already free of centrifugal acceleration. The final result of this deduction is gravitational acceleration from which there is possible to evaluate the attitude. The integrator, used in this part of procedure, can be reset in case of null influence of forward and wind impact acceleration. The mentioned procedure is very effective and precise in all cases except the one that takes place during the attitude changes with simultaneous impact of a wind (turbulence). In this case, the precision decreases with angular rates growing. Therefore, in this case the attitude is evaluated from angular rate sensors with the integration. Under this condition a drift and low resolution of angular rate sensors could affect the precision of the evaluation. Therefore, the method utilizes two Kalman filters to restrict this undesired fact. When an airplane stops its attitude change the evaluation from acceleration has accuracy that corresponds to a resolution of accelerometers and previously determined attitude from angular rate sensing. The attitude changes do not last for a long time, and therefore small angular rate sensors' inaccuracies can not cause rapid increase of an error. When a wind impact is gone as well, the precision relies only on a resolution of accelerometers again. If accelerometers' resolution of 1 mg is considered, the attitude precision is 0.064 deg. and in case of 3 mg the precision is 0.192 deg, which is also sufficient.

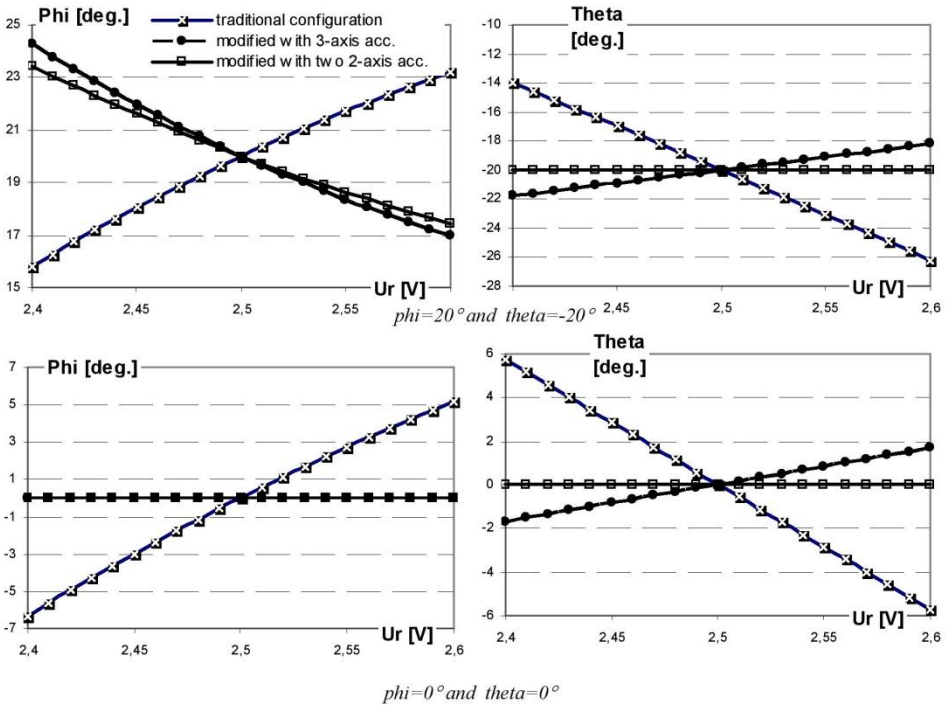

Figure 3. Dependence of the aircraft attitude on a reference voltage deviation

III. METHOD SIMULATION AND ITS RESULTS

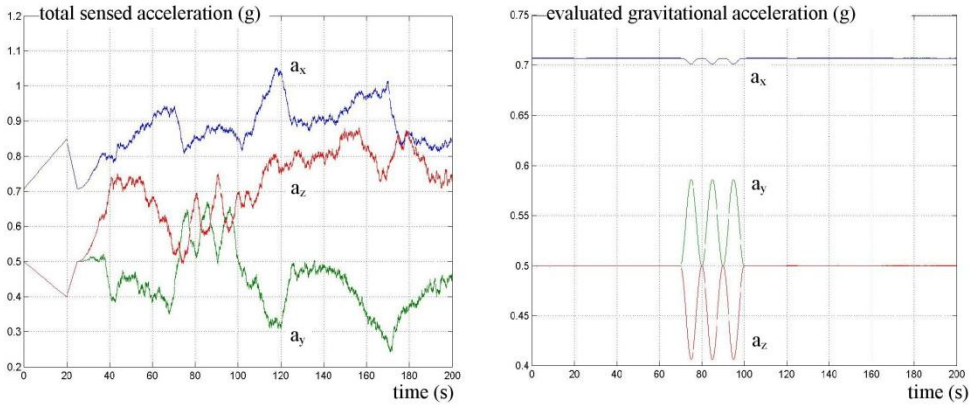

Figure 4. Simulated results of acceleration progresses

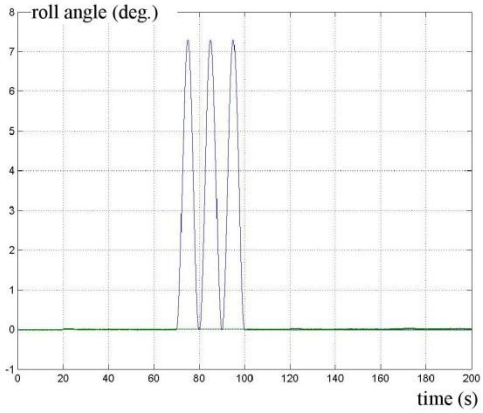

Figure 5. Simulated results of the aircraft attitude progress

In Fig. 4 and Fig. 5 there are shown results of simulation. The simulation included forward acceleration and a turbulence impact. A composition of these accelerations is visible in Fig. 4 – left. Fig. 4 – right shows a gravitational acceleration as a result of a deduction of an evaluated turbulence impact and forward acceleration from the total sensed one. Fig. 5 depicts a simulated attitude progress that corresponds to demands.

IV. MEASUREMENT RESULTS

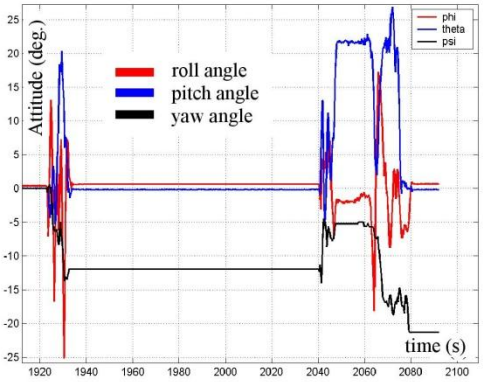

Figure 6. Evaluated attitude by the proposed method, which uses acceleration sensing

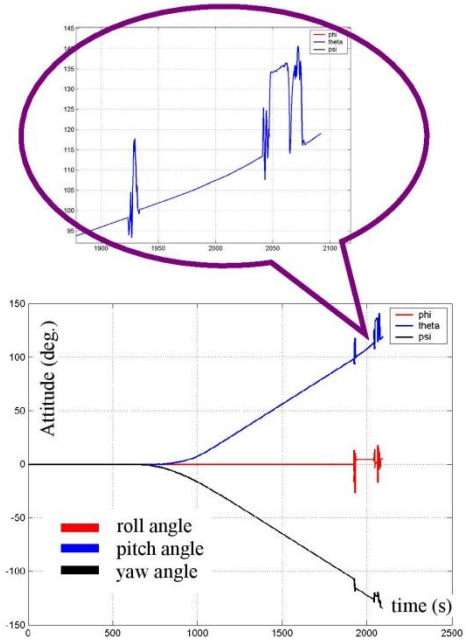

Figure 7. Evaluated attitude based on angular rate sensing

For the measurement there were used angular rate sensors ENV-05D (Murata manufacturer) and 3-axis accelerometer CLX02LF (Crossbow manufacturer). The used measurement unit is shown in Fig. 8. The attitude changes had to be slow, because of 7 Hz update rate of angular rate sensor. There were done various measurements and one measurement results are depicted in Fig. 6 and Fig. 7. In these figures there are shown differences in evaluated attitude that was got by the proposed method, which uses accelerometers, and the one which uses integration of angular velocities. The attitude in Fig. 7 is affected by drifts of angular rate sensors. Unlikely, the proposed method is clearly unaffected by this influence, as it is visible in Fig. 6.

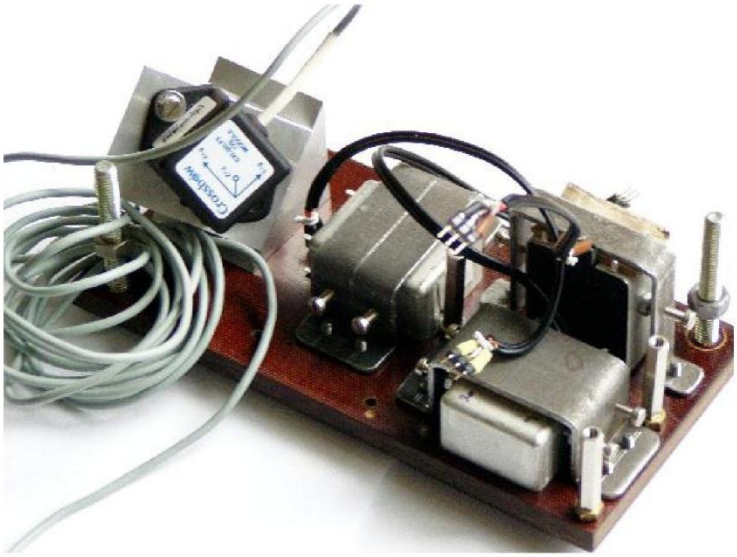

Figure 8. Measurement unit consisted of 3 angular rate sensors and 3-axis accelerometer

V. CONCLUSION

This paper describes a new approach to an aircraft attitude evaluation which utilizes low-cost inertial sensors. Stated method shows suitability of accelerometers' usage for the attitude evaluation and a correction of angular rate sensors via Kalman filtering. The method was verified with simulation in Matlab-Simulink and various measurements and results were presented. The method is mainly determined for an artificial horizon, but it could be also used in a low-cost inertial navigation unit, if the method is extended with GPS receiver or magnetometer implementation.

REFERENCES

[1] M. S. Grewal, A. P. Andrews: Kalman Filtering - Theory and Practice Using MATLAB, NY USA 2001

[2] R. M. Rogers: Applied Mathematics in Integrated Navigation Systems, Reston USA 2003

[3] M.Kayton and W.R.Fried: Avionics Navigation Systems (second edition), NY USA 1996

[4] D.H.Titterton and J.L.Weston: Strapdown Inertial Navigation Technology, London UK 1997

[5] Shmuel Merhav: Aerospace Sensor Systems and Applications, Springer, New York 1996

[6] J. A. Farrell, M. Barth: The Global Positioning System & Inertial Navigation, NY USA 1999

[7] M. Soták, M. Sopata: Integrácia INS a GPS, Vedecký časopis ACTA AVIONICA 8/S, ročník V., Košice, 2003, ISSN 1335-9479

[8] A. B. Chatfield: Fundamentals of High Accuracy Inertial Navigation, Reston USA 1997

4.4. PRINCIPLES OF NAVIGATIONAL DATA EVALUATION AND FUSION

Reinštein, M. - Roháč, J. - Šipoš, M.: Algorithms for Heading Determination using Inertial Sensors. Przeglad Elektrotechniczny. 2010, vol. 86, no. 9, p. 243-246. ISSN 0033-2097. (IF: 0.244)

Michal REINSTEIN, Jan ROHAC, Martin SIPOS
Czech Technical University in Prague

Algorithms for heading determination using inertial sensors

Abstract. *This paper describes the results of comparison analysis regarding three algorithms for heading determination using low-cost inertial sensors: the stand-alone strapdown approach, magnetometer aiding approach, and strapdown approach with errors modelled, estimated and compensated using Kalman filtering. Experimental testing with precise rotational tilt platform was performed. Error analysis was carried out to qualitatively evaluate the best approach intended for implementation into unmanned aerial systems for navigation purposes.*

Streszczenie. *W artykule przedstawiono analizę porównawczą trzech algorytmów szukania kursu nawigacji przy wykorzystaniu czujników inercyjnych: system strapdown, system ze wspomaganiem przez magnetometr, system strapdown z z kompensacją błędu przy wykorzystaniu filtru Kalmana. Przeprowadzono eksperymenty przy wykorzystaniu precyzyjnej platformy z możliwością nastawiania kąta. Oceniono błędy metody.* (***Algorytmy określania kursu nawigacji przy wykorzystaniu czujników inercyjnych***).

Keywords: Kalman filter, inertial navigation, complementary filtering.
Słowa kluczowe: kurs nawigacji, filtr Kalmana.

Introduction

Due to the recent advance in low-cost inertial sensors technology it has become increasingly interesting to construct inexpensive strapdown navigation systems [1]. These systems exploit a traditional concept of an Inertial Measuring Unit (IMU). It consists of three accelerometers to measure the translational acceleration that can be integrated to obtain velocity and position, and three angular rate sensors to measure the rotational motion in order to get the attitude. Such a basic concept is usually enhanced by advanced signal processing and estimation methods to allow sensor errors compensation and improvement in precision of navigation. Generally, this is usually achieved due to data fusion with other supporting multi-sensors systems, such as magnetometer, GPS, odometer etc. Even if the implementation depends on a particular application, this kind of systems can be applied in many areas. For example in a research, especially where autonomous navigation is desired, such as in unmanned vehicle systems (UVS) including automotive [2], [3] and airborne [4] applications, where estimation of displacement [5] and attitude [6] is carried out using various data fusion methods [7].

This paper is the direct continuation of the work presented in [8] which concerned the estimation and compensation of both the deterministic and the random errors that affect the inertial sensors outputs. We have implemented the proposed compensation and modelling mechanisms into Kalman filter (KF) [9], which was based on algorithms for computing the navigation variables, i.e. the position, velocity and attitude, from the accelerations and angular rates. Attitude and heading reference system (AHRS) 3DM-GX2 (MicroStrain) was utilized to provide raw inertial data.

Since precision in heading (or yaw angle in terms of Euler angles) determination is the most crucial issue for any UVS navigation application, we have performed a thorough laboratory comparison analysis of the three most common approaches: the strapdown mechanization algorithm using only inertial sensors [10], [11], the approach based on inertial sensors aided by 3 axial magnetometer, and the extended Kalman filter (EKF) algorithm for error estimation [12], [13]. A precise rotational tilt platform with resolution of 2.6 arcsec in heading was used for this purpose, see Fig 1.

The target UVS application in our case is the Bellanca Super Decathlon aircraft model (Hacker Model Production Inc.) as shown in Fig. 2.

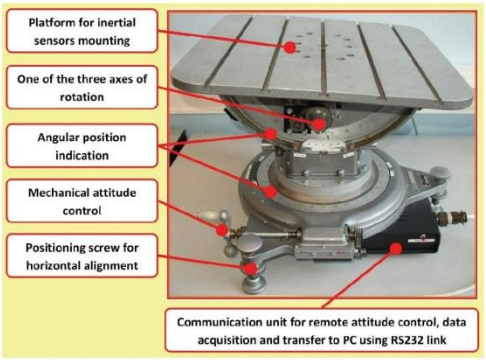

Fig.1. Rotational tilt platform for precise inertial sensors testing and calibration.

Fig.2. Bellanca Super Decathlon (Hacker Model Production Inc.) UAS for field-testing of proposed navigation systems.

Signal processing for inertial sensors

For experimental evaluation of the heading determination algorithms we have tested the three most common approaches.

The first approach is the strapdown mechanization of navigation equations. Strapdown mechanization is an algorithm that converts raw inertial data into navigation variables, i.e. velocity, position, and attitude, by successive integration and transformation to appropriated reference frame [14, pp. 29-39]. The proposed implementation composed different approaches published in [10] - [14], and [15, pp. 61-75], and used raw inertial data being measured with respect to the approximated inertial frame (IF) and

evaluated with respect to body frame (BF). We held to the forward-right-down convention for sensor orientations with rotations obeying the right-hand rule. The navigation variables were resolved in the local level North-East-Down (NED) navigation frame with the Earth-Centered-Earth-Fixed (ECEF) frame used as a transition frame. The differential navigation equations used are [13, p. 29]:

$$\dot{v}^n = C_b^n f^b + g^n - \left(2\omega_{ie}^n + \omega_{en}^n\right) \times v^n \quad (1)$$

$$\dot{C}_n^e = C_n^e \left[\omega_{en}^n \times\right] \quad (2)$$

$$\dot{h} = -v_d \quad (3)$$

$$\dot{C}_b^n = C_b^n \left[\omega_{in}^b \times\right] - \left[\omega_{in}^n \times\right] C_b^n \quad (4)$$

$$\omega_{in}^n = \omega_{ie}^n + \omega_{en}^n \quad (5)$$

where v^n – the velocity vector expressed in NED with v_d – the downwards component, C_b^n – the transformation matrix of the BF to NED, f^b – the measured acceleration in the BF, $\omega_{ib}{}^b$ – the measured angular rates in the BF, g^n – the normal gravity vector computed with respect to the position in the WGS84 reference ellipsoid as defined in [16], $\omega_{ie}{}^n$ – the Earth rate of rotation expressed in NED, $\omega_{en}{}^n$ – the transport rate of the NED with respect to ECEF expressed in NED, h – the altitude, C_n^e – the transformation matrix of the NED to the ECEF, and ()× denotes a skew symmetric matrix.

The structure of the strapdown mechanization algorithm is shown in Fig.3 as proposed in [12, p. 25]. The algorithm covers the following major computational steps: compensation of deterministic sensor errors (such as bias, scale factor and axes misalignment errors), for details see [8], [17]; numerical integration of the sensors output using second order Runge-Kutta method, as suggested in [18]; velocity update to obtain velocity vector; position update to obtain NED and ECEF position, and attitude update to obtain Euler angles (roll, pitch, and yaw). For computation of rotations we have implemented the quaternion approach to ensure compensation of conning effect in the output of angular rate sensors and sculling effect in the accelerometers outputs; for details see [19].

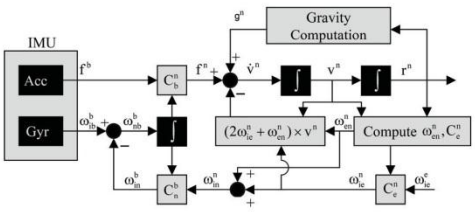

Fig.3. The scheme of strapdown mechanization [12, p. 25]

The second tested approach was based on 3-axial magnetometer aiding the IMU. The magnetometer provided additional information regarding the heading determined from the measurements of the Earth's magnetic field, i.e. the principle of operation of AHRS unit. In this case the heading measurements were given by the standard algorithm of the 3DM-GX2 unit provided by the manufacturer.

The third approach we tested was based on the strapdown mechanization but enhanced by the extended Kalman filter. The classical KF combines all available measurements with prior knowledge about the system and sensors and produces an optimal state estimate that statistically minimizes the error in least mean squares sense [20]. The EKF is a modification of this algorithm designed to deal with non-linearities of the system model equations; for details see [3], [13].

Compared to the KF, the EKF can estimate states of a nonlinear system model (but only up to a certain level of nonlinearity) by applying the Taylor series expansion on the nonlinear system equations and taking the first order terms (or higher). The probability density function is approximated by a Gaussian distribution, which can be completely characterized by its mean and covariance [20, pp. 176-182]. In our application we have proposed the structure of the navigation algorithm according to centralized closed loop complementary filter architecture; see Fig. 4.

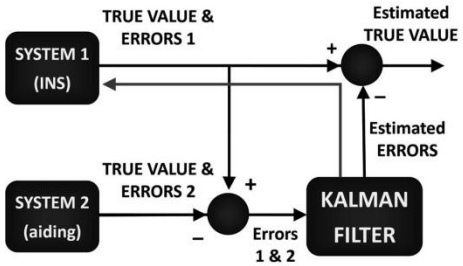

Fig.4. Scheme of centralized closed loop complementary filter architecture for error estimation of an inertial navigation system (INS) with general aiding.

The complementary filtering is usually based on combination of two independent sources of information in such a way that they compensate each other's limitations in order to provide better results of the whole system than the individual source is capable to reach [21]. This was achieved by adding a zero-velocity constraint (system 2 in Fig. 4) as the aiding of the strapdown mechanization algorithm that processed the raw inertial data (system 1 in Fig. 4). Since large values of the state variables could cause biased solutions and inconsistency of the covariance update, only small state values were allowed to be delivered to the EKF [13]. Therefore, instead of using state vector of absolute values we have implemented the EKF to estimate only errors defined by an error model that could describe the error propagation with respect to the navigation equations. We have obtained the error model from the navigation equations (1) to (5) by a perturbation analysis [20, pp. 171-173] followed by linearization; for detailed derivations see the classical 15-state concept [12, pp. 35-41], [22, pp. 24-30] that exploits the uncoupled approach to the classical perturbation analysis as proposed in [12].

Experimental Setup

The experimental setup included the 3DM-GX2 unit mounted on the rotational tilt platform in Fig.1. The platform was aligned to ensure approximately horizontal plane that could provide a desired change in heading by simple rotation about the vertical axis. After stationary initialization, we have measured different data sets of length of 45 minutes. During that time the heading was changed with the step of 10 deg approximately every 1 – 2 minutes. Thus, every dynamical transition was followed by a stationary

period allowing us to observe both the system step response to the change in heading and the drift instability under static conditions. By means of post processing we have determined the complete navigation description of the system's behavior; however, only the heading signal was analyzed and is presented. The heading results obtained from the strapdown mechanization and Kalman filtering based on the EKF with zero-velocity constraint were compared to the reference information from the rotational tilt platform. The reference was provided by optical sensors with resolution of 2.6 arcsec in heading and thus suitable for the reference purposes. The final performance was evaluated by means of root-mean square error (RMSE) developed in time.

Results and Evaluation

Results and their consequent evaluation were obtained using the experimental setup and EKF, both described above. The raw inertial data measured are presented in Fig. 5 and Fig. 6.

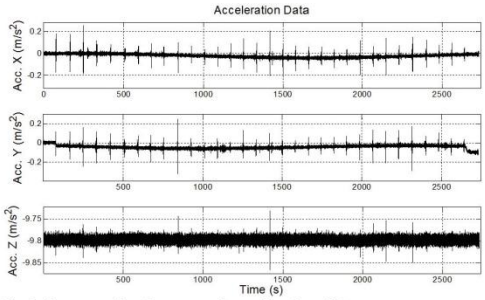

Fig.5. An example of measured acceleration data

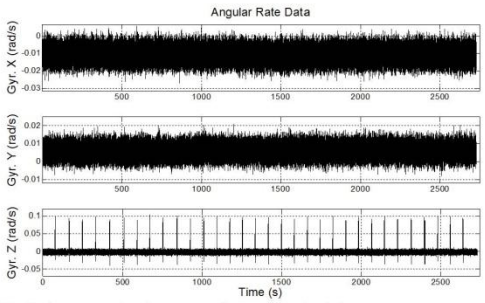

Fig.6. An example of measured angular rate data

In Fig.5 and Fig. 6 there are peaks in acceleration in time spots of the transition as the heading has been changing. The peaks in the measured angular rate signal (z-axis) correspond to the actual rotation given by heading changes. A stationary noise measured in the x-axis and y-axis angular rate sensors correspond to noise parameters specified in the datasheet by the manufacture.

We present the most important results regarding the comparison of the three algorithms for heading determination in Fig. 7; the corresponding RMSE plot is depicted in Fig. 8 (with details highlighted in Fig. 9).

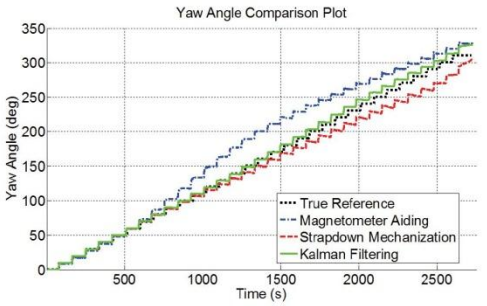

Fig.7. The yaw angle determined by three different heading algorithms.

The comparison plots in Fig. 8 and Fig. 9 clearly show that the performance of all three algorithms is almost identical for the first 10 minutes with the yaw angle RMSE below 3.5 deg.

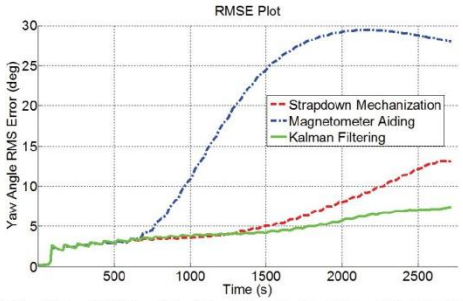

Fig.8. The RMSE plot for different heading determination algorithms compared to the true heading reference

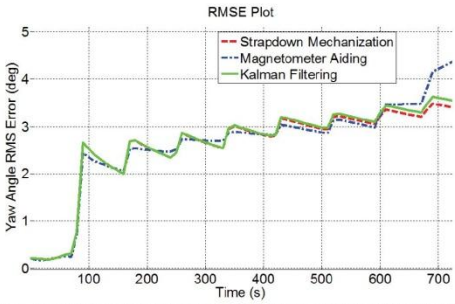

Fig.9. The detailed RMSE plot for different heading determination algorithms corresponding to the first 700 s of data presented in Fig. 8.

As shown in Fig. 8, after the first 10 minutes the yaw angle RMSE with 3-axial magnetometer aiding started to increase more rapidly and reached the limit of RMSE of 5 deg in approx. 12 minutes. This reflected the slower convergence during the heading transition caused by potential disturbances in measured magnetic field. The same RMSE limit of 5 deg was reached by the strapdown mechanization algorithm in approx. 25 minutes whereas with the EKF used in approx. 30 minutes. For the remaining time, the RMSE of the EKF proved to be roughly the half of the strapdown mechanization RMSE value. The reason the EKF algorithm provided superior results when compared to the strapdown mechanization was clearly in the integration

of random sensor errors that contaminated the inertial data in the form of drift and bias instability. These sensor errors were estimated by the EKF as part of the state vector and fed back to correct the strapdown mechanization as shown in Fig. 4. That means the EKF provided correction feedback in all three angles with estimated attitude errors such as in Fig.10.

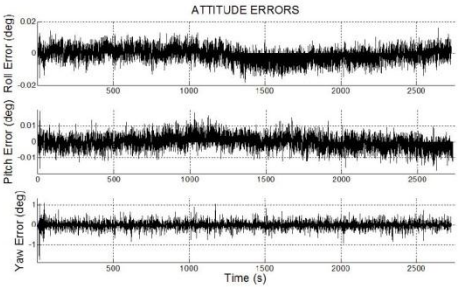

Fig.10. Attitude errors estimated as part of a state vector by the EKF approach presented in Fig. 4.

Conclusions

In this paper we have exploited the error analyses presented in [8] in order to compare and evaluate three possible approaches to heading determination using inertial sensors in 3DM-GX2 AHRS unit (MicroStrain). The analyzed algorithms were: the strapdown mechanization algorithm using only inertial sensors, the approach based on inertial sensors aiding by 3-axial magnetometer, and the extended Kalman filter algorithm for error estimation with zero-velocity constraints.

The presented results highlight the importance of random sensor errors compensation when compared to approaches without compensation. We also showed, that we have achieved results superior to a magnetometer aided solution by exploiting precise sensor error models introduced in [8]. For a short-term application limited by 10 minutes, all three approaches proved comparable performance. For longer period, magnetometer aiding approach began to deviate rapidly from the true values because of slow convergence during heading transitions. The EKF approach proved the best performance by gaining the edge over the strapdown mechanization approach due to the estimation of random sensor errors used for a correction feedback.

This project was partially supported by the research program No. MSM6840770015 "Research of Methods and Systems for Measurement of Physical Quantities and Measured Data Processing" of the CTU in Prague sponsored by the Ministry of Education, Youth and Sports of the Czech Republic, partially by the Czech Science Foundation project 102/09/H082, and by Grant Agency of the Czech Technical University in Prague, grant No. SGS10/288/OHK3/3T/13.

REFERENCES

[1] Zhu R., Zhou Z., A Small Low-Cost Hybrid Orientation System and Its Error Analysis, *IEEE Sensors Journal,* 9 (2009), No. 3, 223-230

[2] Neul R., Gomez U.-M., Kehr K., Bauer W., Classen J., Doring C., Esch E., Gotz S., Hauer J., Kuhlmann B., Lang C., Veith M., Willig R., Micromachined Angular Rate Sensors for Automotive Applications, *IEEE Sensors Journal*, 7 (2007), No. 2, 302–309

[3] Abdel-Hamid W., *Accuracy Enhancement of Integrated MEMS-IMU/GPS Systems for Land Vehicular Navigation Applications*, Ph.D. dissertation, Dept. Geom. Eng., University of Calgary, Calgary, CA, (2005)

[4] Vadlamani A. K., de Haag M. U., Synthesis of Airborne Laser Measurements for Navigation Algorithms, *IEEE Sensors Journal,* 8 (2008), No. 8, 1411–1412

[5] U-Xuan Tan, Veluvolu K. C., Win Tun Latt, Cheng Yap Shee, C. N. Riviere, Wei Tech Ang, Estimating Displacement of Periodic Motion With Inertial Sensors, *IEEE Sensors Journal*, . 8 (2008), No. 8, 1385–1388

[6] Luczak S., Oleksiuk W., Bodnicki M., Sensing Tilt With MEMS Accelerometers, *IEEE Sensors Journal*, 6 (2006), No. 6, 1669–1675

[7] Luo R. C., Chih-Chen Yih, Kuo Lan Su, Multisensor Fusion and Integration: Approaches, Applications, and Future Research Directions, *IEEE Sensors Journal*, 2 (2002), No. 2 , 107–119

[8] Reinstein M., Sipos M., Rohac J., Error Analyses of Attitude and Heading Reference Systems, *Przeglad Elektrotechniczny,* 85 (2009), No. 8, 114-118

[9] Kalman R. E., A new approach to linear filtering and prediction problems, *ASME Journal of Basic Engineering*, 82 (1960), 34-45

[10] Savage P. G., Strapdown inertial navigation integration algorithm design. Part 1: Attitude Algorithms, *J. Guidance, Control, and Dynamics*, 21 (1998), No. 1, 19–28

[11] Savage P. G., Strapdown inertial navigation integration algorithm design. Part 2: Velocity and position algorithms, *J. Guidance, Control, and Dynamics,* 21 (1998), No. 2, 208–221

[12] Shin E-H., *Accuracy Improvement of Low Cost INS/GPS for Land Applications*, M.S. thesis, Dept. Geom. Eng., University of Calgary, Calgary, CA, (2001)

[13] Shin E-H., *Estimation Techniques for Low-Cost Inertial Navigation*, Ph.D. dissetation, Dept. Geom. Eng., University of Calgary, Calgary, CA, (2005)

[14] Titterton D. H., Weston J. L., *Strapdown Inertial Navigation Technology*, Lavenham, UK : The Lavenham Press ltd (1997)

[15] Salychev O., *Applied Inertial Navigation:Problems and Solutions*. ISBN 5-7038-2395-1 : Bauman MSTU Press (2004)

[16] Sotak M., Sopata M., Breda R., Rohac J., Vaci L., *Navigation Systems Integration*, Kosice, published by Robert Breda (2006) ISBN 80-969619-9-3

[17] IEEE Standard for Inertial Sensor Terminology, *IEEE Standard 528*, (2001)

[18] Thong Y. K., Woolfson M.S., Crowe J.A., Hayes-Gill B.R., Jones D.A., Numerical double integration of acceleration measurements in noise, *Measurement*, *Elsevier*, 36 (2004), No 1., 73-92

[19] Sipos M., Paces P., Reinstein M., Rohac J., Flight Attitude Track Reconstruction Using Two AHRS Units under Laboratory Conditions, in *Proc. 8th IEEE Conference on Sensors*, Christchurch (2009), 675-678

[20] Grewal M. S., Andrews A. P., *Kalman Filtering - Theory and Practice using MATLAB*. New York : Wiley-Interscience (2001)

[21] Lazarus S. B., Ashokaraj I., Tsourdos A., Zbikowski R., Silson P.M.G., Aouf N., White B.A., Vehicle Localization Using Sensors Data Fusion via Integration of Covariance Intersection and Interval Analysis, *IEEE Sensors Journal*, 2 (2007), No. 2, 107-119

[22] Vikas Kumar N., *Integration of Inertial Navigation System and Global Positioning System Using Kalman Filtering*, M.S. dissertation, Dept. of Aerospace Engineering, Indian Institute of Technology, Bombay, Mumbai (2004)

***Authors**: ing. Michal Reinštein*, E-mail: reinsmic@fel.cvut.cz, ing. Jan Roháč Ph.D.*, xrohac@fel.cvut.cz, ing. Martin Šipoš*, E-mail: siposm1@fel.cvut.cz, *Czech Technical University in Prague, Technická 2, 166 27 Prague, Czech Republic.*

4.5. DATA PRE-PROCESSING AND VALIDATION

Roháč, J. - Ďaďo, S.: Environmental Vibration Impact on Inertial Sensors' Output. In: Sensors & Transducers. 2012, In Press. ISSN 1726-5479. (IF: --)

Sensors & Transducers Journal, Vol.0, Issue 0, Month 2009, pp.

Sensors & Transducers
ISSN 1726-5479

http://www.sensorsportal.com

Environmental Vibration Impact on Inertial Sensors' Output

Jan ROHÁČ[1], Stanislav ĎAĎO[2]
[1,2]Department of Measurement, Faculty of Electrical Engineering,
Czech Technical University in Prague, Technicka 2, 166 27 Prague, Czech Republic
Phone: [1]+420 2 24353963, [2]+420 2 24352132, fax: +420 2 33339929,
E-mail: [1]xrohac@fel.cvut.cz, [2]dado@fel.cvut.cz

Received: /Accepted: /Published:

Abstract: The paper is dealing with an environmental strong-vibration impact on inertial sensors' output. In our case we measured data on the ultra-light aircraft ATEC 321, which did not have damped cockpit panel, and we recorded the data for post-processing. The main contribution of this paper is in frequency spectrum analyses of measured data, their validation, and filtering to ensure acceptable behavior of navigation systems relying on these data. The data suffered from strong vibration, which had big impact and thus it had to be removed before estimation of navigation parameters was performed. One example of navigation systems is an artificial horizon. Generally, it performs the aircraft attitude estimation just based on accelerometers and angular rate sensors data, and therefore the correctness and efficiency of data filtering as well as consecutive data processing plays a key role.

Keywords: Data Processing, Wavelet Multi-Resolution Filter, Angular Rate Sensors, Accelerometers

1. Introduction

This paper extends the scope of previously published paper [1] concerning applicability of wavelet multi-resolution filters to reduce strong vibration impact on inertial sensors' data and their processing in aircraft navigation systems. The extension deals with methods how to validate data before their processing, with detailed description of different types of the mother wavelets and their comparison from their data filtering performances point of view.

Sensors & Transducers Journal, Vol.0, Issue 0, Month 2009, pp.

1.1 Inertial Sensors' Data Processing

Due to the rapid proliferation of low-cost inertial sensors based on MEMS (Micro-Electro-Mechanical Sensors) technology in recent years, it has become viable to construct inexpensive strapdown navigation systems. These systems can be used in many areas of research, especially where autonomous navigation is required. This includes unmanned vehicle systems and automotive as well as airborne applications, where estimation of attitude and/or displacement information is realized using various data fusion methods, for example a complementary filtering [2]. An artificial horizon is a typical example of these applications. It is a navigation system that belongs to the group of mandatory equipment required for each aircraft based on the regulations of aviation authorities. The system primarily displays aircraft orientation in space, which is described by a bank and elevation angle [3]. Estimation of these angles is based on angular rate measurements along the main aircraft axes [4]. Originally, electro-mechanical gyroscopes were used on board large aircrafts; however, these have been replaced by laser gyros in most cases by now. Laser gyros are very expensive for their usage on small and ultra-light aircrafts, and therefore low-cost MEMS angular rate sensors are a suitable alternative. These sensors have numerous advantages such as small size, weight, price, and power consumption. On the other hand, they suffer from high drift rate, low sensitivity etc., which cause serious drawbacks that have to be dealt with. Because of these characteristics and the fact that an aircraft attitude is estimated by angular rate integration, a stand-alone solution with MEMS angular rate sensors cannot be realized. Integration in the estimation process causes unbound error growth due to noise and, especially, presence of vibrations in the measured data [5],[6]. So it is very useful to use accelerometers to provide the attitude correction under conditions when only a gravitational acceleration is applied to accelerometers, which is an ideal case. Generally, accelerometers are affected by combination of several accelerations, among which the vibrations dominate.

1.2 Environment Characterization

Even if the system is under laboratory conditions, the filtering of sensor outputs is obligatory because of the sensors' noise, which increases inaccuracy after angular rate integration. An additional aspect of inaccuracy is caused by environmental vibrations. In our case we used Inertial Measurement Unit (IMU) ADIS16350 from Analog Devices and measured angular rates and acceleration during all stages of flight such as parking, rolling on a runway, taking off, flying, and landing. The IMU was utilized in EFIS INTEGRA TL-6524 system manufactured by TL-Elektronic Inc. and mounted in the instrument panel of ATEC 321, see Fig.1.

a) b)

Fig. 1. ATEC 321 aircraft (a), EFIS INTEGRA TL-6524 (b).

Data suffered from strong vibration which was also caused by the fact that the instrument panel of ATEC 321 was not equipped with vibration dampers. The sampling frequency was 43 Hz. A vibration character can be seen in Fig.2 and Fig.3. Left parts of these figures present time series of accelerations and angular rates measured in all axes during the parking and right parts correspond to their frequency

Sensors & Transducers Journal, Vol.0, Issue 0, Month 2009, pp.

spectrum.

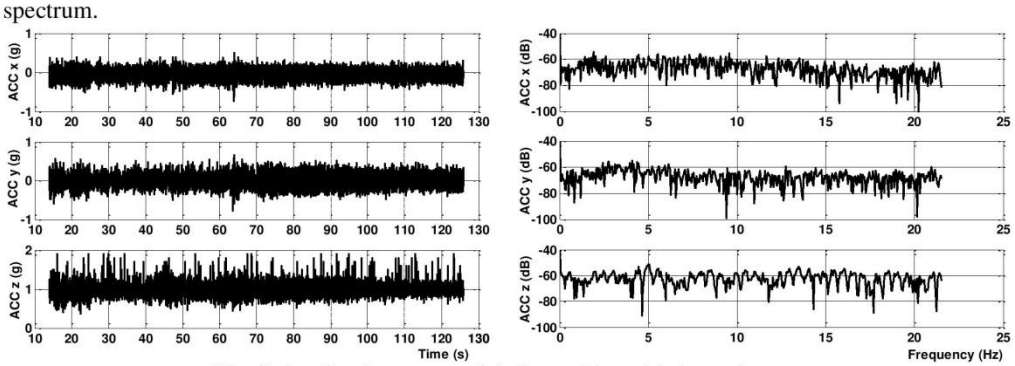

Fig. 2. Acceleration measured during parking with the engine on, time series (left), FFT analysis (right)

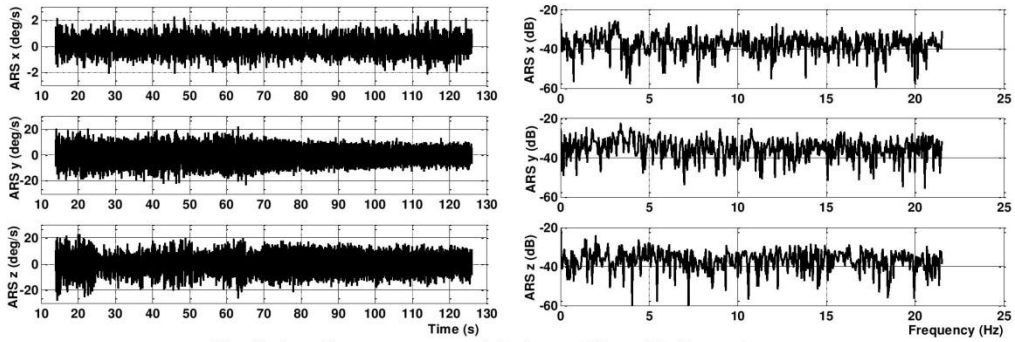

Fig. 3. Angular rates measured during parking with the engine on, time series (left), FFT analysis (right).

Based on FFT analyses it can be seen that the frequency spectrum of vibrations is almost flat; nevertheless, according to Fig. 2 and 3 the vibration has higher impact during the parking in the range of (3 up to 10) Hz. When the aircraft is in the air the frequency range changes according to flight conditions, mostly going up. In cases of engine RPM (Revolution per Minute) suppression during the flight, vibration frequencies go down all the way to 0.5 Hz, as shown in Fig. 4 and 5. The vibration has similar character in all axes except the z-axis in ACC and x-axis in ARS measurements. It is caused by a natural wing damping feature.

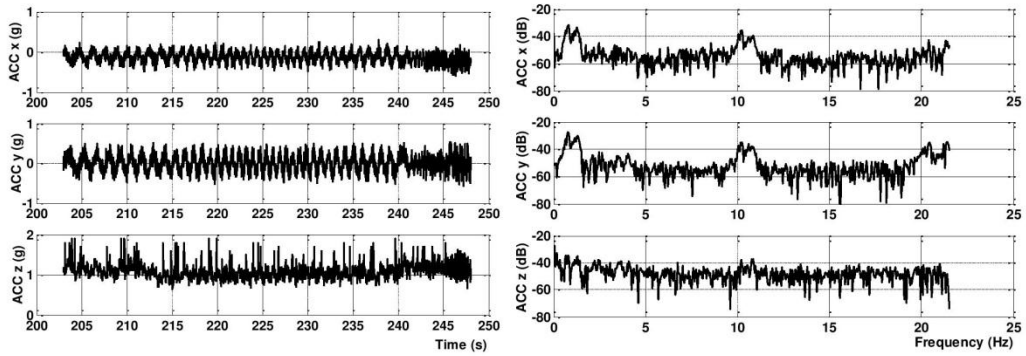

Fig. 4. Acceleration measured during engine RPM suppression,

Sensors & Transducers Journal, Vol.0, Issue 0, Month 2009, pp.

time series (left), FFT analysis (right).

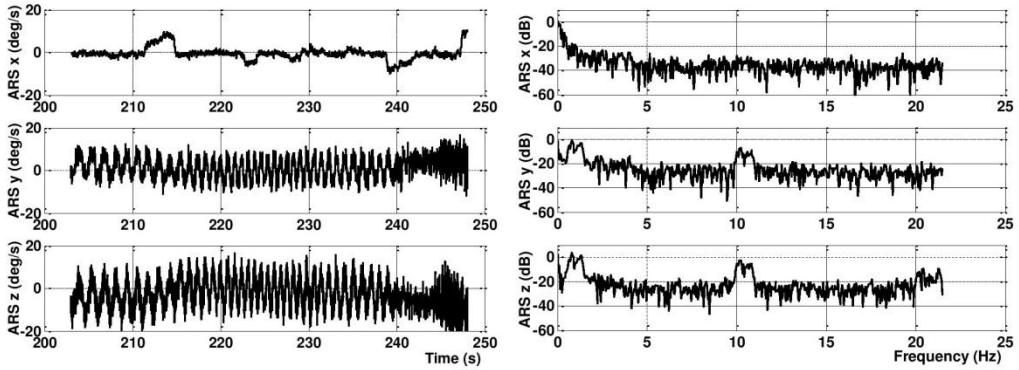

Fig. 5. Angular rates measured during engine RPM suppression,
time series (left), FFT analysis (right).

2. Data Characterization

2.1 Validation of Sensor Data

Vibration could damage the sensor or at least influence its transfer function. From this reason it is advisable to include the diagnostic procedure for checking the consistency of sensor performance. One possibility is to use data validation process based on Probabilistic Data Association Filter (PDAF) [7] described schematically in block diagram of modified Kalman filter system on Fig. 6.

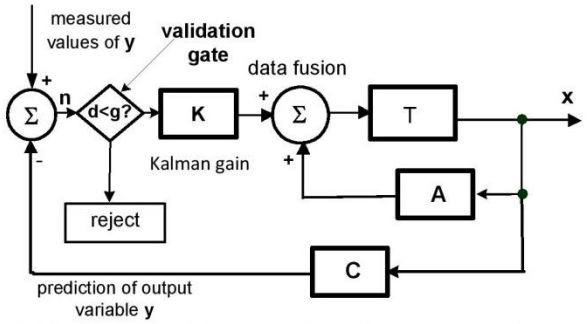

Fig. 6. Principle of the Kalman filter data validation by a PDAF method.
(**A**, **C** correspond to a state and measurement system model matrices, **x** is a state vector, **y** denotes a measurement vector, **K** is a Kalman gain, and **T** represents a delay).

The sensors' output data **y** are compared with the values derived from state equation of system. The statistical parameters of innovation expression

$$\mathbf{n}(t) = \mathbf{y}(t) - \hat{\mathbf{y}}(t \mid t-1) = \mathbf{y}(t) - \mathbf{C}\hat{\mathbf{x}}(t \mid t-1), \tag{1}$$

are examined in a validation gate. The examination process consists in the determination of statistical (Mahalonobis) distance given by the expression

$$d^2(t) = \mathbf{n}(t).\mathbf{S}(t).\mathbf{n}^T(t), \tag{2}$$

Sensors & Transducers Journal, Vol.0, Issue 0, Month 2009, pp.

where S(t) is related to an estimated covariance matrix P and a measurement noise matrix R as follows

$$S(t) = CP(t,t-1)C^T + R. \tag{3}$$

When there is satisfied the condition

$$d^2(t) \leq g, \tag{4}$$

newly measured values **y** are used for a new a-posteriori state estimation. In the opposite case, the inconsistent data are excluded and previously estimated $\hat{x}$ is used. Moreover, the data on rejection output of validation gate are used for diagnostic purposes.

2.2 Characterization of Vibrations Causing Errors by Allan Variance

The effect of vibrations on sensor performance could also be evaluated using Allan variance approach. In terms of Allan variance harmonic components of mechanical vibrations affecting sensor could act as sinusoidal type of noise [8]. Power spectral density (PSD) of this noise can be characterized by a number of distinct frequencies. The PSD of noise containing a single frequency f_0 and amplitude Ω_0 is given by sum of Dirac δ– functions

$$S_\Omega(f) = \frac{1}{2}\Omega_0^2[\delta(f - f_0) + \delta(f + f_0)]. \tag{5}$$

In the case of multiple frequencies f_{0i} of the sinusoidal errors it can be similarly represented by a sum of Dirac δ-functions. As it is well known the procedure of finding Allan variance is equivalent to filtering a noise PSD by a filter with a transfer characteristic

$$H(f) = \frac{sin^4(\pi f\tau)}{(\pi f\tau)^2}. \tag{6}$$

The Allan variance can then be found by performing integration

$$\sigma^2(\tau) = 4\int_0^\infty S_\Omega(f).H(f)df = \Omega_0^2\left(\frac{sin^2\pi f_0\tau}{\pi f_0\tau}\right)^2. \tag{7}$$

Log-log plot of root Allan variance, according to [8], is composed from several peaks with amplitudes falling off rapidly as shown in Fig.7. Estimation of a sinusoidal noise from sensor data might be complicated as it requires the observation of several peaks. Moreover, the peaks due to a sinusoidal noise could be masked by higher order peaks of other frequencies. This fact makes the estimation of error bounds difficult and further justifies the proposed filtering approach to minimization of sinusoidal errors' influences.

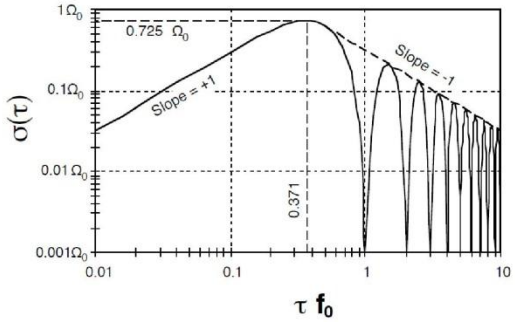

Fig. 7. Square root of Allan Variance plot for a sinusoidal error [8].

Sensors & Transducers Journal, Vol.0, Issue 0, Month 2009, pp.

3. Wavelet Multi-Resolution Filter

3.1 Digital Filters

To reach sufficient results and to smooth inertial signals efficiently we analyzed in [1] different filtering approaches with filters FIR, IIR, MA (Moving Average), and windowed-sinc filters. We suggested the solution using two different filter approaches for accelerometers' and angular rate sensors' data. According to results obtained from FFT analyses a main problem is that a vibration bandwidth and aircraft dynamics overlap and thus the separation of a useful signal from the unwanted one caused by the vibration cannot be done. Therefore, it is required for correct attitude estimation to remove only high frequency noise from angular rate data by low-order low-pass filter, which would respect the aircraft dynamic bandwidth. Nevertheless, in the case of accelerometers the situation is different. It is not required to respect the aircraft dynamics, so it is possible to use high-order low-pass filter with a cut-off frequency set to a level in which a vibration impact can be removed. Its main goal is to restrict the vibration impact on very low frequencies, in our case down to 0.5 Hz. For this reason we had to search for a filter fulfilling requirements on system stability even at such low frequencies. Above mentioned filters did not satisfy these requirements, for details see [1], and thus we searched for other possibility which we found in wavelet multi-resolution filter application. This provided as smooth data as possible with an acceptable time delay which was dealt with in a data fusion process.

Even if the aircraft ATEC321 is light and well maneuverable, we considered flight dynamics bandwidth to 15 Hz and usage of first-order low-pass filter (LPF) for angular rates data. A continuous-time transfer function of LPF is defined as

$$\mathrm{H(s)} = \frac{\mathrm{y(s)}}{\mathrm{u(s)}} = \frac{1}{1+\mathrm{s}\tau}, \tag{8}$$

where τ is a time constant, $y(s)$ denotes the Laplace transform of the filter output, and $u(s)$ corresponds to the input.

The time constant of the LPF is related to its cut-off frequency f_m defined as

$$\mathrm{f_m} = \frac{1}{2\pi\tau}. \tag{9}$$

A discrete form of the LPF can be derived from (8) using difference equation and can be written as

$$\mathrm{y(k)} = (1-\mathrm{a})\,\mathrm{y(k-1)} + \mathrm{a\,u(k)}, \tag{10}$$

where parameter $a = \frac{T_S}{T_S+\tau}$, k denotes the count of time steps, $\mathrm{T_s}$ is a sampling period.

3.2 Principle of the WMRF

Wavelet multi-resolution filtering (WMRF) relies on discrete wavelet transform (DWT) using a finite number of wavelet points. In the case when the spectrum of a useful signal and the one of a noise are overlapped, the WMRF is less harmful to a useful signal than any linear type of other filters. It also has advantages over traditional Fourier methods in analyzing physical situations where the signal contains discontinuities and sharp spikes [9]. Generally, wavelet techniques are based on analyzing a signal through windowing process with variable window size [10]. They allow usage of narrow windows (i.e. short time of observation) in cases when high frequency information is needed and wide windows (i.e. long time of observation) if low frequency information is required [11]. The wavelet transformation can be applied on a discrete signal sequence to decompose it into lower and higher frequency components using predetermined wavelet function, its shifting and scaling coefficients, and

Sensors & Transducers Journal, Vol.0, Issue 0, Month 2009, pp.

the level of decomposition. The DWT definition can be derived from the Continuous Wavelet Transform (CWT) of a time domain signal x(t) as described in [10], [12 p. 84], [13] as

$$CWT(a,b) = \frac{1}{\sqrt{a}} \int_{-\infty}^{\infty} x(t)\,\Psi\left(\frac{t-b}{a}\right) dt, \tag{11}$$

where a and b correspond to the scaling and shifting parameter of the wavelet function *Ψ(t)*.

Scaling the wavelet means stretching or compressing it in the time domain. The smaller the scale, the more the wavelet is compressed. Vice versa, the larger the scale, the more is stretched instead. The lower values of wavelet scales (coefficient a), the more suitable the wavelet is for analysis of high frequency signal components referred to as the signal "details". On the other hand, higher values of wavelet scales allow the analysis of low frequency signal components referred to as the signal "approximations" [10], [12]. The actual integration over time, i.e. Eq. (4), gives the CWT coefficients corresponding to a and b. These coefficients are considered to be the measure of correlation between the used wavelet function and the signal itself for different values of the scales (coefficient a) and different time locations (coefficient b) of the wavelet. The wavelet function *Ψ(t)* is the basis function (or mother wavelet) and it requires to have following properties to ensure the integration (4) is finite: to be short and oscillatory having zero average value and rapid convergence to zero at both ends [12]. The DWT definition is hence as follows, assuming x(n) to be discrete time sequence [12 p. 85] and [13].

$$C_{a,b} = 2^{(-a/2)} \sum_{n} x(n)\,\Psi_{a,b}(n) = 2^{(-a/2)} \sum_{n} x(n)\,\Psi(2^{-a} - b), \tag{12}$$

where $C_{a,b}$ represents DWT coefficients, $\Psi(n)$ denotes the wavelet derived from the mother one based on scaling and shifting coefficients a, b.

The decomposed signal is then reconstructed by applying an inverse DWT (IDWT) on its computed DWT coefficients $C_{a,b}$. It is done by passing the coefficients of selected approximation level through the IDWT low-pass filter and resetting the coefficients of all subsequent details to zero before passing them through the IDWT high-pass filters. The filtered discrete signal $x_f(n)$ can be obtained by

$$x_f(n) = \sum_{a}\sum_{b} C_{a,b}\,\Psi_{a,b}(n). \tag{13}$$

3.3 Performance of the WMRF

The WMRF is mostly used for data post-processing; nevertheless, in [1] we proposed a solution suitable for real-time applications noted as RT WMRF. In our solution a utilized decomposition low-pass filter impulse response was derived from the Symlet 4 mother wavelet. Wavelets of the same kind might differ in number of points (samples) in which the shape of the wavelet and derived decomposition and reconstruction filters are exactly defined. In the case of Symlet 4 the impulse response had 8 points as it can be seen in Fig.8, where also Symlet 8, Daubechies 4, and Daubechies 8 are shown for a comparison. To prove the efficiency of the Symlet mother wavelets (sym4, sym8, sym16, sym32) we ran the analysis in which a wide-band white noise was applied for filtering using WDEN Matlab function with the Level of Decomposition (LoD) equal to 8 and a soft universal 'sqrtwolog' threshold. The results of this analysis are shown in Fig.9. It can be said that the higher number of points of the mother wavelet, the smoother performance from the FFT analysis point of view is. A similar character of a FFT analysis was observed when Daubechies mother wavelets (db4, db8, db16, db32) were applied. Moreover, we compared performances and noise reduction efficiency among Symlet and Daubechies derived mother wavelets; results are denoted in Tab. 1. According to reached results it might seem that Symlet 32 is optimal for a usage due to its smooth frequency domain performance and the highest reduction efficiency, but the number of the mother wavelet

Sensors & Transducers Journal, Vol.0, Issue 0, Month 2009, pp.

points is too high. Therefore, Symlet 4 was utilized in RT WMRF due to its second best noise reduction capability.

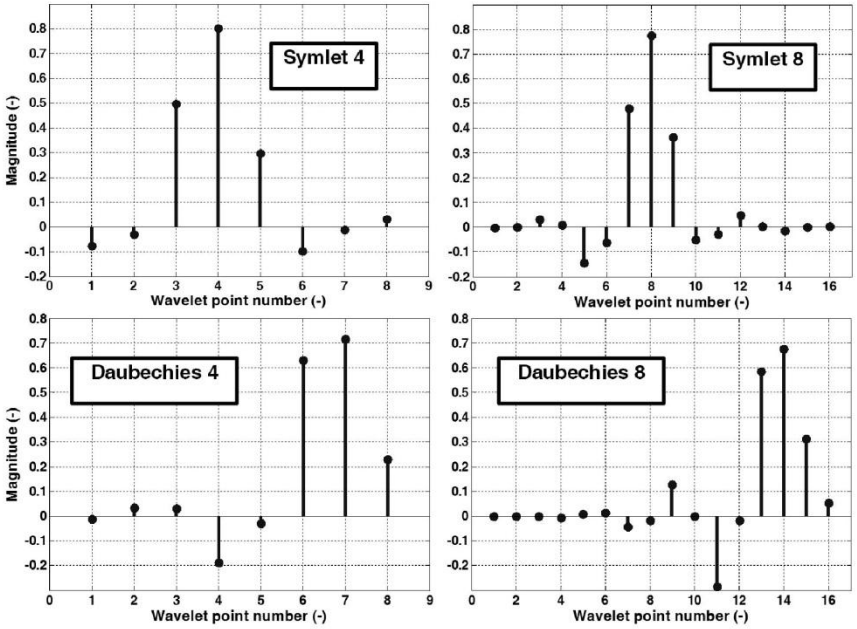

Fig. 8. Definition of discrete mother wavelet functions

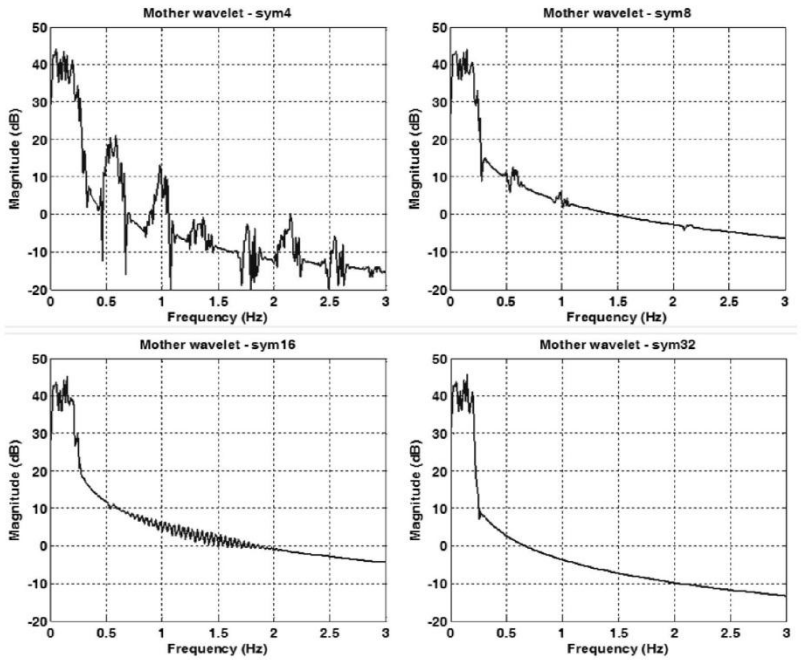

Fig. 9. FFT of WMRF with LoD=8, a soft universal 'sqrtwolog' threshold

8

Sensors & Transducers Journal, Vol.0, Issue 0, Month 2009, pp.

Table 1. Comparison of WMRF results with different mother wavelets applied.

Mother wavelet	Standard deviation (-)	Mother wavelet	Standard deviation (-)	No. of the wavelet points
sym4	0.081	**db4**	0.084	8
sym8	0.086	**db8**	0.087	16
sym16	0.083	**db16**	0.090	32
sym32	0.077	**db32**	0.083	64

4. Results of RT WMRF Application

In [1] proposed RT WMRF utilized a normalized sym4 mother wavelet and a corresponding decomposition low-pass filter. In each Level of Decomposition (LoD) the filter impulse response was convolved with an applied signal or its approximation from a previous LoD. After the last decomposition the algorithm was making an average of the last convolution results. Because the filter impulse response was normalized, the reconstruction was not needed, which reduced a computation load. Results were compared to Matlab WDEN function also utilizing sym4 mother wavelet, the same level of decomposition, in this case equal to 8, and a soft universal 'sqrtwolog' threshold. The performances of both RT WMRF and WDEN function, when a white noise was applied as the input, are shown in Fig.10.

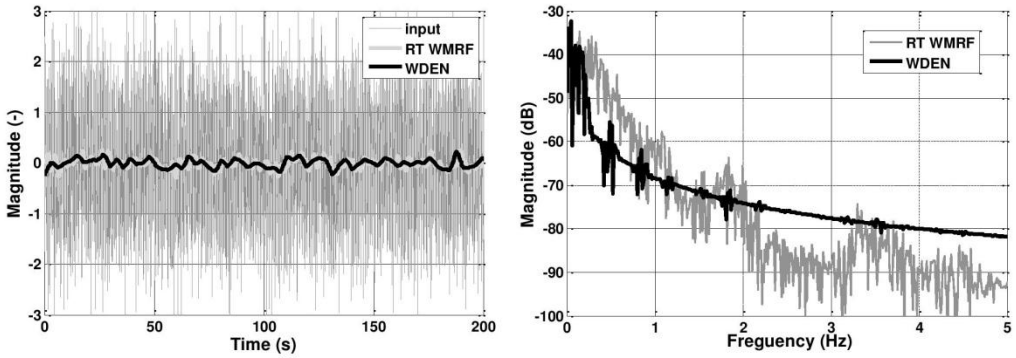

Fig. 10. Performance comparison of a proposed RT WMFR and WDEN function, time domain (left), frequency domain (right)

It can be seen in Fig.10 that WDEN function is more efficient in low-frequency noise reduction due to a sharper edge on its frequency domain performance. Nevertheless, it should be considered that RT WMRF worked with a finite number of signal samples corresponding to 2^{LoD}, which is in contrast to WDEN function using the whole signal at once. In shown performances the LoD was set at 8, thus the number of samples used in RT WMRF was 256. The proposed RT WMRF provided stable solution and fulfilled adequate filtering capabilities required during all flight stages as shown in Fig. 11. Fig.12 depicts zoomed tracks from Fig.11 in different times so as to show different stages of flight. It confirms correct filter behavior even under strong low-frequency vibration conditions.

Sensors & Transducers Journal, Vol.0, Issue 0, Month 2009, pp.

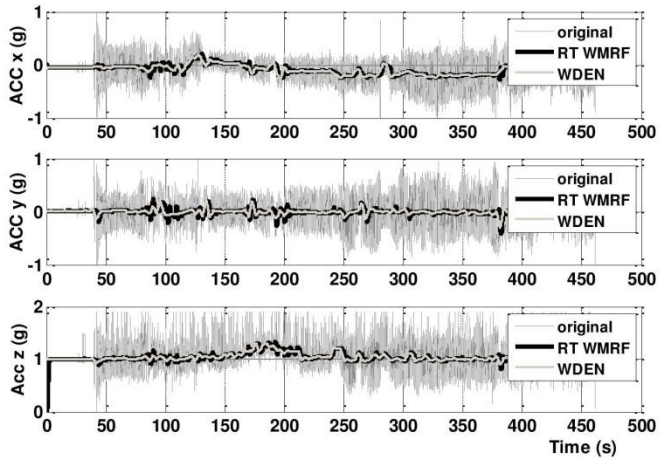

Fig. 11. RT WMRF applied on real flight data

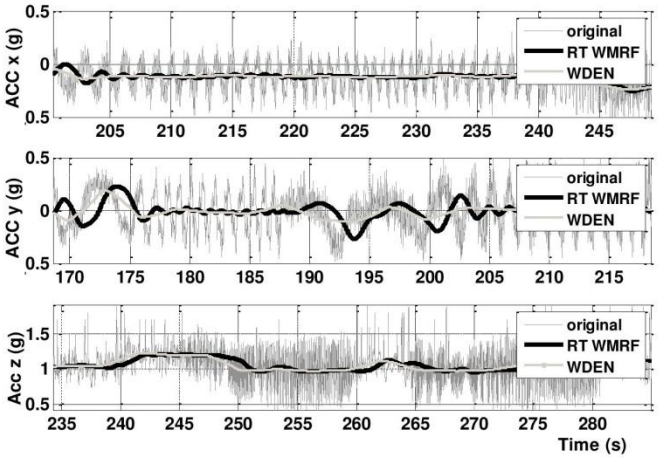

Fig. 12. RT WMRF applied on real flight data – zoomed tracks of Fig. 10

5. Conclusions

This paper extends previously published results about in [1] proposed solution of a real-time WMRF (RT WMRF). This paper provides the frequency spectrum analyses of inertial sensors' data during different stages of flight and points out main problems for data evaluation. The main contribution is in the description of data validation process based on probabilistic data association filter and Allan variance analysis, and in detailed description of WMRF performances and their comparison. It was verified that the Symlet 4 as a mother wavelet applied in RT WMRF provided the best performance when the number of mother wavelet points and noise reduction efficiency was taken into account (the attenuation of components at frequencies around 0.5 Hz is nearly 40 dB). Moreover, it was shown that RT WMRF had approximately a double bandwidth of WDEN function performance for the same level of decomposition. All is targeted at the application of RT WMRF proposed in [1] to prove its suitability to ensure required behavior of aircraft navigation systems relying on inertial sensors' data even in the case of strong vibration environment.

Sensors & Transducers Journal, Vol.0, Issue 0, Month 2009, pp.

Acknowledgements

This research has been partially supported by the research program TA CR Alfa No. TA02011092 "Research and development of technologies for radiolocation mapping and navigation systems", and partially by Grant Agency of the Czech Technical University in Prague grant No. SGS10/288/OHK3/3T/13. Special thanks to TL elektronic Inc. for the aircraft and data provision.

References

[1]. J. Roháč, M. Reinštein, K. Draxler. Data Processing of Inertial Sensors in Strong-Vibration Environment, in Proceedings of the Conference o*n* 'Intelligent Data Acquisition and Advanced Computing Systems (IDAACS 2011)'. Prague, Czech Republic, 15-17 September 2011, vol. 1, pp. 71-75, ISBN 978-1-4577-1426-9.

[2]. V. Kubelka, M. Reinstein. Complementary Filtering Approach to Orientation Estimation using Inertial Sensors Only, in *Proceedings of* '2012 IEEE International Conference on Robotics and Automation (ICRA 2012)', St. Paul, USA, 14-18 May 2012, p. 599-605

[3]. M. Sipos et al. Flight Attitude Track Reconstruction Using Two AHRS Units under Laboratory Conditions, Proceedings of the 8th IEEE Conf. on Sensors, Lecce, Italy, 26-29 October 2008, pp. 675-678.

[4]. D. H. Titterton, J. L. Weston. Strapdown Inertial Navigation Technology. Lavenham, UK, Lavenham Press ltd, 1997.

[5]. P. G. Savage. Strapdown Inertial Navigation Integration Algorithm Design Part 1: Attitude Algorithms, Journal of Guidance, Control, and Dynamics, vol. 21, no.1, pp. 19-28, 1998.

[6]. P. G. Savage. Strapdown Inertial Navigation Integration Algorithm Design Part 2: Velocity and Position Algorithms, Journal of Guidance, Control, an Dynamics, vol. 21, no. 2, pp. 208-221, 1998.

[7]. A.M. Agogino, K. Goebel, S. Alag. Intelligent Sensor Validation and Sensor Fusion for Reliability and Safety Enhancement in Vehicle Control, MOU132, Final Report, UCB-ITS-PRR-95-40, California PATH Research Report, 1995.

[8]. IEEE. IEEE Standard Specification Format Guide and Test Procedure for Single-Axis Interferometric Fiber Optic Gyros, *IEEE Std 952*™-1997 (R2008), [PDF] New York, USA 1997, ISBN 1-55937-961-8.

[9]. M. Sotak, R. Breda, Removing the high frequency noise components from gyro and accelerometer measurements. Acta avionica, Vol. 10, No. 15, pp. 36-40, 2008, ISSN 1335-9479.

[10].S. Nassar. Improving the Inertial Navigation System (INS) Error Model for INS and INS/DGPS Applications, PhD Thesis. Calgary, Canada, Department of Geomatics Engineering, University of Calgary, 2003. Vol. UCEG Reports Number 20183.

[11].M. Sotak. Application of Wavelet Analysis to Inertial Measurements. Science & Military. Vol. 3, No. 2, pp. 17-20, 2008, ISSN 1336-8885.

[12].W. Abdel-Hamid. Accuracy Enhancement of Integrated MEMS-IMU/GPS Systems for Land Vehicular Navigation Applications, PhD Thesis. Calgary, Canada: Department of Geomatics Engineering, University of Calgary, 2005. Vol. UCEG Reports Number 20207.

[13].A. D. Poularikas. The Handbook of Formulas and Tables for Signal Processing. USA, A CRC Handbook Published in Cooperation with IEEE Press, 1999. ISBN 0-8493-8579-2.

4.6. TYPES OF NAVIGATION SYSTEM INTERCONNECTION AND COUPLING WITH AIDING MEANS

Roháč, J. - Šipoš, M.: Sensors and Data Processing Methods Used in Navigation Systems. In Proceedings of the International Scientific Conference Modern Safety Technologies in Transportation. Košice: SUPREMA Ltd., 2011, p. 342-348. ISBN 978-80-970772-0-4.

SENSORS AND DATA PROCESSING METHODS USED IN NAVIGATION SYSTEMS

Jan ROHAC[1] - Martin SIPOS[2]

Abstract: Navigation systems of civil aircrafts are used for vertical and horizontal situation estimation and indication. They provide information about position, velocity, and orientation of the aircraft in a reference framework. They commonly consist of Inertial Measurement Unit (IMU) and computation units. The IMU primary uses inertial sensors, such as accelerometers and angular rate sensors/gyros, which are sometimes supplemented by magnetometers. The vertical situation can be described by altitude and two Euler angles corresponding to roll and pitch. The third angle (yaw) defines the heading and with position it forms the information about the horizontal situation. The navigation systems can be divided into two groups such as Attitude and Heading Reference Systems (AHRS) and Inertial Navigation Systems (INSs). The accuracy of estimated Euler angles also affects the precision of estimated position gotten through two consecutive integrations of acceleration and velocity. Therefore, Euler angles are the main concern of this paper. The angles are estimated via angular rates integration and thus a noise and disturbance can cause an error which grows in time with no boundaries. Therefore, the angles have to be corrected within a flight. There exist several approaches for corrections, which use aiding systems formed by for example accelerometers, magnetometers, and GPS. The approaches have limitations that have to be managed. This paper describes and compares different approaches for the attitude estimation.

Keywords: inertial navigation, accelerometers, angular rate sensors, data fusion, Kalman filtering

1. INTRODUCTION

An accurate tracking of an object attitude plays a key role in wide range of applications, e.g. in aeronautics, astronautics, robotics, automotive industry, underwater vehicles, or human body observation [1-5]. It is primary based on precise measurement of angular rates and accelerations during motion, all in three dimensional space. The most precise device for an angular rate measurement is a ring laser gyroscope, which has the stability better than 0.1 deg/h and the resolution 10^{-6} deg/s [6, 7]. In the case of acceleration, the most precise device is servo accelerometer with the resolution about 10^{-6} g. These devices would have been ideal for all application, if they were not so expensive. Due to this reason other systems, such as Micro-Electro-Mechanical-Systems (MEMSs) have been used in low-cost applications, such as on UAVs or small aircrafts. MEMSs are typically defined as microscopic devices designed, processed, and used to interact or produce changes within a local environment. MEMSs offer reduced power consumption, reduced weight, manufacturing and assembly costs, and increased system design flexibility. Reducing the size and weight of a device allows multiple MEMS components to be used in serial or parallel to increase functionality, device capability, and reliability. In contrast, a MEMS performance has many weak aspects, such as for precise navigation purposes low resolution, noisy output, temperature dependence and so on [5, 8]. Nevertheless, their applicability in navigation is wide due to fast technology improvements, applied data processing algorithms and used aiding systems. In navigation the aiding system is commonly used to provide correction for position or attitude evaluation both coming from accelerometers and angular rate sensors. Examples of possible aiding systems are shown in Fig.1. A typical aiding system for the position and velocity evaluation is GPS. For the altitude ultrasound or laser distance measurement system, or pressure-based one can be used. The main principle of aiding system utilized in applications is to support primary evaluation process by means with zero mean value of the error and known error variance. These properties bound the error growth of estimated attitude and position which would be unbounded due to the presence of integration in the evaluation process when a noise and disturbances occur.

[1] - Ing., PhD.; xrohac@fel.cvut.cz, Czech Technical University in Prague, Technicka 2, Prague, Czech Republic, +420 2 24353963
[2] - Ing.; martin.sipos@fel.cvut.cz, Czech Technical University in Prague, Technicka 2, Prague, Czech Republic, +420 2 24352061

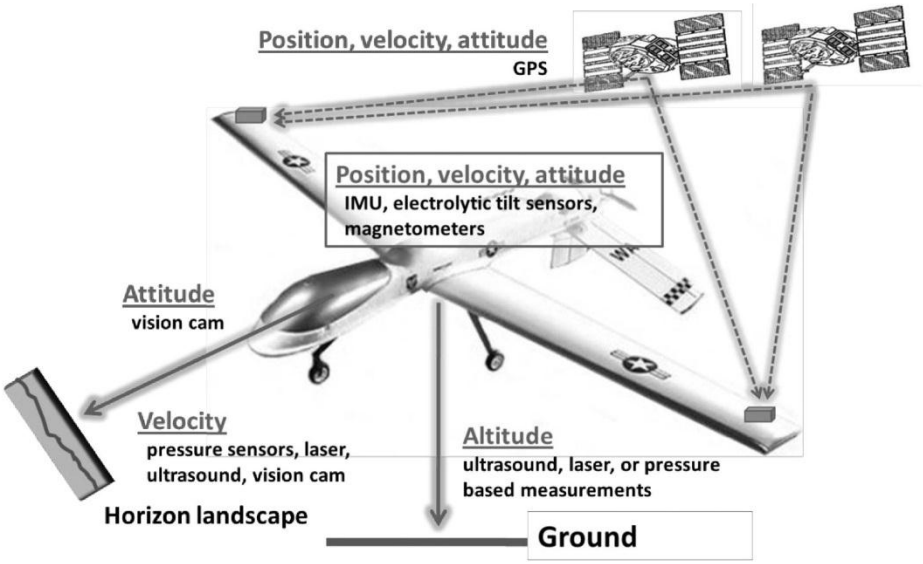

Figure 1 Possibilities of aiding systems

2. DATA PROCESSING

2.1 Complementary filters

A complementary filter (CF) for attitude estimation applies a low-pass filtering on attitude estimates obtained from accelerometer data and a high-pass filtering on a biased attitude estimates obtained by the integration of angular rates [9,10]. Consequently, it fuses both estimates to provide an all-pass attitude solution. An example of a principle block scheme is shown in Fig.2. In this case the CF uses the compensation of accelerometer outputs for centrifugal acceleration to obtain a normalized zero biased gravitation direction defined as

$$\bar{v} = \frac{\hat{g}^b}{\|\hat{g}^b\|}, \tag{1}$$

where $\hat{g}^b$ denotes sensed acceleration compensated for a centrifugal one which is produced within aircraft maneuvers.

The CF can be classified as an observer in the Euler angle form using attitude equations related to angular rate measurements and are defined as

$$\begin{aligned} \dot{\varphi} &= \omega_x + \omega_y \sin\varphi \tan\theta + \omega_z \cos\varphi \tan\theta, \\ \dot{\theta} &= \omega_y \cos\varphi - \omega_z \sin\varphi, \\ \dot{\psi} &= \omega_y \sin\varphi \sec\theta + \omega_z \cos\varphi \sec\theta, \end{aligned} \tag{2}$$

where $\omega_x, \omega_y, \omega_z$ – angular rates, φ, θ, ψ – roll, pitch, and yaw angle [11, 12, 14-16].

The CF uses the feedback respecting the Euler sequence of rotation, and thus an expected gravity can be expressed as

$$\begin{aligned} a_x &= -G \sin\theta, \\ a_y &= G \sin\varphi \cos\theta, \\ a_z &= G \cos\varphi \cos\theta, \end{aligned} \tag{3}$$

where a_x, a_y, a_z denote expected gravity components, $G = 1g = 9.81\ m/s^2$ [12, 14-16].

Measured angular rates are corrected according to feedback as

$$\hat{\omega}^b = \omega^b + \delta, \tag{4}$$

where $\delta = k_P + k_I \int e$ is the correction element with proportional-integral part,
$e = \bar{v} - \hat{v} = \bar{v} - \begin{bmatrix} -G\sin\theta \\ G\sin\varphi\cos\theta \\ G\cos\varphi\cos\theta \end{bmatrix}$ is the difference between normalized measured acceleration and estimated acceleration.

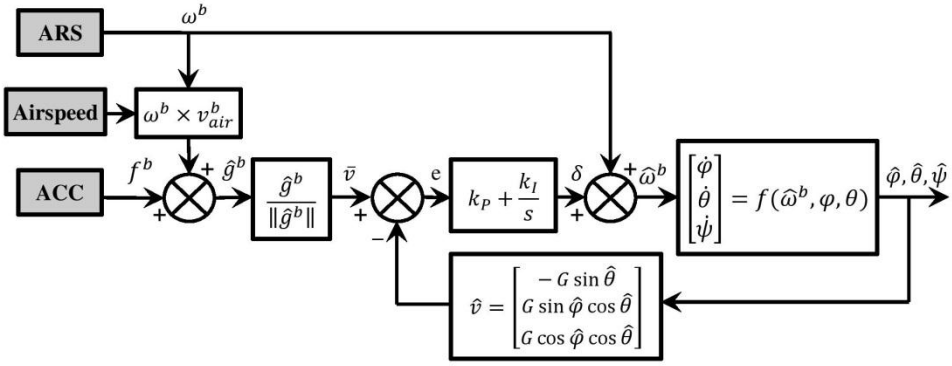

Figure 2 Complementary filter principle block scheme with centrifugal acceleration correction

The CF in Fig.2 uses proportional-integral (PI) compensation. The "P" term governs the frequency cross-over between accelerometer (ACC) based attitude estimates and angular rate sensor (ARS) based attitude estimates. The "I" term is to correct ARS biases. A main advantage of CFs lies in its simplicity and that is a reason why it is sometimes preferred to other approaches, e.g. using Kalman filtering.

2.2 Kalman filtering

Principles of Kalman filtering were originally published in 1960 [13]. A rapid development of microprocessor technologies enables Kalman filters (KFs) to be implemented in real-time applications. The KFs have several alternatives depending on an inner state-space modes and data coupling. For detailed description see [14-16]. The inner state-space model can be expressed as

$$x_{k+1} = \Phi_k x_k + w_k, \tag{5}$$
$$z_k = H_k x_k + v_k, \tag{6}$$

where x denotes a state vector,
z a measurement vector,
Φ a state transition matrix,
H a measurement matrix giving the ideal connection between the measurement and the state vector,
w, v vectors of the process and measurement noise,
index k corresponds to time t_k at which the vectors and matrices are processed.

In the case of characteristics of w_k, v_k it is required Gaussian distribution defined as

$$w_k \sim N(0, Q_k),\ v_k \sim N(0, R_k), \tag{7}$$

where

$$E\left[w_k w_i^T\right] = \begin{cases} Q_k, & i = k \\ 0, & i \neq k \end{cases}$$
$$E\left[v_k v_i^T\right] = \begin{cases} R_k, & i = k \\ 0, & i \neq k \end{cases}$$
$$E\left[w_k v_i^T\right] = 0, \text{ for all k and i.}$$

When conditions stated in (7) cannot be satisfied it is required to apply a shaping filter (SF) and integrate it into the state-space model. The SF uses a white noise (Gaussian distributed random process) as an input and shapes it to respect the real noise character [14-16]. Kalman filters commonly employ so called Kalman filter loop, see Fig.3, periodically repeated in accordance with a sampling frequency of measured data. It has also the alternative, in which a projection step is repeated N-times (N is an integer number) without the correction of the estimate with the measurement. This alternative is commonly used when measurements have different sampling frequencies, for example in the case of INS and GPS integration (GPS up to 10 Hz, INS up to about 100 Hz).

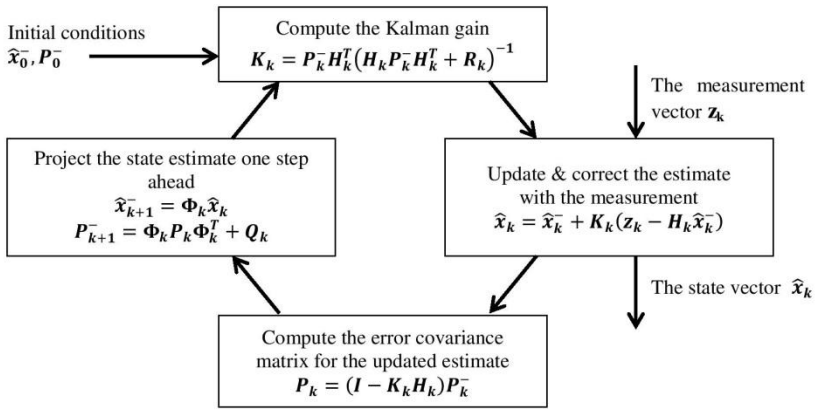

Figure 3 Kalman filter loop [14]

3. ATTITUDE ESTIMATION APPROACHES

A following part will concern only Kalman filtering approach. Generally, two kinds of applications can be distinguished. The first one uses data gotten just from Inertial Measurement Unit (IMU), whose primary sensors are only accelerometers (ACCs) and angular rate sensors (ARSs). In contrast, the second group uses ACCs, ARSs, and magnetometers (MAGs). The main difference between them is in the usage of quaternions in the case of MAGs being available. In the context of the attitude estimation it is assumed that the ACCs measure only gravity and MAGs only Earth's magnetic field [17]. In both cases of chosen sensors there does not exist a unique attitude solution if there are used independently. It is caused by all possible attitude solutions achievable by the rotation along the axis parallel with the axis of the field. It leads to unobservable solution in yaw angle in the case of ACCs. However, when ACCs and MAGs are used to aid ARSs, the quaternions and all Euler angles can be estimate due to the full observability of the calculation process.

In some applications it is acceptable to use only ARSs and ACCs for attitude estimation; however, it allows estimating only two Euler angles (roll and pitch). A quaternion representation requires a complete solution to be found [17].

3.1 Attitude estimation with ARSs & ACCs

The attitude estimation based on angular rate measurements is defined as in (2). The gravity distribution respecting the Euler sequence of rotation can be expressed as in (3). The process model for attitude estimation combines both (2) and (3). By substituting (2) into the results of differentiation of (3) the process model can be written as

$$\begin{aligned} \dot{a}_x &= -\dot{\theta}\cos\theta = \omega_z a_y - \omega_y a_z, \\ \dot{a}_y &= \dot{\varphi}\cos\varphi\cos\theta - \dot{\theta}\sin\varphi\sin\theta = -\omega_z a_x + \omega_x a_z, \\ \dot{a}_z &= -\dot{\varphi}\sin\varphi\cos\theta - \dot{\theta}\cos\varphi\sin\theta = \omega_y a_x - \omega_x a_y. \end{aligned} \tag{8}$$

The equation (8) can be rewritten in the matrix-vector form as

$$\begin{bmatrix} \dot{a}_x \\ \dot{a}_y \\ \dot{a}_z \end{bmatrix} = \begin{bmatrix} 0 & \omega_z & -\omega_y \\ -\omega_z & 0 & \omega_x \\ \omega_y & -\omega_x & 0 \end{bmatrix} \begin{bmatrix} a_x \\ a_y \\ a_z \end{bmatrix} + w(t). \tag{9}$$

The process model can be further extended by angular rate sensor model which can be defined as

$$\dot{\omega} = -\frac{1}{\tau}\,\omega + \frac{1}{\tau}\,w(t), \tag{10}$$

where τ corresponds to the correlation time.

The measurement model considers only gravity being measured by ACCs and can be expressed as

$$\begin{bmatrix} f_x \\ f_y \\ f_z \\ 1 \end{bmatrix} = h(a_x, a_y, a_z) = \begin{bmatrix} -G\,a_x \\ -G\,a_y \\ -G\,a_z \\ a_x^2 + a_y^2 + a_z^2 \end{bmatrix}. \tag{11}$$

The used design of KF utilizes for the process model angular rates which are not significantly affected by disturbances. In contract to angular rates, accelerations are influenced by disturbances as well as by other accelerations caused by changes in the motion. Therefore, there is a need to evaluate reliability of measured acceleration to be defined only by the gravity. In other cases the process model should be processed without the corrections coming from the measurements.

3.2 Attitude estimation with ARSs & ACCs & MAGs

The attitude estimation can be done in this case via quaternions calculation. The quaternions have several advantages against the Euler angles, such as no singularities occur and a lower computational load due to the avoidance of trigonometric function evaluations. Nevertheless, the Euler angles represent easier description of the object attitude/orientation in space [18, 19].

Generally two approaches can be used in this kind of applications and used sensors. First approach employs all 9-dimentional measurement (3x ARSs, 3x ACCs, 3x MAGs) as a measurement vector. Angular rates are linear related to the state vector; however, the other ones are non-linear related, which increases computational load and Kalman filter design is computationally inefficient.
The other approach can use either Newton method, Gauss-Newton method, or the steepest descent method to find a corresponding quaternion for all measurements of ACCs and MAGs , as shown in Fig.4. Results are then combined with angular rate measurements and provided to the Kalman filter as the measurement vector. This solution simplifies the Kalman filter design and thus it is computational more efficient than the previous case.

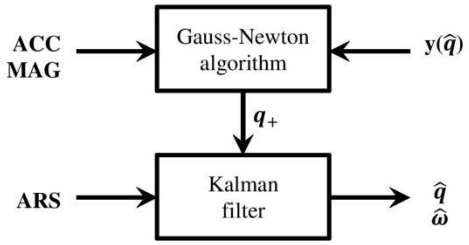

Figure 4 Principled filter block scheme [19]

Xiaoping et al. in [19] proposed improved quaternion-based design of KF which further reduced computational load of the estimation process. A reduced-order Gauss-Newton algorithm is shown in Fig. 5.

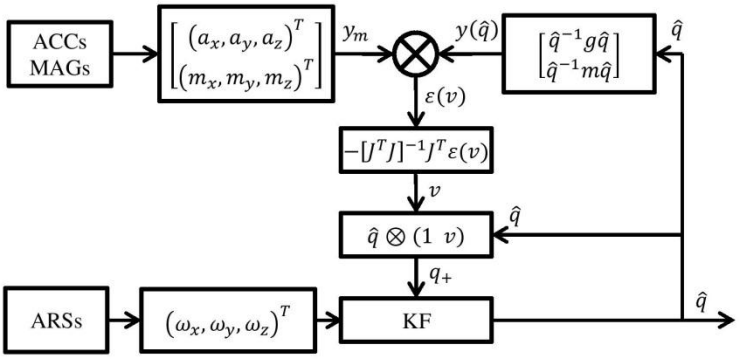

Figure 5 Reduced-order Gauss-Newton algorithm block scheme [19]

The reduced-order Gauss-Newton algorithm for a quaternion update q_+ uses two compounded rotations around the current quaternion estimate $\hat{q}$ followed by the one around the correction quaternion v. The quaternion update q_+ is then applied to the measurement vector and is defined as

$$q_+ = \hat{q} \otimes (1 \quad v), \tag{12}$$

where $v = -[J^TJ]^{-1}J^T\varepsilon(v)$ defines the correction three dimensional quaternion,
$\varepsilon(v) = y_m - y(\hat{q})$ denotes the difference between the measurements of ACC, MAG and their expected values estimated according to $\hat{q}$,
J represents the Jacobian with respect to the variable $\varepsilon(v)$,
$\begin{bmatrix}\hat{q}^{-1}g\hat{q} \\ \hat{q}^{-1}m\hat{q}\end{bmatrix}$ governs the rotation of gravity and magnetic vector defined in local reference frame according to estimated quaternion $\hat{q}$.

4. CONCLUSION

This paper is focused on the description of different approaches to estimate the attitude of an object. The estimation process differs according to used sensors. As previously mentioned, the attitude would have suffered from unbound growing error if there were not aiding systems available. For purposes of attitude estimation there can be used accelerometers, magnetometers, vision camera, electrolytic tilt sensors, and GPS to support the primary angular rate sensors/gyroscopes. This paper describes the situation when only accelerometers or accelerometers and magnetometers are available. Furthermore, some examples are discussed and related to the complementary filter and Kalman filter applications. Both filters can have strong and weak points. Performances of both filters depend on data-preprocessing, data availability, and environmental conditions under which the flight or the motion is executed.

This research has been partially supported by the research program No. MSM6840770015 "Research of Methods and Systems for Measurement of Physical Quantities and Measured Data Processing" sponsored by the Ministry of Education, Youth and Sports of the Czech Republic, partially by Grant Agency of the Czech Technical University in Prague grant No. SGS10/288/OHK3/3T/13, and partially by Czech Science Foundation project 102/09/H082.

REFERENCES

1. REINSTEIN M. et al.: Error Analyses of Attitude and Heading Reference Systems, Przeglad Elektrotechniczny, vol. 85, no. 8, 2009, pp. 114-118.
2. ALISON K., BROWN A.: Test Results of a GPS/Inertial Navigation System Using a Low Cost MEMS Unit, Proceedings of 11 Annual Saint Petersburg International Conference on Integrated Navigation System, Saint Petersburg, Russia, 2004, pp. 1-8.
3. SIPOS M. et al.: Flight Attitude Track Reconstruction Using Two AHRS Units under Laboratory Conditions, 2009 IEEE Sensors, VOLS 1-3, 2009, pp. 630-633.
4. SOTÁK M.: Coarse alignment algorithm for ADIS16405, Przegląd elektrotechniczny, vol. 9, no. 86, 2010, pp. 247-251.
5. BABOUR, N., SCHMIDT, G.: Inertial Sensor Technology Trends, IEEE Sensors Journal, vol. 1, 2001, pp. 332-339.
6. TITTERTON, D. H., WESTON J. L.: Strapdown Inertial Navigation Technology. London UK, Peter Peregrinis Ltd., 1997, pp. 16.
7. RIPKA P., TIPEK A.: Modern Sensors Handbook, Wiley-ISTE; 1 edition, 2007, pp. 403-410.
8. KOUREPENIS A. et al.: Performance of MEMS Inertial Sensors, IEEE Position Location and Navigation Symposium, 1998, pp. 1-8.
9. EUSTON M. et al.: A complementary Filter for Attitude Estimation of a Fixed-Wing UAV, Proceeding of The IEEE/RSJ International Conference on Intelligent Robots and Systems, Nice, France, 2008, pp. 340-345.
10. FOURATI Hassen et al.: A Nonlinear Filtering Approach for the Attitude and Dynamic Body Acceleration Estimation Based on Inertial and Magnetic Sensors: Bio-Logging Application, IEEE Sensors Journal, vol. 11, no. 1, 2011, pp. 233 – 244
11. HEO, O. Ch., Park K.: *Estimating Accelerated Body's Attitude Using an Inertial Sensor*, ICROS-SICE International Joint Conference 2009, Japan, 2009, pp. 5474-5478.
12. KANG Ch. W., PARK Ch. G.: Attitude Estimation with Accelerometers and Gyros Using Fuzzy Tuned Kalman Filter, Proceedings of the European Control Conference 2009, 2009, pp. 3713-3718.
13. KALMAN R. E.: A new approach to linear filtering and prediction problems, ASME Journal of Basic Engineering, 82 (1960), pp. 34-45

14. BROWN R. G., HWANG P. Y. C.: Introduction to Random Signals and Applied Kalman Filtering, John Wiley&Sons, New York, USA, 1997.
15. SOTÁK M. et al.: Navigation System Integration, Košice: Robert Breda, Kosice, Slovak Republic, 2006.
16. GREWAL M. S., ANDREWS A. P.: Kalman Filtering: Theory and Practice Using MATLAB, John Wiley & Sons, Inc., Second Edition, 2002.
17. MADGWICK S. O. H.: An Efficient Orientation Filter for Inertial and Inertial/Magnetic Sensor Arrays, Report, [online], 2010, available on www: http://sharenet-wii-motion-trac.googlecode.com/files/An_efficient_orientation_filter_for_inertial_and_inertialm agnetic_sensor_arrays.pdf, [Accessed: 29-Jun-2011].
18. KIM A., GOLNARAGHI M. F.: A Quaternion-Based Orientation Estimation Algorithm Using an Inertial Measurement Unit, Position Location and Navigation Symposium, 2004, pp. 268-272.
19. XIAOPING Yun et al.: An improved Quaternion-Based Kalman Filter for Real-Time Tracking of Rigid Body Orientation, Proceeding of The IEEE/RSJ International Conference on Intelligent Robots and Systems, Las Vegas, USA, 2003, pp. 1074-1079.

Reviewer: Prof. Ing. Name SURNAME, PhD., e-mail, address, phone

4.7. USAGE OF A NAVIGATION IN AN APPLICATION OF METAL DETECTORS

Nováček, P. - Roháč, J. - Ripka, P.: Complex Markers for a Mine Detector. IEEE Transactions on Magnetics. 2012, vol. 48, no. 4, p. 1489-1492. ISSN 0018-9464.

IEEE TRANSACTIONS ON MAGNETICS, VOL. 48, NO. 4, APRIL 2012 1489

Complex Markers for a Mine Detector

Petr Nováček, Jan Roháč, and Pavel Ripka

Czech Technical University in Prague, Faculty of Electrical Engineering, 166 27 Prague, Czech Republic

This paper describes a novel type of metal markers for eddy current metal detection systems using precise positioning information. The new design for metal markers which are compounded by an ordered array of metal plates with different magnetic parameters has three fundamental advantages: 1. the markers are sensed directly by the metal detector, and no additional hardware is required; 2. the signatures are sharp; 3. not only the position but also the speed of the detector head can be evaluated. In the case of a stand-alone inertial navigation system for evaluating the position of the detector, the precision would be low due to the sensor noise and its integration. However, knowledge of the relative positions and potentially of the detector head speed over the markers can be used as auxiliary information, and so the eddy-current mapping system will be capable of determining the size of the magnetic imprint of a detected metal object and its position relative to the markers. This increases the reliability of the object discrimination during humanitarian demining, and decreases the numbers of false alarms, which nowadays constitute 99.9% of all alarms emitted by an ordinary mine detector.

***Index Terms*—Eddy currents, inertial navigation, magnetic field measurement, signal processing.**

I. INTRODUCTION

HUMANITARIAN demining is a very important activity, in which efforts are directed at clearing land contaminated with unexploded ordnance (UXO) after military conflicts all round the world. It is nowadays becoming more and more difficult to differentiate between UXO and clutter during demining procedures. Moreover, the detection ability of metal detectors is further decreased when searching in magnetic soils [1]. The numbers of false alarms can rise to 99.9% [2]. This high percentage of garbage that is detected instead of UXO enormously increases the cost of demining.

In recent years, several research groups have been developing innovative intelligent metal detectors with a high impact on decreasing the risk of injuries. Remotely controlled vehicles have been developed for demining, e.g. hovering detectors [3], unmanned vehicles [4], and robots [5], [6]. The improved ability of standard metal detectors to discriminate is mostly due to advanced signal processing [7], [8]. The magnetic signature of the suspected conducting object, in the form of a 2-D intensity map, is often compared with known patterns created by mines, and with ammunition used in the relevant region. In order to create this kind of map, it is necessary to scan the area using a metal detector and to have precise information about the position of the detector search head available.

The use of specialized vehicles or robots is mostly limited to flat terrain. Hand-held metal detectors, such as the All Terrain Mine Detector (ATMID) [9], equipped with additional systems, will offer a possible solution in areas that are difficult to access (forests, sloping terrain, etc.)

A precise positioning system for a hand-held metal detector is a challenging task, as the required resolution is 1 cm, and the required precision is 2 cm. We believe that only a simple, lightweight and inexpensive fully autonomous system has a chance of being adopted by the demining community. We therefore use an inertial positioning system based on acceleration and angular rates sensed by accelerometers and rate gyros. Metal detectors are generally equipped with low-cost Micro-Electro-Mechanical System (MEMS) sensors, which have significant drift and noise. Considering the integration from speed to position (and double integration from acceleration) these sensor errors very quickly lead to gross errors in evaluated position. In this paper, we use knowledge about metal marker relative positions to aid the positioning system. On the other hand, optical flow sensors provide information only about velocity, which alone is also not sufficient. The complex markers that we propose here provide information on both position and velocity, and this potentially allows all offsets in the system to be periodically nullified. The markers are sensed by the eddy-current detector itself. Unlike in the case of optical aiding methods, this requires no additional hardware.

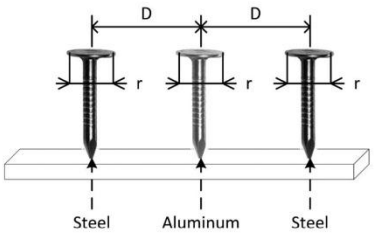

Fig. 1. Possible complex magnetic marker structure.

The novel contribution of this work is the utilization of complex markers as an auxiliary source of information for a precise positioning and navigation algorithm.

II. METHODOLOGY

Complex magnetic markers (CMMs) consist of a specially ordered array of tiny metal plates with known magnetic characteristics, see Fig. 1, where D represents plate distances and r is the diameter.

The proposed CMMs are designed to have precise center localization characteristics and to affect as small area as possible by their presence. The second characteristic enables the user to detect a UXO in a major part of the space between CMMs, which are commonly located in about 1 m distance, and does not decrease the sensitivity of the detector. The whole system is able to detect a UXO up to tens of centimeters in depth, depending on the environment, and to localize it due to the positioning capabilities of the detector head.

Manuscript received August 15, 2011; revised October 07, 2011; accepted October 11, 2011. Date of current version March 23, 2012. Corresponding author: P. Nováček (e-mail: petr.novacek@fel.cvut.cz).

Digital Object Identifier 10.1109/TMAG.2011.2172933

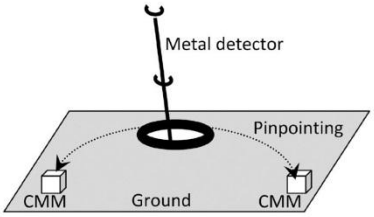

Fig. 2. "Pinpointing" character of the demining procedure (CMM—Complex Magnetic Marker).

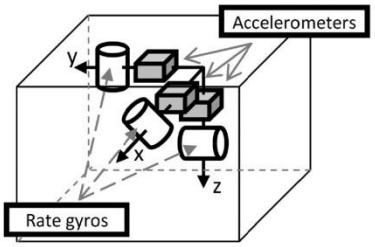

Fig. 3. Inertial measurement unit configuration.

We show that complex magnetic markers can be used not only to indicate the presence of the detector head above the markers, but also to measure the head velocity. In the case of complex markers with a known signal profile, the output voltage is highly dependent on the detector head velocity during the passage of the markers.

The standard demining process consists of two phases. In the first phase, the operator scans the strip of land using the conventional method. Once he detects a metal object, he stops moving forward and starts to pinpoint the exact location of the object. He signals the most probable location by two markers located on both sides of the object at a distance of 50 cm. The signal from the metal detector is collected during a pinpointing between these markers, see Fig. 2.

It must always be ensured that the detector head goes over the magnetic markers to identify the end of area being searched. This feature can be used to aid the positioning system, which continuously evaluates the position on the basis of the sensed acceleration and angular rates. This measurement is performed by the Inertial Measurement Unit (IMU), which generally consists of accelerometers and rate gyros, sometimes supplemented by magnetometers. According to the measured data, the position and attitude of the detector head can be estimated and then used to map the magnetic imprint of the detected object. This forms a system capable of observing the imprint more closely and determining its size and position. When low-cost sensors are used, it is necessary to have an auxiliary system to provide position corrections to reduce the effect of noise integration within the navigation data algorithm.

A. Inertial Sensors

Inertial sensors, i.e. a tri-axial accelerometer and a tri-axial rate gyro, form the Inertial Measurement Unit (IMU), see Fig. 3.

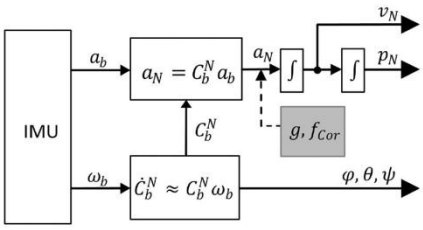

Fig. 4. Principle block scheme of the navigation algorithm.

Accelerometers measure the transitional acceleration, and rate gyros measure the angular rate. This data is used consecutively to evaluate the attitude (roll, pitch, and heading angle), based on which the sensed acceleration is transformed into the local navigation frame and then integrated to obtain the velocity and the position. A block scheme of this procedure is shown in Fig. 4, where ω_b, a_b denote the sensed angular rates and accelerations, $\mathrm{C}_\mathrm{b}^\mathrm{N}$ represents the transformation matrix from the body to the local navigation frame, v_N, p_N correspond to the velocity and the position in the local frame, and φ, θ, ψ are Euler angles related to the attitude.

The navigation algorithm further includes corrections for gravitational force and Coriolis force, denoted in Fig. 4 as g and f_{Cor}.

As mentioned above, both accelerometers and rate gyros suffer from noise which, after integration, causes unbounded error in the system output. This factor has to be minimized by an auxiliary system which is formed, in our case, by knowledge of the precise positions of the metal reference markers. In each sweeping cycle, the position estimated via the inertial sensors and the navigation algorithm is corrected, and this approach reduces the system error. In our experiments, we used IMU ADIS 16405, with a sampling frequency of 25 Hz. The usage, design and performance of the Kalman filter are not described in detail here, because they are beyond the scope of this paper.

B. Position Reference Markers

As presented by Bruschini [10], the signal phase measured by an eddy current metal detector depends on the material parameters, with the dependency defined as

$$\varphi = arctg\left(\frac{\mathrm{Im}(f)}{\mathrm{Re}(f)}\right), \tag{1}$$

where f represents the output signal of the metal detector, $\mathrm{Im}(f)$ and $\mathrm{Re}(f)$ denote the imaginary and real part of the output signal f, and φ is the evaluated signal phase.

In this paper, we propose a new design for metal markers which are compounded by a specially ordered array of metal plates with different magnetic parameters (permeability and conductivity). The array forms a magnetic marker with a defined impact on the detector output. This performance can be used to indicate the precise position of the detector head when the head is right above the marker.

The array of plates can be composed of different conductivity materials with a known relative permeability μ_r and conductivity σ. In our case, the marker consists of Aluminum (Al: $\mu_{rAl} = 1$, $\sigma_{Al} = 3.6\ 10^7\ \mathrm{S/m}$) and Chrome Steel (St: $\mu_{rSt} = 150$, $\sigma_{St} = 0.46\ 10^7\ \mathrm{S/m}$) circular plates with the same diameter $r = 9.4\ \mathrm{mm}$.

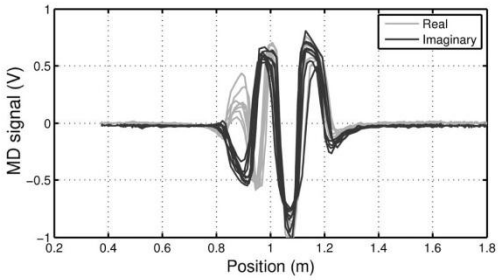

Fig. 5. Imprint of CMM consisting of two plates—Steel and Aluminum; distance between the plates: 50 mm.

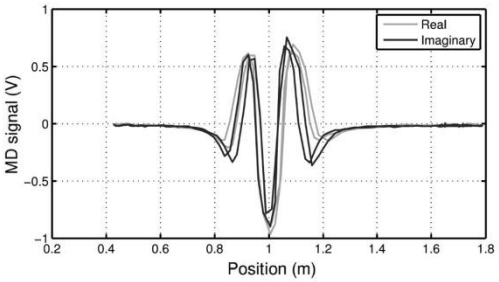

Fig. 6. Imprint of CMM consisting of two plates—Steel and Aluminum; distance between the plates: 40 mm; the signal phase shift is unobservable.

The possibility to differentiate CMMs just by choosing different plate array structures (the sequence of steel and aluminum plates) is another advantage of the proposed CMM. The use of a multiple CMM system with different structures (codes) enables more complex navigation tasks to be defined with absolute position accuracy, which is in contrast with the technology currently available on market.

III. Measurement Setup

The measurement setup included a modified ATMID metal detector equipped with a subsystem capable of measuring the real and imaginary part of the detector output signal and of communicating with a PC. Moreover, the IMU ADIS16405 was mounted on the detector head. An optical measurement system utilizing an industrial camera [11] was used as a position reference. All experiments were performed under laboratory conditions. The measured data was synchronized with a sampling frequency of 25 Hz.

IV. Experimental Results

The aim of this paper is to prove the suitability of CMM characteristics for providing adequate position determination accuracy. Precise navigation algorithms are beyond the scope this paper, and only CMM characteristics are therefore further analyzed and discussed here.

First of all, we analyzed the influence of the distance between the St and Al plates on the performance of the detector. Fig. 5 shows one imprint of a real and imaginary part of the detector output voltage. In this case, the distance between the plates was 5 cm. This was evaluated as the smallest distance in which the real and imaginary part was still distinguishable. When the distance was smaller, the difference decreased, as shown in Fig. 6, and the difference was hardly detectable. In contrast, when the distance was increased, no improvement was observed, and the CMM extended the size of its imprint, which was undesirable.

Knowledge of the precise position within the range of the imprint is defined by the local maximum or minimum (depending on the number of plates and on the structure). The sharper the local minimum or maximum is, the better the CMM localization accuracy will be. Therefore, due to the different design of CMM with more than two plates, a sharper local minimum or maximum can be achieved. A complex CMM imprint with four plates (Fe-Al-Fe-Al) is shown in Fig. 7. In this case, the local maximum is 2 times sharper than the local minimum in Fig. 5.

The imprints shown in Figs. 5–7 were evaluated from experiments in which the CMM was moved under the detector head.

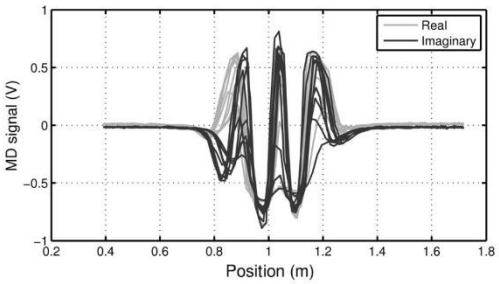

Fig. 7. Imprint of CMM consisting of four plates—Steel, Aluminum, Steel and Aluminum; distance between plates is 50 mm.

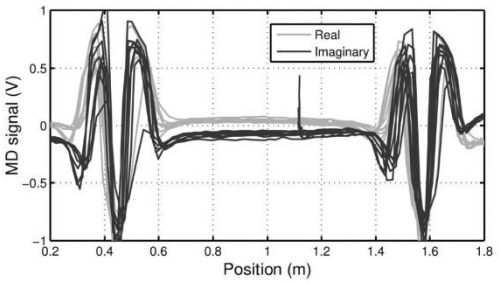

Fig. 8. CMM signal stamp for left and right CMM influenced by noise.

This ensured steady environmental conditions from the conductivity point of view. When the situation was opposite, i.e. when the detector head moved and the two CMMs were steady with a known relative position, the influence of the unsteady conductive conditions affected the mean values of the real and imaginary part, as shown in Fig. 8. The phase shift is small; however, it disables the use of CMM with a smaller distance than 5 cm the between plates. This situation corresponds to real demining conditions, and small phase shifts therefore have to be considered as undesirable.

We implemented an algorithm using a convolution function to localize the local minimum or maximum within the range of the imprint. This also took into account the differences between the minima and maxima in order to restrict false localization. In addition, the algorithm can compare the evaluated imprint

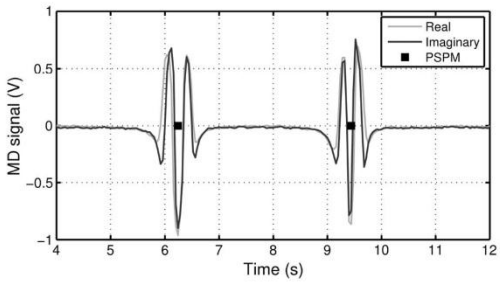

Fig. 9. CMM signal stamp for left and right CMM influenced by noise.

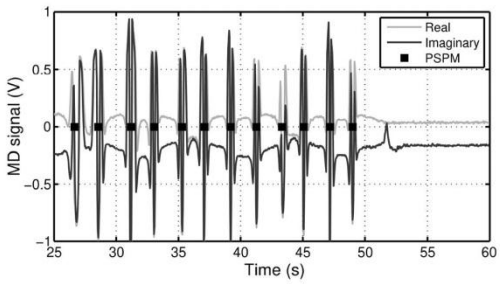

Fig. 10. Localization of imprint minima—unsteady conductive conditions.

with the imprint stored in the memory. This functionality further limits potential false imprint identification and localization. The algorithm is also able to estimate the metal detector search head transit time above the reference mark, and this enables it to be used in velocity estimation. The results of the algorithm are shown in Figs. 9 and 10. In the first case, the measurement was made under steady conductive conditions (CMM was moved under the detector head). By contrast, Fig. 10 depicts the measurement in which the detector head moved ("swept") between two CMMs, and thus the influence of an unsteady conductive environment can be seen in the imprint.

V. Conclusion

Continuous positioning of the metal detector is crucial in demining procedures. Since low-cost inertial sensors are used, additional (aiding) information about the position is needed. In this paper, we have proposed a new design for magnetic markers (CMM) composed of a specially ordered array of metal plates with different magnetic parameters. In the case of a complex marker (see Fig. 7), this design provides precise positioning capability due to the sharp identification of minima or maxima. The accuracy is better than 45 mm under all conditions. This accuracy makes the knowledge of proposed CMM relative positions, which are precise due to CMM parameters, suitable to aid an inertial sensor based position estimation process.

In addition, the character of CMM and its imprint minimize false localization of the marker. This is one of the main advantages of the design.

During preliminary experiments, we used markers in the form of nails made from two metal materials, non-magnetic aluminum and chrome steel, which are available in developing countries, where most demining operations are carried out. Some preliminary experiments have been performed under laboratory conditions; however, other tests are now planned under real conditions in the Joint Research Centre (ISPRA, Italy) testing area, where the whole metal detector system with magnetic markers will be tested.

Acknowledgment

This work was supported by the Grant Agency of the Czech Technical University in Prague under Project SGS10/288/OHK3/3T/13, by the Czech Science Foundation under Project 102/09/H082, and by Research Program MSM6840770015 Research on Methods and Systems for Measurement of Physical Quantities and Measured Data Processing of the CTU in Prague, sponsored by the Ministry of Education, Youth and Sport of the Czech Republic.

References

[1] P. Ripka, J. Vcelak, P. Kaspar, and A. M. Lewis, "Bomb detection in magnetic soils: AC versus DC methods," in *Proc. 5th IEEE Conf. Sens.*, 2006, pp. 1389–1391.
[2] D. Guelle, *Metal Detector Handbook for Humanitarian Demining*. Luxembourg, Norwich: Office for Official Publications of the European Communities; Stationery Office distributor, 2003.
[3] M. Hussain, "RF controlled GPS based hovering mine detector," in *Proc. 9th Int. IEEE INMIC*, 2005, pp. 1–4.
[4] M. Yagimli and H. Varol, "Mine detecting GPS-based unmanned ground vehicle," in *Proc. 4th Int. Conf. RAST*, 2009, pp. 303–306.
[5] E. Heußlein, B. W. Patullo, and D. L. Macmillan, "Robot navigation: Implications from search strategies in exploring crayfish," *Robotica*, vol. 28, no. 3, p. 465, May 2009.
[6] J. Estremera, J. A. Cobano, and P. Gonzalez de Santos, "Continuous free-crab gaits for hexapod robots on a natural terrain with forbidden zones: An application to humanitarian demining," *Robot. Autonomous Sys.*, vol. 58, no. 5, pp. 700–711, May 2010.
[7] P. Ripka, M. Janosek, and P. Novacek, "Depth estimation of metal objects," *Procedia Eng.*, vol. 5, pp. 280–283, 2010.
[8] J. Svatos, J. Vedral, and P. Fexa, "Metal detector excited by frequency-swept signal," *Metrology Meas. Syst.*, pp. 57–68, 2011.
[9] Schiebel, Maintenance Manual MT5001/16/010E 2003.
[10] C. Bruschini, "A Multidisciplinary Analysis of Frequency Domain Metal Detectors for Humanitarian Demining," PhD thesis, Vrije Universiteit Brussel, , Brussels, 2002.
[11] P. Novacek, P. Ripka, O. Pribula, and J. Fischer, "Mine detector with discrimination ability," *J. Electr. Eng.*, vol. 61, no. 7, pp. 141–143, 2010.

5. METHODS AND TECHNOLOGY APPLIED IN NAVIGATION SYSTEMS– UNPUBLISHED RESULTS

5.1. MODIFICATIONS OF MEASUREMENT FRAMES

Within the research project #1 in chapter 3.2 a new concept of a navigation system has been developed. Its design uses a resulting concept motivated from the original paper presented in chapter 4.3 whose utility design was patented under Intellectual Rights Properties under No. PUV 2011-24979 named "Measurement Unit of an Artificial Horizon". A basic principle of the navigation system, shown in Fig. 11, implements the ACC framework modification supplemented by other frame defined by three-axis IMU ADIS16405 in a typical frame configuration. Side board 2-axis ACCs ADIS16204 are turned 45 deg with respect to the Earth gravity vector when the main board is horizontal. This navigation system fuses inward obtained data from ACCs and ARSs with external aiding systems, i.e. GPS receiver and magnetometer.

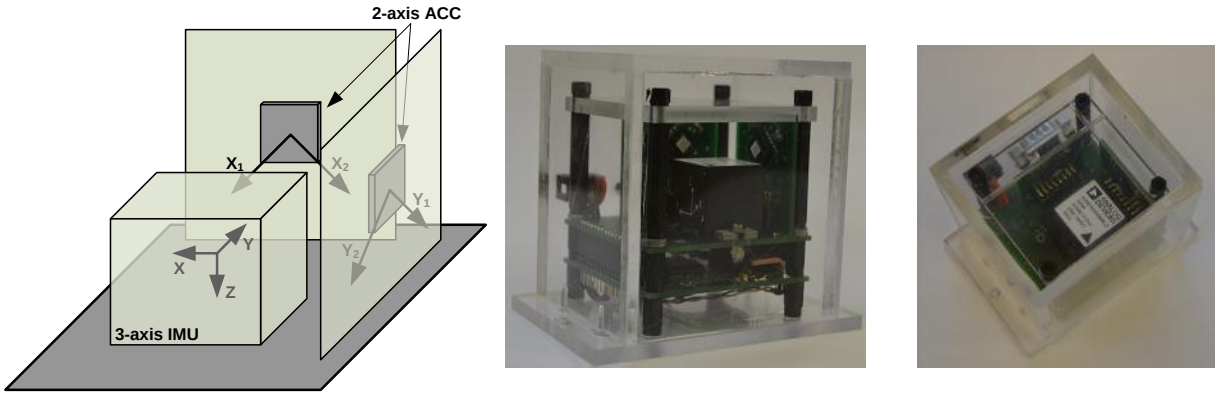

Fig. 11 –The modified accelerometer framework,
a principle scheme (left), two shots of the realized navigation system (middle, right)

The concept of the navigation system, shown in Fig. 11, integrates sensors with digital outputs. Even if they are considered as smart sensors with a temperature and misalignment compensation their signal processing units work with a limited number of inputs and thus the signal to noise ratio (SNR) can be further improved just by an inner filtering capability. The filter increases a group delay which is the disadvantage of the concept. Unlikely, to improve the signal to noise ratio it is necessary to utilize sensors with analog outputs and increase their number per a sensitive axis. Therefore, a new concept has been developed. Its entire design, shown in Fig. 12, is composed by four 3-axis ACCs ADXL337, four 2-axis ACCs ADXL203, and three 1-axis ARSs ADIS16136, all from ADI manufacturer. All ACCs are analog, unlikely the ARSs which are digital. Chosen ARSs are the only tactical grade angular rate sensors available on market, which was the reason for their implementation. Since the frame modification was previously applied only on ACC frame, it is so in this new concept as well. The ARS frame has not been modified. The whole concept can be divided from the ACC point of view into three parts having different frames, see Fig. 12. The first part utilizes two 2-axis ACCs placed on two side boards as has been used in previous case of the navigation system shown in Fig. 11. Each ACC on side boards are turned 45 deg with respect to the Earth gravity vector when the main board is horizontal. This concept brings benefits in sensing the gravity vector by ACCs with a low resolution around 1 mg under conditions close to horizontal. The second part is already placed on the main board whose axes correspond to the main aircraft ones. This second part includes two groups; each consisted of two 3-axis ACCs forming two ACC frames. In a group one part of the ACC frame is always oriented in order to form the opposite to the other one. For each ACC axis then exists the other one in which an applied acceleration produces the same output magnitude but with an opposite sign; those ACCs are coupled. Thus three ACC couples are within each group, as depicted in Fig. 12. Each couple outputs are led into a differential amplifier as shown in Fig. 13 to perform

$$U_1 - U_2 = U_{10} \pm \Delta U_1 - U_{20} \mp \Delta U_2 = U_{10} - U_{20} \pm (\Delta U_1 + \Delta U_2), \qquad (5.1)$$

where U_i corresponds to outputs of an ACC couple,

U_{i0} is a DC value when no acceleration is applied,
ΔU_i reflects the output change when acceleration applied.

When opposite directions of sensitive axes within an ACC couple are considered and $U_{10} - U_{20} = 0$ in ideal case, there can be (5.1) rewrite into the form

$$U_1 - U_2 \approx \Delta U_1 + \Delta U_2 = 2\Delta U \approx 2a_i, \tag{5.2}$$

where a_i is an applied acceleration in i-axis of the main board frame.

When a noise is considered with respect to (5.1.-5.2) the resulting value σ_{Ti} can be evaluated as

$$\sigma_{Ti} = \sqrt{\sigma_{1i}^2 + \sigma_{2i}^2}, \tag{5.3}$$

where σ_{ji} is a standard deviation of the noise for *j*-direction (j = {1,2}) along i-axis of the main board (i = {X_L, Y_L, Z_L}).

From (5.2-5.3) there can be seen that the sensitivity was doubled and a noise level increased, but not two times. That improves the signal to noise ratio (SNR). To further improve the SNR the outputs from both groups can be:

1. averaged, which will produce estimated acceleration value in i-axis $\hat{a}_i \approx 2a_i$ and $\hat{\sigma}_{Ti} = \frac{\sigma_{Ti}}{\sqrt{2}}$,
2. added to each other, which will produce estimated acceleration value in i-axis $\hat{a}_i \approx 4a_i$ and $\hat{\sigma}_{Ti} = \sqrt{\sigma_{T1i}^2 + \sigma_{T2i}^2}$,
   where σ_{Tgi} corresponds to the resulting value σ_{Ti} obtained from (5.3) for *g*-group (g = {1,2}).

In both mentioned cases the final SNR is improved. The last third part of the new concept, see Fig. 12, utilizes two 2-axis ACCs whose sensitive axes are horizontal and also differentially oriented. In this case the ACCs were chosen in order to provide forward and lateral acceleration sensing with as low noise as possible. The sensors ADXL203, according to the datasheets, reach the lowest noise density parameter in the ADI production of multi-axial ACCs, which was the reason for their implementation.

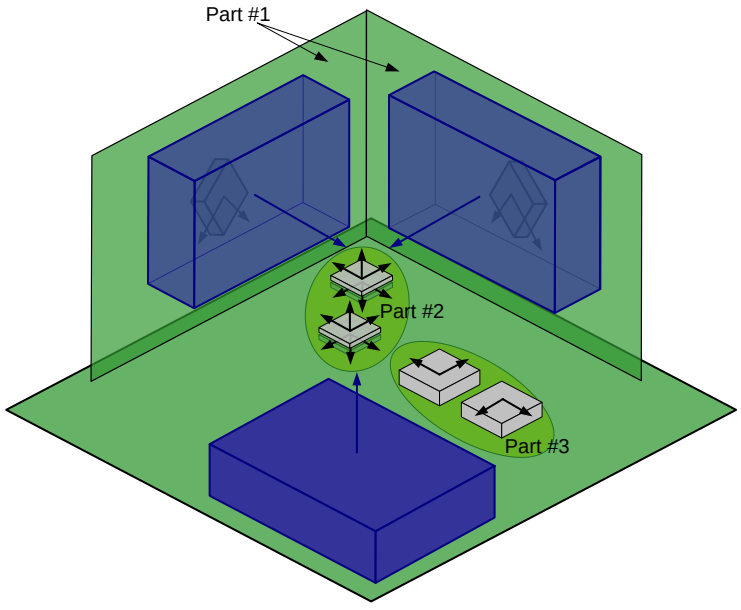

Fig. 12 – A new concept of a navigation system in multi-sensor configuration
ARSs with their axes – blue, ACCs with their axes – grey

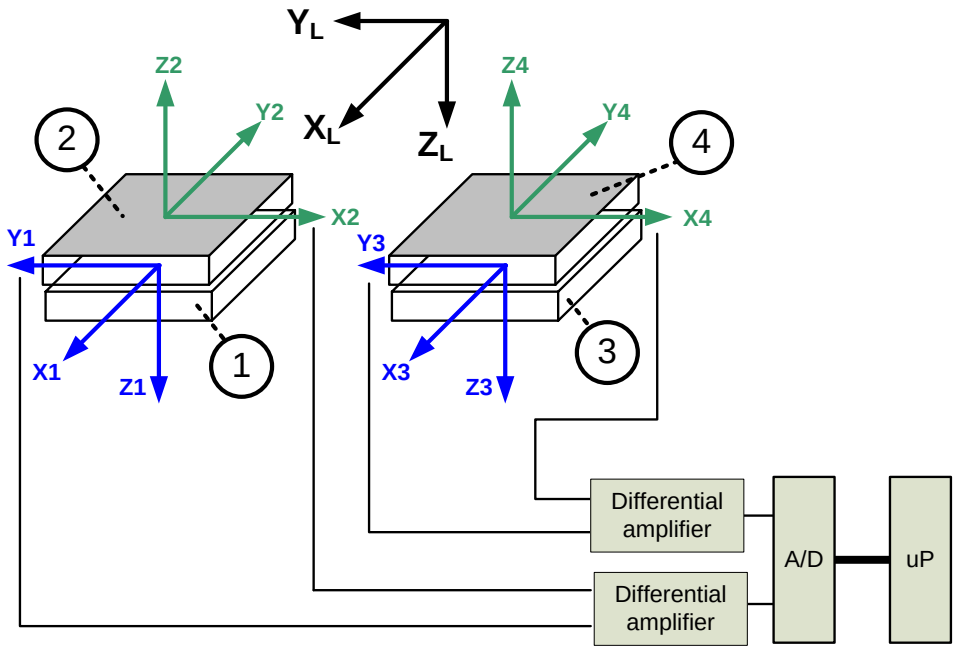

Fig. 13 – A principle scheme of 3-axis ACCs' output data processing (one channel), X_L, Y_L, Z_L form the main measurement frame

The new proposed concept of a navigation system is advantageous for its multi-sensor configuration which brings the capability of the signal handling the way as described by (5.1-5.3) as well as the SNR improving, data fusion, plus increased sensitivity of ACC based attitude evaluation with increased reliability by side-boards ACCs. The ACCs are accompanied by tactical grade ARSs and thus the whole system should reach the best performance for this MEMS based navigation system category. The system is still under development.

5.2. MODULAR NAVIGATION SYSTEM FOR PRECISE POSITION AND ATTITUDE EVALUATION

The design and development of a modular navigation system for precise attitude and position evaluation was the objective of the research project #3 specified in chapter 3.2. The final solution was a product of a collective work of PhD. students, master degree students, and the applicant. The applicant managed the project, coordinated and led partial tasks, as well as partially worked on particular solutions. A principle scheme is depicted in Fig. 14. A core part of the system consisted of modules involving IMU, GPS receiver, tilt sensor, magnetometer (MAG), and pressure sensors. The core was extendable for arbitrary data modules, which could be connected but not necessarily. All modules were connected via CAN bus with a master module using the CANaerospace communication protocol. The master module controlled the data flow and acquired obtained data. Raw data were compensated for deterministic errors, pre-processed, and used for attitude and position evaluation. Furthermore, all data were stored in SD card for later acquisition. The extended Kalman filter was used for navigation data evaluation and its results were sent via wireless connection to the ground station SW, which displayed them. The whole airframe part of the system was mounted on board of the UAV Bellanca Super Decathlon XXL depicted in Fig. 15 the way as shown in Fig. 16. For the performance verification the core part was extended by arbitrary data modules involving a reference position and attitude system PolaRx2e@, which was a multi-antenna and multi-functional GPS receiver, and multiple electrolytic tilt modules (ETMs) for their performance observation and testing. All arbitrary modules had to be designed with respect to IEEE1451 which assured automatic module identification and configuration within the CAN bus.

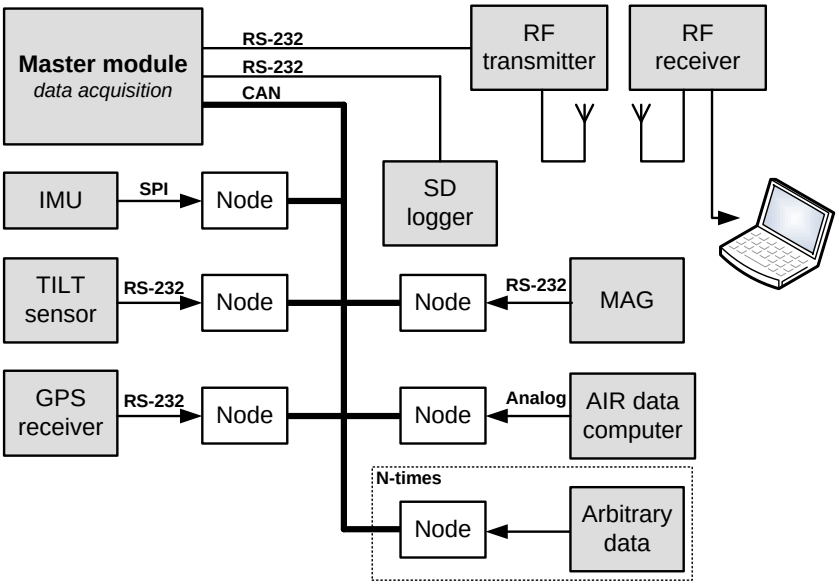

Fig. 14 – A modular concept of the navigation system

Fig. 15 - Bellanca Super Decathlon XXL (Hacker Model Production)

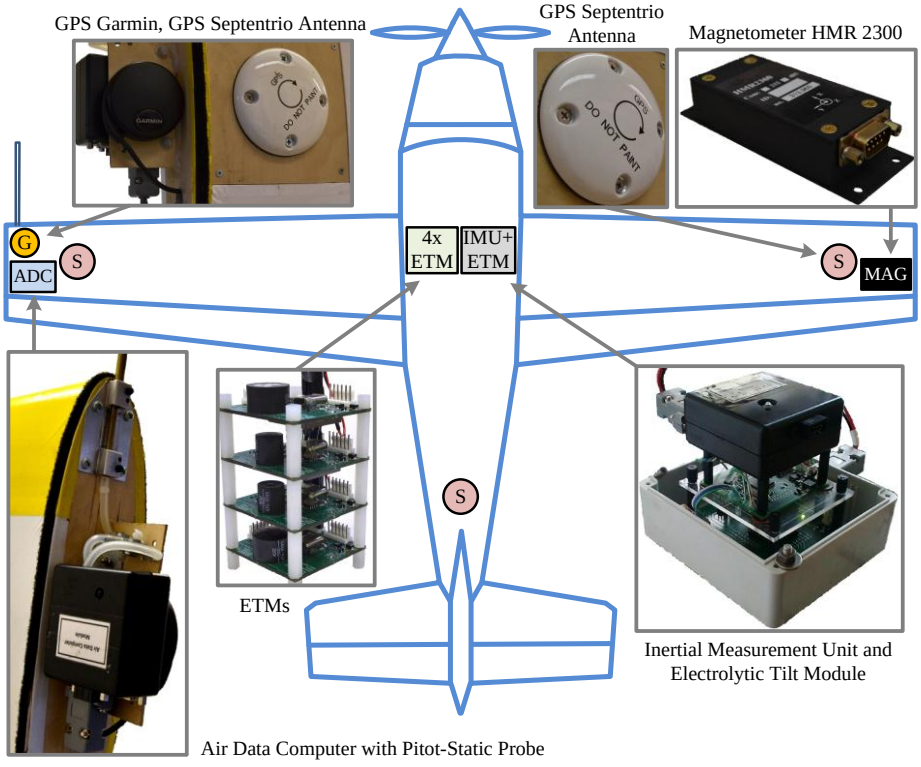

Fig. 16 – The modular system configuration

The ground station SW had two parts, the first one displayed the data measured and stored with the capability to read data from the SD card, see Fig. 17. It was used in pre-flight system verification when all data were transmitted. The other part, shown in Fig. 18, provided the overview of onboard evaluated navigation data transmitted from the UAV to the ground station. The SW was also designed to receive system monitoring data but this part has not been used so far.

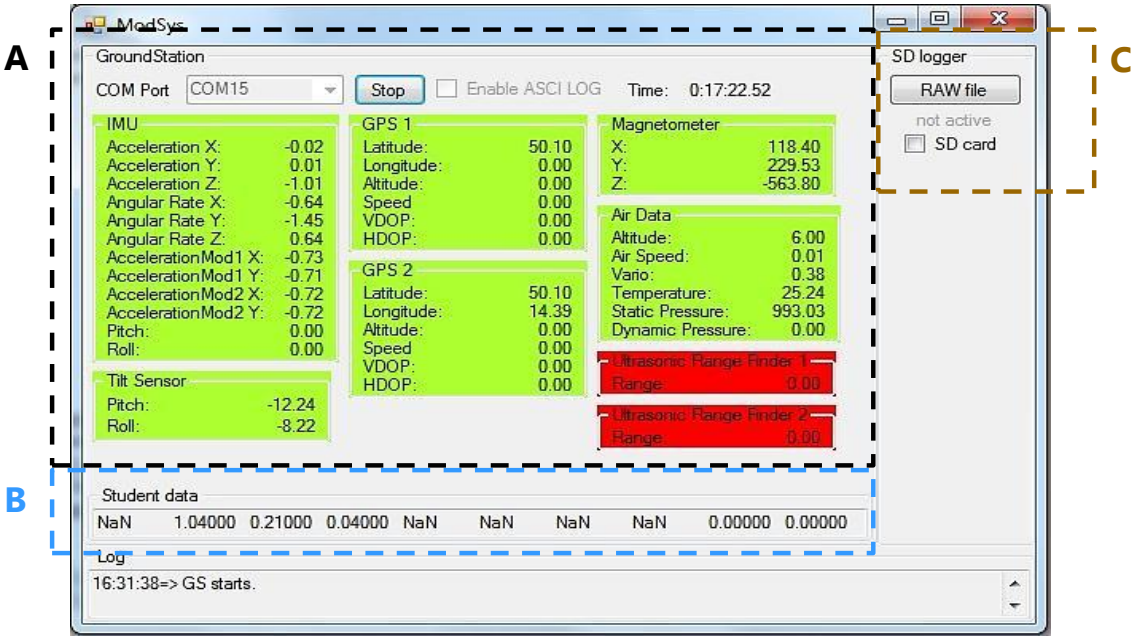

Fig. 17 – The modular navigation SW (ModSys)
A – measured and stored data, B – arbitrary data, C – SD logger data proceeding

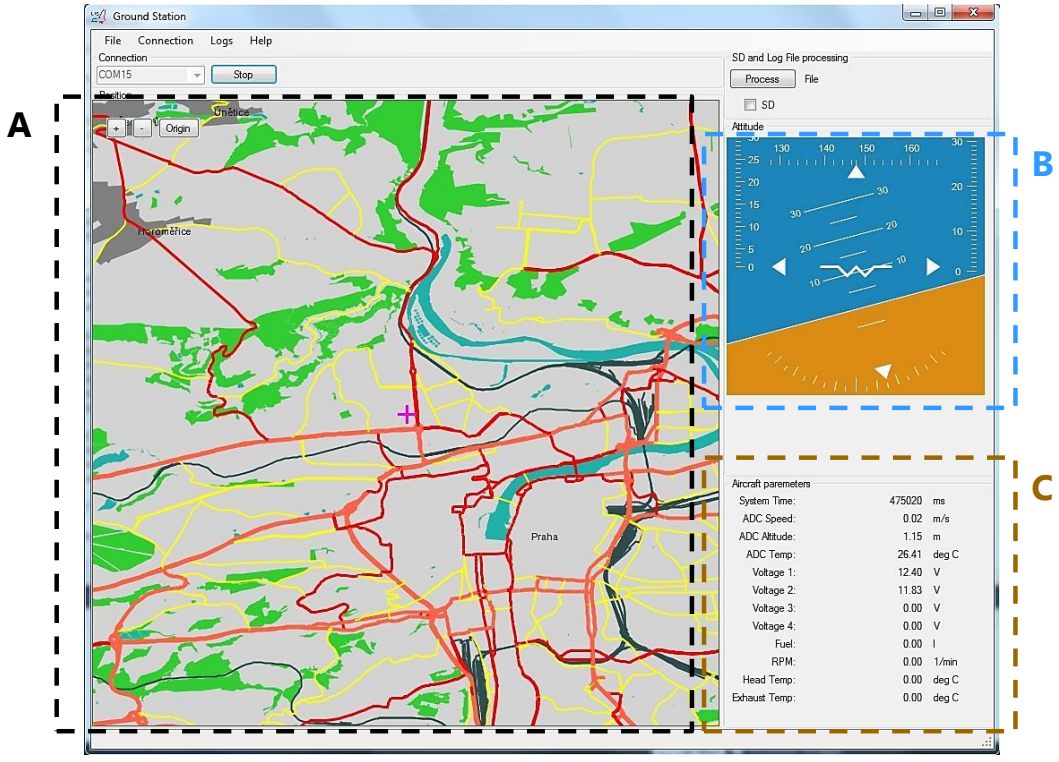

Fig. 18 – ModSys ground station SW
A – maps with localization, B – artificial horizon, C – system monitoring data

To verify the performance of the navigation system, there has been performed a test flight with the UAV, which was remotely controlled to perform various flying patterns illustrated in Fig. 19. The whole flight took 30 minutes.

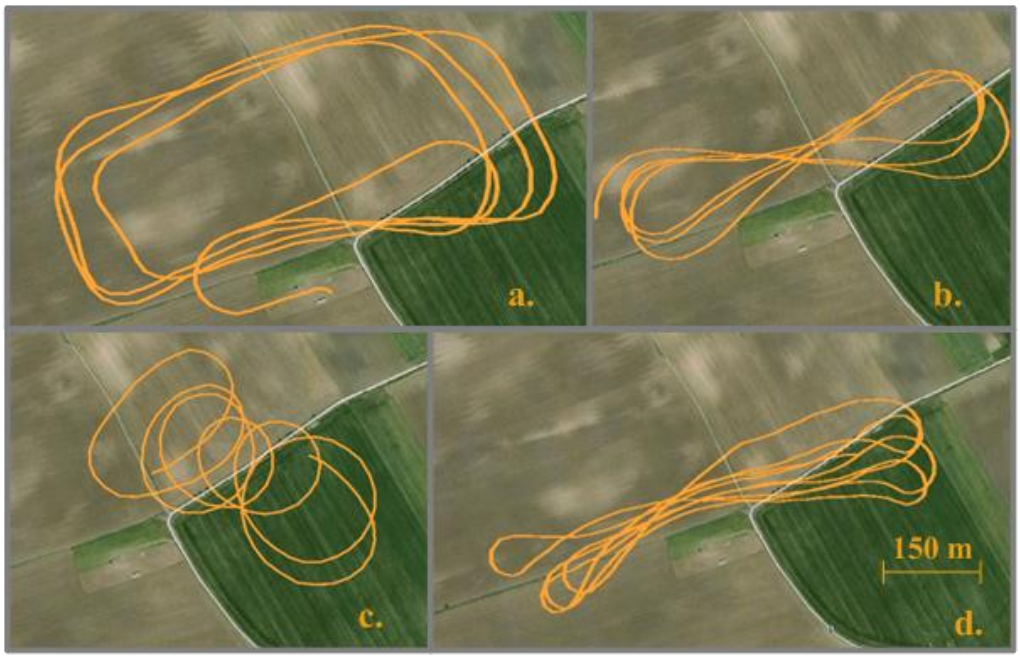

Fig. 19 – Flight tracks of the experiment with the UAV with different shape
a. – rectangular, b. – eight-pattern, c. – circular, d. – rapid attitude changing trajectories

To determine the precision of position evaluation there has been applied an algorithm using extended Kalman filter fusing INS and GPS (INS/GPS EKF) and for the attitude accuracy estimation there has also been used another algorithm utilizing attitude EKF with Gauss-Newton compensation feedback. To minimize a vibration influence on measure data, data were pre-processed by a 10^{th} order low-pass filter with a cut-off frequency at 5 Hz. All results were compared with the reference obtained from a multi-antenna GPS receiver Septentrio PolarX2@e and are shown in Table 3. The typical standard deviation (1σ) of the reference in all channels is given in Table 4. The performance corresponded to standard settings of the receiver not using any enhancements by augmentation systems or a differential GPS. The attitude accuracy was proportional to the baseline lengths among antennas, 3 meters between wing antennas and 0.9 meters between the wing-baseline and the tail antenna.

	Position INS/GPS EKF (m)			**Attitude INS/GPS EKF (deg)**			**Attitude EKF + Gauss-Newton Algorithm (deg)**		
	North	East	Down	Roll	Pitch	Yaw	Roll	Pitch	Yaw
RMSE	4.54	4.89	5.94	1.17	1.98	5.17	2.28	3.07	6.07
1 σ	2.96	3.40	4.67	1.09	1.75	4.41	2.12	2.87	5.58

Table 3 – The precision of the attitude and position evaluation process

	Position accuracy (m)		**Attitude accuracy (deg)**		
	Horizontal	Vertical	Roll	Pitch	Yaw
1 σ	1.1	1.9	0.2	0.6	0.3

Table 4 – The precision of the multi-antenna GPS system

The algorithms accuracy estimation partially suffered from the inaccuracy of the reference which was the only one available for flight experiments. A disadvantage of the reference was also in its functionality in harsh-vibrating environment which was causing outages in data flow.

6. FUTURE WORK

An R&D in the field of navigation systems is progressive as there still exists a broad demand for their usage in variety of new applications. In the field of terrestrial navigation an attention is given to navigation provided inside buildings or in places with low availability of a GPS signal mainly in urban areas where the accuracy rapidly decreases. In these cases the primary role is put on inertial sensors and other aiding systems, e.g. laser scanners, Wi-Fi positioning, optic vision etc. In the case of aircraft operation the safety is always considered. Nowadays, large aircrafts are going to flight according to GPS coordinates instead of VOR and DME navigation means. So GPS technology cannot be omitted; however, to increase the safety the demand addresses a system redundancy as well as its independency on other external means but the ones influenced just by the flight dynamics. Therefore, stand-alone functionality of navigation means should not be omitted as well. According to a current R&D in the field of navigation systems it seems that the attention is still focused on all aspects of design and development of navigation means including improvements in sensor technology and sensors' performance, signal/data processing, calibration methodology, plus measurement systems integration and data fusion. Although the range of potential activities in the area of navigation is wide and none is less interesting, the applicant wants to give his main attention to investigate new methods and potential solution of navigation objectives and to design and develop:

- A precise navigation system primary using only inertial sensors, such as fiber optic gyroscopes DSP-3100 (KVH manufacturer) and quartz ACCs INN-204 (Innalabs manufacturer), all available at the laboratory K13138-LIS. Hence, the task lies in its development and realization including design and implementation of algorithms needed for attitude and position determination that is not relying on other aiding systems. Based on the first look it seems that the task is just to implement already known methods and algorithms, but based on the closer look the development and realization bring many challenges the applicant has not dealt with or dealt just partially before. It includes a precise design of sensor beds and holders, analog ACC outputs signal processing and conversion into a digital form, measurement unit calibration, complete INS mechanization implementation, and the system verification. The INN-204 has the resolution of 5 μg which leads to a current output value being units of nA and with the sensor range 50 g it provides a big dynamic range for the AD converter. There is already knowledge of possible calibration methods suitable to calibrate an IMU; however, these methods have been generally applied on MEMS based units with resolution about 1 mg and 0.1 deg/s. In this case the sensors have the resolution about 5 μg and 10^{-8} deg/s, which requires a different approach and equipment. The final application can address small aircrafts where price is still a key factor and in this case the costs would be around 350 000 CZK (just the sensors) which is low with respect to potential competitors in this category of navigation systems.
- A miniature and low-cost navigation system, which could be used for general navigation purposes. Although a navigation system can be found even in smart phones, its application is simple and has strict limits of functionality. Advantages of a proposed system will be in broad functionality under different conditions provided by a unique integration of up-to-date sensors, not just inertial ones, supported by algorithms improving the precision of the position and attitude estimates. The final application could be oriented for instance at hand-held navigation units for blind people, light UAV navigation, mobile robots, intelligent mine detectors etc.
- An attitude and heading reference system with an optic vision aiding capability. This capability will be provided by a camera observing a horizon and will assure the attitude and heading stabilization. A challenge in this task is in an image processing, which is not the field of applicant interest thus it will be solved in cooperation, but also in adaptive data fusion, which is the applicant main concern.
- Optimized methods for navigation data processing in harsh environment conditions, plus for increasing capability of low-cost MEMS based navigation units through a measurement frame modification and signal processing as well as their integration with aiding measurement systems. Objectives of this point also consider the continuation of activities paid to the modular navigation system proposed by the applicant in cooperation with his PhD. students.

7. SUMMARY AND CONCLUSION

Summary: This thesis is devoted to the problems of modern sensors implementation in preferably low cost navigation systems. The design of a navigation system is generally a complex issue and requires profound knowledge in navigation principles, sensor technology, signal and data processing, calibration methodology as well as knowledge in measurement system modeling, fusion and implementation. Inertial navigation systems for aircraft navigation are in general very expensive, because of high precision requirements (1 NM/hour in position). Moreover, they are designed to be standalone which gives excessively demanding requirements on applied sensors. Such sensors are thus very expensive, and therefore this kind of navigation system is mainly determined for large aircrafts or ships. In other applications there prevails an effort to use cost-effective solutions often utilizing MEMS based sensor. In this case "aided navigation systems" have to be used, because inertial sensors (accelerometers, angular rate sensors/gyros) performance cannot sufficiently satisfy demanding precision requirements. Therefore, additional external measurement systems (aided navigation) have to be implemented.

First chapter guides a reader in a development process of an aided navigation system and points out specific areas in which the applicant has contributed. Chapter 2 introduces current state-of-of-the-art in navigation systems and deals with theoretical background necessary for understanding the methods and technology the applicant applied for fulfilling the goals of his motivation and predetermined objectives. Chapter 3 further reports areas of R&D activities included in this thesis. They are mainly focused on the development of methods leading to the improvement of navigation systems' performance. Besides theoretical solutions and laboratory applications, the thesis also addresses practical needs being solved in cooperation with aircraft industry partners. Therefore, the mainstream of the thesis is devoted to a completeness of navigation systems design. Main topics of the thesis might be summarized as:

- estimation of deterministic sensor parameters and calibration procedures,
- estimation of the stochastic sensor parameter and modeling,
- measurement frames modification,
- navigation data evaluation and their fusion,
- data pre-processing and validation,
- aiding systems and their integration.

The applicant contribution is presented in chapter 4 by selected papers which were published in both journals and conference proceedings. The content of this chapter is then extended in chapter 5 by the description of other applicant contribution which has not been published yet.

Conclusion: The theoretical background and experience in R&D included in the thesis were fully exploited in the applicant educational activities. There have been bachelor, master, and PhD degree students involved in his practically oriented research projects which led to the stimulation of their interest and motivation to work in technical branches. In years 2008-2012 6 bachelor theses, 5 master theses, and one finished PhD thesis were inspired by topics closely related to navigation system design and supervised by the applicant. Moreover, currently other three PhD students deal with navigation system applications using the new ideas and results presented in this thesis. The work of the applicant in the field of navigation systems formed a corner stone of the establishment of new specialization "navigation systems" in the Department of Measurement. It also has undoubtedly positive influence on educational activities by making a study branch "Aircraft and space systems" taught at CTU in Prague attractive for young people. At the same time involving modern methods and technology contained in this thesis enhances quality of applicant lecturing activities for foreign and Czech students. The aerospace oriented study branch creates a platform for establishing international relationships within PEGASUS Network representing the net of cooperating European universities in the field of aerospace. A main goal of this international cooperation is in student exchange as well as in cooperation with industry in the level of student interships which in both cases enhance the level of education at CTU in Prague.

8. SUMMARIZED LIST OF THE APPLICANT PUBLISHED PAPERS

[8.1] Roháč, J.: Accelerometers and their Usage in an Aircraft Attitude Evaluation . In Applied Electronics 2005 - International Conference Pilsen. Pilsen: University of West Bohemia, 2005, p. 285-288. ISBN 80-7043-369-8.

[8.2] Roháč, J.: Low-Cost System of an Artificial Horizon. In MOSATT 2005 - Modern Safety Technologies in Transportation. Košice: Slovak Transport Society at the Slovak Academy of Sciences, 2005, p. 343-347. ISBN 80-969106-1-2.

[8.3] Roháč, J.: Accelerometers and an Aircraft Attitude Evaluation. In IEEE Sensors 2005 - The 4-th IEEE Conference on Sensors [CD-ROM]. Irvine, CA: IEEE Sensors, 2005, p. 784-788. ISBN 0-7803-9057-1.

[8.4] Roháč, J.: Calibration of an Artificial Horizon Unit. In Nové trendy rozvoja letectva - Zborník 7. medzinárodnej vedeckej konferencie [CD-ROM]. Košice: Slovenský letecký inštitút a. s., 2006, ISBN 80-8073-520-4. (in Czech).

[8.5] Roháč, J.: Accelerometers and their Usage in Angular Rate Evaluation. In MDS palubních soustav letadel - 6. odborný seminář. Brno: Univerzita obrany, Fakulta vojenských technologií, 2006, s. 8-12. ISBN 80-7231-155-7. (in Czech).

[8.6] Roháč, J. - Pačes, P. - Draxler, K. - Jakl, P.: Air Speed Measurement by Low-cost Sensors. In MDS palubních soustav letadel - 6. odborný seminář. Brno: Univerzita obrany, Fakulta vojenských technologií, 2006, s. 68-74. ISBN 80-7231-155-7. (in Czech).

[8.7] Roháč, J.: Calibration and Its Effect on Precision of a Low-Cost Artificial Unit. In ICIT 2006 International Conference on Industrial Technology [CD-ROM]. Kolkata: Cygnus Advertising, 2006, p. 1777-1781. ISBN 1-4244-0726-5.

[8.8] Beňo, L. - Bugaj, M. - Draxler, K. - Fábera, V. - Chalas, R. - et al.: Aircraft Maintenance Technician. 1. vyd. Brno: CERM, 2006. 166 s. (in Czech).

[8.9] Reinštein, M. - Roháč, J.: Signal Processing and Data Transfer Concerning Angular Rate Sensors. In The third AIAA-Pegasus Student Conference [CD-ROM]. Napoli: Universita degli Studi di Napoli "Federico II", 2007,

[8.10] Reinštein, M. - Roháč, J.: Measuring System for Angular Rate Sensors. In POSTER 2007 [CD-ROM]. Prague: CTU, Faculty of Electrical Engineering, 2007,

[8.11] Reinštein, M. - Roháč, J.: System for Verification of Adaptive Algorithms Enhancing the Precision of Low Cost Inertial Sensors. In MOSATT 2007, Proceedings of the International Scientific Conference "Modern Safety Technologies in Transportation". Košice: Slovak Transport Society at the Slovak Academy of Sciences, 2007, p. 224-230. ISBN 978-80-969760-2-7.

[8.12] Roháč, J.: GPS and its Usage in Attitude Evaluation. In MOSATT 2007, Proceedings of the International Scientific Conference "Modern Safety Technologies in Transportation". Košice: Slovak Transport Society at the Slovak Academy of Sciences, 2007, p. 237-244. ISBN 978-80-969760-2-7.

[8.13] Reinštein, M. - Roháč, J.: Modelling and Evaluation of Inertial Sensors. In MDS - Měření, diagnostika, spolehlivost palubních soustav letadel - 7. mezinárodní vědecká konference. Brno: Univerzita obrany, Fakulta vojenských technologií, 2007, p. 97-105. ISBN 978-80-7231-281-8.

[8.14] Pačes, P. - Roháč, J. - Ramos, H.: Intelligent Sensing in a Design of a Distributed Engine Control Unit. In ICST 2007 - The 2nd International Conference on Sensing Technology [CD-ROM]. Palmerston North: Massey University, Institute of Information Sciences and Technology, 2007, p. 205-210. ISBN 978-0-473-12432-8.

[8.15] Roháč, J.: Artificial Horizon with a Modified Low-Cost IMU. In The Navigation Conference and Exhibition ARE WE THERE NOW? [CD-ROM]. London: Royal Institute of Navigation, 2007, p. 1-16.

[8.16] Soták, M. - Sopata, M. - Bréda, R. - Roháč, J. - Váci, L. (ed.): Inertial Systems Navigation. 1. vyd. Košice: Bréda Róbert, 2006. 344 s. ISBN 80-969619-9-3. (in Slovak).

[8.17] Roháč, J.: Primary Sensors Used in Navigation. In Integrácia navigačných systémov. Košice: Bréda Róbert, 2006, s. 85-130. ISBN 80-969619-9-3. (in Slovak).

[8.18] Reinštein, M. - Pačes, P. - Roháč, J. - Šipoš, M.: Advanced Implementations Techniques in Kalman Filtering. In 2008 PEGASUS-AIAA Student Conference [CD-ROM]. Prague: Czech Technical University, 2008,

[8.19] Šipoš, M. - Roháč, J. - Reinštein, M.: Measurement with Electrolytic Tilt Sensor. In 2008 PEGASUS-AIAA Student Conference [CD-ROM]. Prague: Czech Technical University, 2008,

[8.20] Šipoš, M. - Reinštein, M. - Roháč, J.: System for Measuring Tilt-Angle. In New Development Trends In Aeronautics. Košice: Technical University of Košice, 2008, p. 120-121. ISBN 978-80-553-0067-2.

[8.21] Šipoš, M. - Reinštein, M. - Roháč, J.: Levenberg-Marquardt Algorithm for Accelerometers Calibration. In Sborník z 8. mezinárodní vědecké konference Měření, diagnostika a spolehlivost palubních soustav letadel. Brno: Univerzita obrany, Fakulta vojenských technologií, 2008, p. 39-45. ISBN 978-80-7231-555-0.

[8.22] Reinštein, M. - Roháč, J. - Šipoš, M.: Improving Performance of a Low-cost AHRS. Acta Avionica. 2008, vol. X, no. 16, p. 132-137. ISSN 1335-9479.

[8.23] Reinštein, M. - Roháč, J. - Šipoš, M.: Turbulence Modelling for Attitude Evaluation Purposes. In Sborník z 8. mezinárodní vědecké konference Měření, diagnostika a spolehlivost palubních soustav letadel. Brno: Univerzita obrany, Fakulta vojenských technologií, 2008, p. 46-54. ISBN 978-80-7231-555-0.

[8.24] Roháč, J. - Reinštein, M.: New Trends in Angular Rate Sensing and Attitude Evaluation. In Nové trendy v civilním letectví. Praha: ČVUT, Fakulta dopravní, 2008, p. 155-161. ISBN 978-80-7204-604-1.

[8.25] Pačes, P. - Šipoš, M. - Reinštein, M. - Roháč, J.: Sensors of Air Data Computers - Usability and Environmental Effects. In ICMT'09 - Proceedings of the International Conference on Military Technologies. Brno: Univerzita obrany, 2009, p. 401-409. ISBN 978-80-7231-649-6.

[8.26] Reinštein, M. - Šipoš, M. - Roháč, J.: Error Analyses of Attitude and Heading Reference Systems. Przeglad Elektrotechniczny. 2009, vol. 85, no. 8, p. 114-118. ISSN 0033-2097.

[8.27] Šipoš, M. - Pačes, P. - Reinštein, M. - Roháč, J.: Flight Attitude Track Reconstruction Using Two AHRS Units under Laboratory Conditions. In IEEE SENSORS 2009 - The Eighth IEEE Conference on Sensors [CD-ROM]. Christchurch: IEEE Sensors Council, 2009, p. 675-678. ISBN 978-1-4244-5335-1.
[8.28] Šipoš, M. - Roháč, J.: Integration of Low-cost Inertial Navigation Unit with Secondary Navigation Systems. In Workshop 2010 [CD-ROM]. Praha: ČVUT v Praze, 2010, p. 146-147. ISBN 978-80-01-04513-8.
[8.29] Reinštein, M. - Roháč, J. - Šipoš, M.: Algorithms for Heading Determination using Inertial Sensors. Przeglad Elektrotechniczny. 2010, vol. 86, no. 9, p. 243-246. ISSN 0033-2097.
[8.30] Roháč, J.: Aided Navigation Systems for UAVs. In 2nd Conference for Unmanned Aerial Systems. Praha: FSI ČVUT, 2010, . ISBN 978-80-86059-53-2.
[8.31] Nováček, P. - Roháč, J.: GPS Based Attitude Estimation. In 2nd Conference for Unmanned Aerial Systems [CD-ROM]. Praha: FSI ČVUT, 2010, p. 1-8. ISBN 978-80-86059-53-2.
[8.32] Ripka, P. - Nováček, P. - Reinštein, M. - Roháč, J.: Position Sensing System for Eddy-current Mine Imager. In EUROSENSORS XXIV - Proceedings [CD-ROM]. Linz: Elsevier BV, 2010, p. 276-279. ISSN 1877-7058.
[8.33] Roháč, J.: Navigation Data Denoising. In MDS - Měření, diagnostika, spolehlivost palubních soustav letadel 2010. Brno: Univerzita obrany, 2010, p. 133-140. ISBN 978-80-7231-741-7.
[8.34] Šipoš, M. - Roháč, J.: Calibration of Tri-axial Angular Rate Sensors. In MDS - Měření, diagnostika, spolehlivost palubních soustav letadel 2010. Brno: Univerzita obrany, 2010, p. 148-152. ISBN 978-80-7231-741-7.
[8.35] Roháč, J. - Šipoš, M. - Nováček, P. - Pačes, P. - Reinštein, M.: Modular System for Attitude and Position Estimation. In Workshop 2011 [CD-ROM]. Praha: České vysoké učení technické v Praze, 2011, p. 1-4.
[8.36] Draxler, K. - Pačes, P. - Roháč, J. - Fetr, M.: Use of Differential Air Pressure Sensor for Barometric Difference Altitude and Vertical Speed Measurement. In ICMT'11 International Conference on Miltary Technologies 2011 [CD-ROM]. Brno: Univerzita obrany, 2011, p. 605-610. ISBN 978-80-7231-788-2.
[8.37] Roháč, J.: Artificial Horizon without Kalman Filter Applied. In ICMT'11 International Conference on Miltary Technologies 2011 [CD-ROM]. Brno: Univerzita obrany, 2011, p. 679-684. ISBN 978-80-7231-788-2.
[8.38] Šipoš, M. - Roháč, J.: Usage of Electrolytic Tilt Sensor for Initial Alignment of Tri-axial Accelerometer. In ICMT'11 International Conference on Miltary Technologies 2011 [CD-ROM]. Brno: Univerzita obrany, 2011, p. 685-691. ISBN 978-80-7231-788-2.
[8.39] Šipoš, M. - Pačes, P. - Roháč, J. - Nováček, P.: Analyses of Triaxial Accelerometer Calibration Algorithms. IEEE Sensors Journal. 2012, vol. 12, no. 5, p. 1157-1165. ISSN 1530-437X.
[8.40] Šipoš, M. - Roháč, J. - Nováček, P.: Analyses of Electronic Inclinometer Data for Tri-axial Accelerometer's Initial Alignment. Przeglad Elektrotechniczny. 2012, vol. 88, no. 01a, p. 286-290. ISSN 0033-2097.
[8.41] Šipoš, M. - Roháč, J. - Nováček, P.: Improvement of Electronic Compass Accuracy Based on Magnetometer and Accelerometer Calibration. Acta Physica Polonica A. 2012, vol. 121, no. 4, p. 945-949. ISSN 0587-4246.
[8.42] Roháč, J. - Řeřábek, M. - Hudec, R.: Multi-Functional Star Tracker - Future Perspectives. Acta Polytechnica. 2011, vol. 51, no. 6, p. 61-64. ISSN 1210-2709.
[8.43] Roháč, J. - Reinštein, M. - Draxler, K.: Data Processing of Inertial Sensors in Strong-Vibration Environment. In Intelligent Data Acquisition and Advanced Computing Systems (IDAACS). Piscataway: IEEE, 2011, vol. 1, p. 71-75. ISBN 978-1-4577-1426-9.
[8.44] Roháč, J. - Šipoš, M.: Practical Usage of Allan Variance in Inertial Sensor Parameters Estimation and Modeling. In New Trends in Civil Aviation 2011. Praha: ČVUT v Praze a OSL ČR, 2011, p. 107-112. ISBN 978-80-01-04893-1.
[8.45] Nováček, P. - Roháč, J. - Ripka, P.: Complex Markers for a Mine Detector. IEEE Transactions on Magnetics. 2012, vol. 48, no. 4, p. 1489-1492. ISSN 0018-9464.
[8.46] Roháč, J. - Šipoš, M.: Sensors and Data Processing Methods Used in Navigation Systems. In Proceedings of the International Scientific Conference Modern Safety Technologies in Transportation. Košice: SUPREMA Ltd., 2011, p. 342-348. ISBN 978-80-970772-0-4.
[8.47] Šipoš, M. - Roháč, J.: Improvement of Electronic Compass Accuracy Based on Magnetometer and Accelerometer Calibration. In SPM 2011 - X Symposium of Magnetic Measurements. Czestochowa Branch: Polish Society of Theoretical and Applied Electrical Engineering, 2011, p. 33.
[8.48] Nováček, P. - Ripka, P. - Roháč, J. - Paroulek, L.: Explosive Remnants of Wars Differentiation. In SPM 2011 - X Symposium of Magnetic Measurements. Czestochowa Branch: Polish Society of Theoretical and Applied Electrical Engineering, 2011, p. 28.
[8.49] Roháč, J. - Šipoš, M. - Nováček, P.: Azimuth Determination Based on Magnetometer Measurements. In MDS - Měření, diagnostika, spolehlivost palubních soustav letadel 2011 - Sborník příspěvků z 11.mezinárodní vědecké konference. Brno: Univerzita obrany, Fakulta vojenských technologií, 2011, p. 11-17. ISBN 978-80-7231-828-5.
[8.50] Nováček, P. - Roháč, J.: Inertial Sensors Utilization in Humanitarian Demining. In MDS - Měření, diagnostika, spolehlivost palubních soustav letadel 2011 - Sborník příspěvků z 11.mezinárodní vědecké konference. Brno: Univerzita obrany, Fakulta vojenských technologií, 2011, s. 138-144. ISBN 978-80-7231-828-5. (in Czech).
[8.51] Šipoš, M. - Roháč, J. - Stach, M.: System for Vibration Testing. In MDS - Měření, diagnostika, spolehlivost palubních soustav letadel 2011 - Sborník příspěvků z 11.mezinárodní vědecké konference. Brno: Univerzita obrany, Fakulta vojenských technologií, 2011, p. 213-225. ISBN 978-80-7231-828-5.
[8.52] Roháč, J. - Ďaďo, S.: Environmental Vibration Impact on Inertial Sensors' Output. In: Sensors & Transducers. 2012, In Press. ISSN 1726-5479.
[8.53] Roháč, J. - Šipoš, M.: Measurement Unit of an Artificial Horizon. Užitný vzor Úřad průmyslového vlastnictví, 23268. 2012-01-16. (in Czech).
[8.54] Roháč, J. - Šipoš, M. - Šimánek, J. - Tereň, O.: Inertial Reference Unit in a Directional Gyro Mode of Operation. In IEEE SENSORS 2012 - Proceedings [CD-ROM]. Piscataway: IEEE Service Center , 2012, p. 1356-1359. ISBN 978-1-4577-1765-9.